THE DYNAMICS OF SHAKEN BABY SYNDROME

by

CHRISTOPHER NEIL MORISON

A thesis submitted to
The University of Birmingham
for the degree of
DOCTOR OF PHILOSOPHY

School of Manufacturing and Mechanical Engineering
The University of Birmingham
June 2002

ABSTRACT

Shaken Baby Syndrome is a form of child abuse estimated to occur to one in 20,000 babies and presumed to occur when a carer cannot cope with a constantly crying child and so gives it a sharp shake. This causes the brain to move within the skull, stretching and possibly tearing the veins that bridge the fluid filled gap. To better understand this condition, experiments were performed to measure the mechanical properties of bridging veins followed by detailed mathematical modelling of the motion of a baby's brain in response to shaking. Few finite element models of shaken baby syndrome exist, and those either ignore the fluid surrounding the brain or model it as a soft solid. The importance of modelling the fluid properly is demonstrated, and the reliability of MSC.Dytran's fluid-solid interaction modelling is confirmed. The first three-dimensional finite element model of shaken baby syndrome which accurately includes the cerebrospinal fluid is created and used to estimate tolerance criteria for causing subdural haematoma by shaking. This research concludes that shaking of a baby could produce bridging vein strain close to the tolerance for failure and hence should be considered a possible cause of subdural haematoma.

ACKNOWLEDGEMENTS

The author would like to acknowledge the following people for their contribution to this project:

- **Dr D.C. Hodgson**, Senior Lecturer,
  Manufacturing and Mechanical Engineering, Birmingham University.
  For his invaluable assistance and guidance throughout the whole of the research and thesis preparation.

- **Dr R. Sunderland**, Consultant Paediatrician, Birmingham Children's Hospital
  For his enthusiasm for the research and interest in the results achieved, and also for lending his expertise by helping with extraction of the pig bridging veins and interpretation of the magnetic resonance images.

Furthermore, both of these people should be acknowledged for their initial collaboration in realising that this research was needed and for laying its foundations.

CONTENTS

LIST OF FIGURES

LIST OF DEFINITIONS

Apnoea Cessation of breathing.

Arachnoid Membrane (meninge) covering the brain, like a cobweb, covered with or consisting of soft fibres or hairs so entangled as to give a cobwebby appearance.

Bridging Veins Veins which drain blood from the upper surface of the brain into the superior sagittal sinus

Bulk Modulus Property of a material defined as the ratio of pressure to volumetric strain.

Cerebellum Part of the vertebrate hindbrain, concerned primarily with somatic motor function, the control of muscle tone and the maintenance of balance.

Cerebrospinal Fluid (CSF) A clear, colourless fluid that contains small quantities of glucose and protein. Cerebrospinal fluid fills the ventricles of the brain and the central canal of the spinal cord.

Cerebrum The portion of the brain (frontal lobes) where thought and higher function reside.

Computed Tomography (CT) A special radiographic technique that uses a computer to assimilate multiple X-ray images into a 2 dimensional cross-sectional image.

Coup injury An injury occurring directly beneath the skull at the area of impact.

Contrecoup injury An injury occurring beneath the skull opposite to the area of impact.

Diffuse Axonal Injury (DAI) Damage to the nerve cells of the brain caused by high shearing forces.

Dura Mater The outermost, toughest and most fibrous of the three membranes (meninges) covering the brain and spinal cord.

Falx Cerebri The scythe-shaped fold of dura mater in the longitudinal fissure between the two cerebral hemispheres; it is attached anteriorly to the crista galli of the ethmoid bone and caudally to the upper surface of the tentorium.

Fontanelle A soft spot, such as one of the membrane covered spaces remaining in the incompletely ossified skull of a foetus or infant.

Goniometer A calibrated device designed to measure the arc or range of motion of a joint.

Hypoxia Reduction of oxygen supply to tissue below physiological levels despite adequate perfusion of the tissue by blood.

Ischaemia A low oxygen state usually due to obstruction of the arterial blood supply or inadequate blood flow leading to hypoxia in the tissue.

Magnetic Resonance Image (MRI) A special imaging technique used to image internal structures of the body, particularly the soft tissues.

Pia Mater The delicate and highly vascular membrane immediately investing the brain and spinal cord.

Poisson Ratio The ratio of transverse contraction strain to longitudinal extension strain in the direction of stretching force.

Shear Modulus Property of an elastic material relating shear stress to shear strain.

Sphenoid Ridge Sphenoid bone, an irregularly shaped bone in front of the occipital in the base of the skull of the higher vertebrates.

Strain Elongation as a percentage of initial length.

Stretch Ratio Ratio of stretched length to initial length.

Subdural Haematoma (SDH) A serious type of head injury characterised by a collection of blood under the dura mater adjacent to the brain. Acute subdural haematomas are a surgical emergency that usually result from head trauma.

Tentorium Cerebelli A fold of the dura mater which separates the cerebellum from the cerebrum

Vertex The highest point of the brain or head.

Viscoelasticity The property of a viscous material that also shows elasticity.

Young's Modulus Property of an elastic material relating stress to strain.

Medical definitions courtesy of the CancerWEB On-line Medical Dictionary
http://cancerweb.ncl.ac.uk/omd/

INTRODUCTION

Shaken baby syndrome has received much media attention over the past few years due to the well-publicised trials of several parents or carers accused of shaking a baby to death. During these trials expert witnesses for the prosecution and defence can present opposing opinions on the forces necessary to kill a baby, which often go as far as vigorous pathological shaking almost certainly followed by an impact of the baby's head. But how accurate are these estimations, and do we actually yet know how much you might have to shake a baby in order to kill it?

Babies are particularly vulnerable to head injury for several reasons. Firstly, their underdeveloped neck muscles and relatively large head means that babies cannot support their own head. Secondly, a baby's brain is surrounded by an increased volume of cerebrospinal fluid (CSF), which can be up to 10 mm thick, compared to only 1-2 mm in older children and adults, which gives the brain more room for movement within the skull. As a child is gripped by its torso and shaken, its head oscillates back and forth and the brain can move significantly within the skull. This can cause several injuries to the child including retinal haemorrhages, subdural haematoma (SDH), hypoxia and shearing injuries within the brain tissue which can lead to brain damage or even death. The subdural haematoma is caused when the 'bridging veins' (which span the CSF layer between the upper surface of the brain and the inner surface of the skull) are stretched by the movement of the brain and is commonly the primary diagnostic evidence of shaking. Therefore it was decided to concentrate this research on the bleeding which leads to subdural haematoma since understanding the necessary forces would assist in determining

the minimum levels of violence exhibited to a child. The clinical consequences of handicap or death are due to damage to the brain tissue itself, but the causative mechanism for this are even less well understood.

An experimental study (Duhaime *et al.*, 1987) related the results of previous shaking experiments on monkeys to tolerance criteria for concussion, diffuse axonal injury (DAI) and SDH in babies. The result of this study was that the tolerance levels for DAI and SDH were well above the levels of acceleration experienced within the heads of life-like baby dolls as they were shaken, but below the levels caused by impacting the dolls' heads against hard or padded surfaces. Therefore this study concluded that you cannot kill a baby merely by shaking it, some form of impact must be involved. Since the publication of this study many people have favoured the term 'Shaken-Impact Syndrome' and have taken the conclusions of this report at face value.

However, there are various factors that cast doubt on these findings. The experiments on the monkeys involved shaking their heads at frequencies around 100 Hz, whereas an adult can only shake a baby at up to 4 Hz. Furthermore, the method employed to scale the tolerance levels from the monkey experiments to human babies was originally developed to scale internal brain stresses and only takes into account the different brain masses. It ignores the wider CSF layers present in babies and also the different nature of concussion and DAI (which are caused by internal brain stresses) compared to SDH (which is caused by movement of the brain as a whole). These issues, coupled with the results of many clinical studies which have found that about one-third of all suspected shaken baby cases have no evidence of impact (skull fracture or even minor scalp bruising) suggest that it may be possible to kill a baby just by shaking it.

There have been very few attempts to produce computer (Finite Element) models of Shaken Baby Syndrome. Most past research has concentrated on modelling adult head injuries in road accidents. Also, because of the difficulties involved with modelling the interactions between fluids and solids, all previous models have either completely ignored the CSF which surrounds the brain, or modelled it as a soft solid.

This thesis reviews the previous clinical, experimental and computer modelling research relevant to shaken baby syndrome, and then investigates the ability of modern finite element modelling software to model the fluid/solid interaction forces necessary to realistically include the CSF in models of shaken baby syndrome. This thesis then presents the development and application of the first three-dimensional finite element model specifically designed to answer questions about shaken baby syndrome.

This model has demonstrated the importance of accurate representation of the cerebrospinal fluid, and has for the first time confirmed its vital role in protecting against head injuries. Since the early 1940's it has been understood that the brain is much more vulnerable to injury caused by head rotation compared to just straight-line motion. Previously this has been thought to be the result of the brain being much more delicate in shear than it is in compression, since the brain is sheared in rotational motion but compressed in straight-line motion. However, recently is has been argued that this difference is largely caused by the protection of the CSF (Hodgson, Shippen and Sunderland, 2001) which greatly reduces the linear movement of the brain within the skull but does very little to stop the brain rotating, as is explained within this thesis and confirmed by the model.

The model agrees with this theory, and shows that the presence of the CSF reduces the translational acceleration of the brain within the skull by about 99.7% without applying any concentrated forces to the brain surface. Yet the model has also shown that the rotational component of the shaking motion can cause significant rotation of the brain within the skull. This rotation could stretch the bridging veins by up to 50% which may easily be enough to break them according to previous research and also experiments reported in this thesis, which found that bridging veins usually break at strains between 30-70%, perhaps even lower for weaker veins.

Due to the inherent variability of biological tissues there is a corresponding variability in the failure properties of the bridging veins, and this makes it impossible to develop precise tolerance criteria for Shaken Baby Syndrome. However, this research has demon-

strated that shaking a baby at 4 Hz may easily be enough to cause subdural haematoma, and hence much less violence may be required than has previously been reported.

1.1 Aims and Objectives

The original objective of this research was *"To develop the first finite element model of shaken baby syndrome which realistically includes the cerebrospinal fluid, and to use this model to develop tolerance criteria for causing bridging vein failure by shaking a baby"*. In the process of achieving that objective, various other aims were met, including:

- All current research relevant to shaken baby or shaken/impact syndrome is presented, showing both schools of thought and the reasons behind them.
- The important role of the CSF was investigated, and was shown to be crucial when modelling head injury.
- The ability of modern finite element modelling software to reliably combine fluids and solids in the same model was confirmed, paving the way for the final objective and hopefully encouraging the adoption of more accurate and representative finite element models of head injury than have previously been used.

1.2 Thesis Overview

Chapter 2 of this thesis contains the review of the current literature and is split into several sections. Firstly, papers in support of shaken baby syndrome are reviewed, followed by those preferring shaken/impact syndrome. These include mainly clinical studies which report incidences of subdural haematoma with or without evidence of head injury but also includes some animal and physical model experiments. The current understanding of the importance of rotation in head injury is also reviewed, and the current theories used to explain the danger of rotation are presented. Research into the failure properties of

human bridging veins is limited to three experimental studies, all of which are compared, highlighting the different methods used in all the experiments which perhaps explains the lack of agreement in their results. Experiments on the material properties of human brain tissue are then tabulated with a similarly diverse range of results despite the increased attention brain tissue research has received. Finally, relevant finite element models of human or primate head injury are reviewed showing both a lack of realistic treatment of the CSF and fluid/solid interactions and also an absence of a model specifically designed for shaken baby syndrome research.

Chapter 3 describes the development of a mechanical testing rig designed to test the failure properties of human infant bridging veins and the strain rate dependence thereof. In order to determine the effect of strain rate the rig needed to stretch the veins at a wide range of speeds, and hence was designed to be actuated either by a DC motor for the slow speeds or by an impact with a pendulum for the high speeds. Human bridging veins were to be provided by the Birmingham Children's Hospital, Birmingham Women's Hospital and the Birmingham Coroner. Unfortunately very few parents were willing to sign the required consent form, which perhaps was partly caused by the negative publicity surrounding the Alder Hey organ retention scandal at the time. This meant that only a very limited number of human bridging veins were available and hence reliable conclusions could not be made. However, those samples which were successfully tested did produce results consistent with the previous research, and it should be noted that these were the first experiments performed on human *infant* veins.

Chapter 4 presents the forces that act on a submerged solid body, and how these forces may or may not contribute to brain protection from inertial translation or rotation. The most significant forces are Archimedes' buoyancy force (which acts under any inertial acceleration, not just gravity) and the acceleration reaction force (whereby the fluid's inertia opposes any acceleration of the body). The ability of the finite element modelling software MSC.Dytran to model these forces is then successfully confirmed by using it to model simple systems for which the theoretical result is known.

Chapter 5 completes this research by describing the development of the finite element model of a baby's head, and the application of the model to estimating shaken baby syndrome tolerance criteria. The development of the model includes creation of the geometry and mesh through to choices of material properties and boundary conditions. Various aspects of the model are tested, including the effectiveness of the CSF in protecting the brain against translational motion, its inability to protect against combined rotation and translation, and the partial ability of the tentorium cerebelli (the membrane which separates the cerebrum and cerebellum) to protect against rotation. Finally the stretch ratio of the bridging veins is shown for shaking the model at a range of frequencies and amplitudes, and is compared to impacts of the head against hard and soft surfaces.

1.3 Conclusions

As already stated, the imprecision in the knowledge of bridging vein failure properties makes the development of precise tolerance criteria impossible. However, the results presented within this thesis provide a valuable new insight into the range of brain motion possible during baby shaking and should hopefully provide the medicolegal community with added information, including reasons to doubt the currently favoured 'shaken impact syndrome' and evidence to support the original 'shaken baby syndrome' hypothesis (Guthkelch, 1971; Caffey, 1974). Furthermore, should future testing of human infant bridging veins clarify their failure properties, then when combined with the results contained within this thesis is should be possible to develop more accurate tolerance criteria for causing subdural haematoma by shaking a baby.

LITERATURE REVIEW

2.1 Introduction

The current literature on shaken baby syndrome can be divided into a number of categories, each of which is dealt with separately in this chapter. Firstly, research into the existence of shaken baby syndrome is presented and is further divided into that which supports the existence of shaken baby syndrome and that which concludes that some form of impact must be necessary. Then the results of previous research into the material properties of the contents of the human head are compared, and finally previous finite element models will be summarised.

2.2 Shaken Baby Syndrome

Historically subdural haematoma were attributed to the deformation of the skull during birth, until Caffey (1946) first made the association between subdural haematomas and fractures of the long bones. Emerging awareness of the scope and scale of child abuse initially met considerable resistance as, at that time, many child experts presumed that parents would not injure their own children. Then in 1962 Kempe defined a new syndrome in his paper "The Battered-Child Syndrome", which combines evidence of fracture of any bone with subdural haematoma, or where the degree and type of injury is at variance with the history given regarding the occurrence of the trauma. Kempe emphasised the possibility of pathological violence by parents or carers towards the child, and put the onus on physicians to properly manage the case, suggesting techniques for questioning

the carers to gain a more accurate history, diagnostic methods and protective measures for the child.

Eventually the number of reported cases of battered child syndrome with no evidence of external head trauma caught the attention of various researchers who collated these cases and used them as the basis for defining *'whiplash shaken infant syndrome'*. Since then the question *"Does shaken baby syndrome exist?"* has been the cause of much debate. The following two sections contain brief summaries of the current literature reporting instances of subdural haematoma and which specify evidence of impact or inertial loading. Where numeric data is available it is further summarised in Table 2.1.

2.2.1 In Support of Shaken Baby Syndrome

Guthkelch (1971) was perhaps the first to explain the unusually high incidence of subdural haematoma occurring in battered children compared to head injuries of other origin, and also remarked on the similarity between injuries caused by severe whiplash in an automobile accident (with no head impact) and those which are known to exist in the many cases of the battered child syndrome. She studied 23 cases of proven or suspected parental assault on children, and found no evidence of direct violence to the head in 5 out of the 13 cases involving subdural haemorrhage. In addition she described two cases in which there was a very strong reason to suppose that the mechanism of production of the subdural haemorrhage had been shaking rather than battering. She also remarks that " 'a good shaking' is felt to be socially more acceptable and physically less dangerous than a blow on the head or elsewhere."

The term *'whiplash shaken infant syndrome'* was probably first coined by Caffey in 1974 to differentiate injuries sustained from the habitual shaking of infants—where there is no evidence of external trauma to the head—from the so-called *'battered child syndrome'* which had previously been used to categorise most cases of suspicious infant death or injury. Caffey felt strongly that it was important to educate parents, carers and physicians to the dangers of shaking infants, which had previously been "considered innocuous by

both the parent-assailant and the questioning physician." Caffey's research (1972 and 1974) collated many previous reported cases of bilateral subdural haematomas, intraocular bleedings and multiple traction changes in the long bones (including Guthkelch, 1971) where there is no evidence of external head trauma and/or strong testimony suggesting that the injuries could only have been the product of shaking. Perhaps one of the most striking of these cases (*Newsweek*, 1956, 48(1), p90) is quoted by Caffey (1974),

> By far the most extensive anecdotal proof of pathogenic manual whiplash-shaking comes from the confessions to the savage shakings of dozens of infants by an infant-nurse who whiplashed three infants to death, maimed two others, and shook uncounted others during a period of nine years. She stated that "one of her babies" died after she had "pounded it on the back to get a bubble up." Prior to a coroner's inquest she broke down and confessed that "baby K refused to drink her bottle so I seized her by both arms and shook her until her head bobbed and she became faint. Then I quickly put her down." After a preliminary investigation the coroner charged that this infant-nurse had caused the infant's deaths during her "uncontrollable fits of anger and uncontrollable urge to grasp infants between the elbows and shoulders and shake them as long as they persisted in crying." Two others of the whiplashed babies were said to have been manhandled so severely that they became painfully injured. One year after the coroner's inquest, two fathers, who had employed this same nurse to care for their two infants earlier, reported that each of the infants had become retarded mentally. As soon as the coroner's report became known to the community, "dozens" of mothers reported that their infants had been significantly injured by this same nurse, and a review of the office records of several paediatricians confirmed additional injuries to many other infants from the same source. It is amazing that this infant-nurse was able to continue her brutal whiplash-shaking practices during the long period of nine years in an enlightened academic community, on the infants of well-educated parents and

> on the patients of well-trained expert paediatricians. This was due in large part to the absence of external signs of trauma after violent often repeated pathogenic shaking.

A study of 134 battered children was published by Smith and Hanson (1974) from the University of Birmingham only a few months before Caffey (1974) defined 'whiplash shaken infant syndrome'. Intracranial haemorrhages were found in 47 children, consisting of 30 subdural, 9 subarachnoid and 8 cerebral. Of these 15 had no skull fractures, and 7 (15%) had no head bruises but instead showed finger and thumb shaped bruises on the trunk and arms. The authors believe that these children were violently shaken and are in support of Guthkelch's (1971) suggestions that whiplash injury rather than direct blows accounts for intracranial bleeding.

McClelland *et al.* (1980) examined 21 patients with cerebral injury as a result of child abuse. Shaken baby syndrome was suspected in 6 of these cases (median age of $5\frac{1}{2}$ months) due to the presence of subdural haematoma, retinal haemorrhage, severe central nervous system dysfunction, bulging fontanelle, hemiplegia (paralysis affecting only one side of the body) or extensor posturing (stiffly extended and internally rotated arms and/or legs). X-rays showed normal skulls in 5 of these 6 patients and an occipital skull fracture in the remaining case. Unfortunately bruising is not mentioned in this study, so it is difficult to isolate pure shaking from shaking with soft impact.

A biomechanical study (Gennarelli and Thibault, 1982) proved that impact is not necessary to cause acute subdural haematoma in primates. In this study, the heads of rhesus monkeys where securely fitted into a helmet that was attached to a pneumatic actuator and linkage system. The system was programmed to deliver a single acceleration-deceleration pulse to the head by rotating it though a 60° arc (centred in the lower cervical area) in times varying from 5 to 25 milliseconds with magnitudes between 100 and 3,000 G. Angular acceleration produced acute subdural haematoma of sufficient size to cause the animal's death in 37 of 128 cases. The haematomas were usually bilateral overlying the ruptured parasagittal bridging veins, although most often much larger on

one side. It should be noted however, that the acceleration magnitudes and especially the frequencies used in this study are much higher than could probably be produced by an adult manually shaking an infant. The definition of acute subdural haematoma used in this study it also noteworthy, since acute subdural haematoma was considered present only if sufficient blood was present in the subdural space to cause death. There was no separate classification for non-fatal subdural haematomas which could eventually have lead to brain damage and mental disorders. The choice of the magnitude of the deceleration phase of the loading as the criteria has also been criticised by various authors (Lee and Haut, 1989, Lee *et al.* 1987), who correctly highlight the fact that the majority of bridging veins have been shown to drain forwards from the brain into the venous sinus and hence they would be stretched more during forwards acceleration whereas forwards deceleration would cause compression before tension. Therefore, even though the deceleration used by Gennarelli and Thibault was several times the magnitude of the prior acceleration, use of the deceleration magnitude as the failure criteria may have significantly overestimated the tolerances for subdural haematoma.

Hadley *et al.* (1989) found 13 (36%) patients suspected of having a clinical history of shaking injury without direct cranial trauma in 36 infants identified has having nonaccidental head injury. This was a prospective study over a period of 6 years. The criteria met by these 13 patients were 1) a documented history of infant shaking as admitted by the perpetrator and 2) no historical, clinical or radiographic evidence of direct impact trauma to the craniofacial region. Eight of these 13 patients died. Computed Tomography findings reported the presence of subdural haematoma in all 13 patients ranging from 'present' in 3 patients, 'moderate' in 7 patients to 'severe' in 3 patients. They conclude that direct cranial impact is "not always" required, especially in the very young. They also report a new pathological finding of sub- or epidural haematomas on the high cervical spinal cord and cervical spinal cord contusions which were found during 5 of the 6 autopsies. They suggest that spinal cord damage caused during the rapid acceleration-deceleration of the infants head could contribute to infant morbidity and mortality. This theory was further

developed by Geddes *et al.*(2001*a*, 2001*b*) which is discussed later in this section.

A study by Alexander *et al.* (1990) was specifically designed to determine the presence of external signs of head trauma in suspected cases of shaken baby syndrome. Over a $4\frac{1}{2}$ year period 24 infants between the ages of 3.5 and 59 weeks were diagnosed as having injuries consistent with the intracranial injuries attributed to shaking. All patients underwent physical examination, or autopsy examination if the child died, specifically looking for signs of direct head trauma. It was found that 12 (50%) of these cases had no signs of external head trauma, also from a total of 9 fatal cases, 5 had no signs of external head trauma. This supports the hypothesis that shaking alone is sufficient to cause serious intracranial injury. Furthermore, the lack of a relationship between mortality and evidence of impact suggests that severe injury can occur with shaking alone.

A review of the non-accidental head injury literature by Brown and Minns (1993) mentions 30 children with non-accidental head injury seen by the authors. Shaking was thought to be the cause of 17 (57%) of these cases with impact attributing to the other 13 (43%) cases. A subdural haematoma was diagnosed in 16 of the 30 cases, and was the only finding in 3 cases.

Gilliland and Folberg (1996) did a prospective study of 169 child deaths, and found 80 deaths due to head trauma. Evidence of shaking was considered present if two or more of the following criteria were met: 1) finger marks and/or rib fractures; 2) subdural and/or subarachnoid haemorrhage; or 3) a history of vigorous shaking. Direct head trauma was defined as either scalp or skull injuries. They found that 9 (11.3%) of the deaths only had evidence of shaking, 30 (37.5%) had evidence of shaking and impact, and the remaining 41 (51.3%) only had evidence of impact. Their evidence supports the theory that "shaking alone is a lethal mechanism of injury", however they do point out that in their study most infants believed to have been shaken had some evidence of impact injury.

Lazoritz *et al.* (1997) noticed that Caffey's original definition of 'whiplash-shaken infant syndrome', and today's 'shaken baby syndrome' or 'shaken impact syndrome' is now commonly used in cases which clearly involve impacts and even in some cases of

impact without shaking, and so he undertook a study for comparison with Caffey's original study (1974). Seventy-one patients identified as having a subdural haematoma caused by nonaccidental means were included in the study. The incidence of subdural haematoma with no evidence of impact trauma is not explicitly stated, although he states that shaking was admitted initially in 9 (12.7%) cases and after the conclusion of an investigation in two additional cases. No explanation was given for the injuries in 24 (33.8%) cases, with falls or head impacts being reported in the remaining cases. Skull fractures were found in 13 (18.3%) cases, and rib or long bone fractures in 23 (32.4%) cases. Scalp bruising without underlying fractures is not reported. The report concludes that "the term shaken impact syndrome should be avoided, and that it should be acknowledged that shaken infant syndrome is a syndrome of severe head injury to infants caused by either shaking alone or by shaking plus impact."

The causes of 33 subdural haematomas occurring in children under 2 years of age in south Wales and south west England during 1993 and 1995 were researched by Jayawant *et al.* (1998). Nine infants died, 15 had profound disability and the remaining 9 were reported as normal after 1 year. Sixteen of the 27 infants who had a skeletal survey were found to have fractures, 5 of which were of the skull, the remaining were of the rib (9), tibia or fibula (4), femur (2), clavicle (1) and radius (1). Ten infants were reported to have bruising, but the location of the bruising is not given. In 14 cases a clear history of shaking was obtained, although it was never the first explanation put forward. In these cases it was not uncommon for carers to propose up to three different explanations for the injuries, or to deny any trauma and attribute the symptoms to an illness. Unfortunately this study is mainly concerned with signs suggestive of abuse in general and suggests complete and mandatory clinical investigations in cases of infantile subdural haematoma in order to increase the accuracy of the diagnosis of abuse. Therefore there is no clear distinction between infants that were purely shaken and those which may have suffered shaking and impacts, although it does conclude that "[the] study confirms that a shaking injury was inflicted in many cases of subdural haemorrhage, but that subdural haemorrhages can

also arise from severe trauma such as a road traffic accident."

Tzioumi and Oates (1998) found a very high incidence (76%) of shaking only cases in their 10-year retrospective study of subdural haematomas in children under 2 years. They found subdural haematomas in 38 children, 21 of which were ascribed to nonaccidental causes, with a mean age of 5.3 months. Shaking—diagnosed when there were no associated injuries to the head or where there was an admission by the care giver—attributed for 16 (76%) of these 21 cases. Surprisingly 38% of the "shaken" patients were found to have only unilateral subdural haemorrhages , whereas shaking is usually thought to produce bilateral haemorrhages as reported by Caffey (1974) and Gennarelli and Thibault (1982). However, they refute that child abuse was over-diagnosed in children with unilateral subdurals since in one of these cases the mother admitted shaking the infant.

In a report on four pairs of twins, five of which suffered from shaken baby syndrome, Becker *et al.* (1998) reported that shaking was admitted to in three of the cases. Also, confirming one of Guthkelch's (1971) observations, "Two parents believed that the shaking was a less violent approach than striking."

Research relating intracranial pressure to outcome in non-accidental head injury by Barlow and Minns (1999) focused on 17 subjects with an average age of 5.1 months. Seven (41%) of these subjects had subdural haematomas, retinal haemorrhages, rib fractures but no evidence of impact and so were thought to be victims of pure whiplash-shaking. Evidence of impact was defined as bruising to the head, subgaleal haematoma (found either clinically or with imaging) or where there was a skull fracture.

Research by DiScala *et al.* (2000) examined the cases of 1997 abused and 16,831 unintentionally injured children under the age of 5, extracted from a database covering the 10 years between 1988 and 1997. The sex, age, history, nature and severity of injury, diagnostic procedures used and outcomes were compared between both groups. The median age for child abuse was 8 months, compared with 28 months for accidental injury, also 53.0% of abused infants had a previous medical history compared with 14.1% of accident victims. Battering was reported in 53% of the abuse cases and shaking in 10.3%. Children

in the abuse group were significantly more likely to sustain injury to the thorax (12.5% vs 4.5%) and abdomen (11.4% vs 6.8%). Both groups sustained similar numbers of injuries to the head (62% for abused, 59.9% for accidental), and of those subgroups the abused children suffered more intracranial injury (42.2% vs 14.1%) but less skull fracture without intracranial injury (13.7% vs 19.2%) and less concussion or other unspecified closed head injury (6.2% vs 26.6%). Unfortunately those are the only head injuries distinguished in this report—there is no data for scalp bruising which again makes it difficult to isolate pure shaking cases from cases with shaking and soft impact.

A review of all intracranial haemorrhages seen by a child protection team during 1997 was performed by Morris *et al.* (2000), extracted from more than 400 cases of alleged physical abuse. A total of 32 cases of intracranial haemorrhage (subarachnoid, epidural and subdural) were found, 19 of which were possible child abuse. Eight of these 19 cases were excluded form further study because they had inflicted bruises and/or fractures of abuse and/or retinal haemorrhages, leaving 9 infants with pure subdural haematoma who lacked external bruises, fractures and retinal haemorrhages. This gives an incidence of 47% of subdural haematomas with no evidence of head impact, a figure which excludes cases which may have had retinal haemorrhages and bruising of the thorax, both of which are common in the classical shaken baby syndrome.

A report by Maxeiner (2001) mentions 10 cases of subdural haematoma in which 4 had no external or internal injuries on the face or head. In one of these cases a detailed confession of violent shaking was made which was consistent with the findings.

A recent study by Geddes *et al.* (2001*a*, 2001*b*) confirms the presence of acute subdural haematoma in infants who have been shaken, but suggests that a different mechanism may be responsible for the majority of nonaccidental head injury cases. Their neuropathological study of 53 cases of non-accidental head injury in infants (37, age < 1 year) and children (16, age ≥ 1 year) revealed only 8 cases, all infants, where no bruising or fracture was found at autopsy. These cases were assumed to have been shaken, and in one of these cases the carer confessed to having shaken the infant. Eighty-one percent (43 out of 53) of

the total cases (31 of the infants) were found to have subdural haemorrhages, including 7 of the 8 shaken infants. However, 34 of the subdurals are described as "trivial in terms of quantity of blood", with the 4 large haematomas all occurring in older subjects. Instead, the most common cause of death (82%) was raised intracranial pressure resulting from brain swelling. Diffuse axonal injury could not account for this, since it was only present in 3 of the cases, whereas severe hypoxic brain damage was present in 77% of the cases. Localised axonal damage focussed near the craniocervical juncture or cervical cord was found in 11 of the 37 infants. This lead the authors to suggest that hyperextension of the neck during shaking or battering may damage the axons in or near the craniocervical juncture, possibly causing loss of respiratory control leading to hypoxia-ischaemia, raised intracranial pressure and death. This research has yet to be critically reviewed by the medical community, and it is likely that the reported insignificance of subdural haematoma will cause controversy, since it seems to contradict the findings of the past 30 years of the shaken baby syndrome debate.

2.2.2 In Support of Shaken *Impact* Syndrome

The main proponent of *'Shaken Impact Syndrome'* is a team in Philadelphia (Duhaime *et al.*, 1987) whose study concluded that it was unlikely that shaking alone could generate enough force to cause acute subdural haematoma. Their initial hypothesis was based on the review of 48 patients identified with suspected shaken baby syndrome, the patients ranging in age from 1 month to 2 years. Only 25% of these cases had intra-cranial damage without any evidence of impact trauma, and all of the 13 fatal cases had some evidence of blunt head trauma (although in 7 of these cases the impact findings were only noted at autopsy and had not been apparent prior to death).

They tested their hypothesis by fixing accelerometers inside the head of lifelike dolls of 1-month-old infants and subjecting these dolls to repetitive violent shaking followed by an impact against either a metal bar or a padded surface. The mean peak tangential acceleration of the shaking and impacts was 9.29 G and 428.18 G respectively, with mean

time intervals of 106.6 ms and 20.9 ms respectively. When these values were compared with known tolerance criteria for brain injury in primates (scaled to the brain mass of an infant), the angular acceleration and velocity associated with shaking were below the injury range, while the values for impacts spanned concussion, subdural haematoma and diffuse axonal injury (DAI) ranges. This led to the conclusion that "shaken baby syndrome, at least in its most severe acute form, is not usually caused by shaking alone."

The primate experiments (Thibault and Gennarelli, 1985) involved exciting monkeys heads with known accelerations and velocities, thus inducing varying degrees of cerebral damage ranging from concussion through to ASDH and DAI. This produced tolerance criteria in the form of minimum accelerations and velocities required to cause different levels of damage in the primate. The frequencies used the in the primate experiments are not known, however, the same Philadelphian team consistently used frequencies between 50 and 100 Hz in their experiments (Ommaya and Gennarelli, 1974, Gennarelli *et al.*, 1982, Margulies *et al.*, 1985, among others) and if such high frequencies were used to develop these tolerance levels then they may not be directly applicable to manual shaking which was found to produce frequencies around 4 Hz (Duhaime *et al.*, 1987). The scaling function then used to scale these tolerances to the brain mass of an infant is reviewed in more detail later.

Evidence of impact was found in all 10 cases reported by Elner *et al.* (1990). This paper primarily reports the incidence of ocular injuries (which were present in 7 out of 10 sequential cases of suspected child abuse) but also highlights the difficulty of spotting evidence of direct head impact which, although present in all 10 cases, were sometimes subtle or hidden beneath the hair. In 2 of the 7 detailed cases with ocular injuries, evidence of blunt head trauma was only apparent at autopsy, during which one of these cases was found to have a skull fracture.

A retrospective study by Howard *et al.* (1993) considered 28 cases of infantile subdural haematoma over 20 years and also found little or no evidence to suggest that shaking alone is enough to cause subdural haematoma. This evidence is presented in a variety of formats:

- Ten of the cases resulted in legal action, 5 of which had history of assault or evidence of impact injury, with carers of the 5 remaining cases claiming that their infant had fallen but had no unbiased witnesses to verify their history. On physical examination of the 5 claimed fall cases, all were found to have retinal haemorrhages with minimal scalp injury in 1 case and and no evidence of scalp injury in 4 cases. However, the data seems to show that CT scans showed skull fracture in 2 of these final 4 cases. In other words, only 2 of the 28 subdural haematomas could possibly be caused by shaking alone, because they could not be satisfactorily explained by witnessed injury or evidence of head impact.

- Three of the 28 cases were reported to have been shaken, however in all three cases the history and clinical findings revealed that the infants has also sustained a direct impact injury.

- In total, 14 of the 28 subdural haematoma cases showed no external signs of head injury, a figure in line with that of Guthkelch (1971) and Alexander *et al.* (1990) among others. However, 13 of these 14 infants with normal scalp examination either sustained a fall observed by multiple unbiased witnesses (6), had an underlying skull fracture (2) or scalp contusion on post-mortem examination (1) or were likely to have been caused by an impact injury sustained more than 1 week prior to evaluation (4).

In her general review of child abuse, Norton (1983) appears to be of the belief that shaking cannot produce the forces required to cause serious injury. She argues, "Since children have fallen prodigious distances without sustaining serious brain injury, it is difficult to formulate a reasonable mechanism, considering both neuroanatomy and the forces involved, for this to occur as the result of merely shaking the child, no matter now violently." Surprisingly this came after Holbourn (1943) demonstrated the importance of rotation in head injury (see Section 2.2.4) due to the shear modulus of brain material being substantially lower than its bulk modulus. Since shaking a baby causes rotation and thus

high shear strains in the brain, it is quite conceivable that shaking is more likely to cause serious brain injury compared to falls which mainly cause translation and compressive strains. However, she does demonstrate the difficulty of spotting head bruising without autopsy by comparing a photograph of an apparently normal shaved scalp to a photograph of the massive, multiple areas of subgaleal haemorrhages underneath.

2.2.3 Brain Mass Scaling Function

The scaling relationship employed to scale tolerance criteria for primates to human infants was presented by Ommaya *et al.* (1967) after it was proposed in a private communication from Holbourn in 1956. Formally, it may be written as:

$$\ddot{\theta}_p = \ddot{\theta}_m \left(\frac{M_m}{M_p} \right)^{2/3} \tag{2.1}$$

where M_m and M_p are the masses of the so-called model and prototype, and $\ddot{\theta}_p$ and $\ddot{\theta}_m$ are their critical angular accelerations. This relationship is based on the following assumptions:

1. The brain, although incompressible much like water, acts as an elastic medium.
2. The brain tissue is homogeneous and isotropic.
3. Density of the brain tissue in the model and prototype are equal ($\rho_m = \rho_p$).
4. Model and prototype brains are geometrically similar, through one scale factor.
5. Injury is the result of shear strains exceeding a certain value.
6. The skull is very stiff, such that deformations of the skull do not contribute significantly to the strains in the enclosed brain.
7. Model and prototype brains have the same stiffness.

Experimental work also described in this report indicates a >99% probability of concussion in the rhesus monkey (brain mass 70–100 gram) at accelerations of 40,000 rad/s^2,

Authors	Year	Non-accidental head injury cases	Shaking only cases		Median age (months)
			n	%	
Guthkelch	1971	15	7	46.7	
Smith and Hanson	1974	47	7	15	
McClelland *et al.*	1980	21	5	23.8	5.5
Duhaime *et al.*	1987	48	24	25	7.85
Hadley *et al.*	1989	36	13	36	3
Alexander *et al.*	1990	24	12	50	
Elner *et al.*	1990	10	0	0	
Howard *et al.*	1993	28	2	7	
Brown and Minns	1993	30	17	57	5
Gilliland and Folberg	1996	80	9	11.3	
Lazoritz *et al.*	1997	71	11	15.5	
Tzioumi and Oates	1998	21	16	76	5.3
Barlow and Minns	1999	17	7	41	5.1
Barlow *et al.*	1999	12	7	58	5.7
Gleckman *et al.*	1999	17	7	41	4.5
DiScala *et al.*	2000	1997	206	10.3	8
Morris *et al.*	2000	19	9	47	5
Geddes *et al.*	2001	37	8	21.6	
Maxeiner *et al.*	2001	10	4	40	
			Averages:	32.7	5.5

Table 2.1: Summary of shaken baby syndrome research in which clear distinction is made between shaking and impact.

which predicts a >99% probability of concussion in man (brain mass 1300 gram) of about 7500 rad/s^2.

Despite the number of assumptions and simplifications, the scaling relationship was somewhat verified by later research by the same team (Ommaya and Hirsch, 1971). This involved producing cerebral concussion in 3 primate species (squirrel monkey, rhesus monkey and chimpanzee) by both direct impact to the occipital zone of the head and whiplash injury caused by impact to the base of a mobile chair carrying the seated animal. Each test produced a point of maximum angular velocity and acceleration which either did or did not cause concussion, allowing tolerance levels at which the animals had a 50% chance of concussion. The points of concussion and non-concussion were highly inter-scattered, especially in the case of the squirrel monkey tests, but tolerance levels for 50% concussion in rhesus monkeys, squirrel monkeys and chimpanzees were estimated as 300–350, 300 and 70 rad/s respectively. The corresponding critical angular acceleration was obtained from the equation:

$$\dot{\theta} = \frac{\ddot{\theta}}{\omega} \tag{2.2}$$

where $\dot{\theta}$ is the damaging rotational velocity (rad/s)

$\ddot{\theta}$ is the damaging rotational acceleration (rad/s^2)

ω is the natural frequency of brain rotation (rad/s)

This relied on the knowledge of the natural frequency of brain rotation for each species. The Rhesus monkey brain was said to have a frequency of 5–10 Hz, and the rotational frequency of a human subject's brain was found to be 4–5 Hz. Therefore it was assumed that the squirrel monkey and chimpanzee had frequencies also in the 5–10 Hz range and so 5 Hz was assigned (seemingly arbitrarily) to the chimpanzee and 10 Hz to the squirrel monkey, resulting in 50% tolerance levels of approximately 15,000, 19,000 and 2,200 rad/s^2 for the rhesus monkey, squirrel monkey and chimpanzee respectively. These values, when plotted against the brain weights for each species (70–100, 20–27 and 350–500 gram for the

rhesus monkey, squirrel monkey and chimpanzee) seem to compare favourably with the scaling relationship given by Equation 2.1, although it should be noted that small changes in the estimation of either the 50% tolerance level for angular acceleration or the assigned values of the natural frequency of rotation has a significant detrimental impact on this fit. Nevertheless, using an adult human brain mass of 1300 gram this scaling relationship predicts an angular acceleration of 1800 rad/s^2, at which the chances of concussion are about 50%. This is compared with the value of 1636 rad/s^2 estimated by Ommaya and Yarnell (1969) at which a road traffic accident victim suffered "a level of injury reasonably close to the threshold for cerebral concussion" (this paper is reviewed in detail later).

More recent work has also successfully employed this scaling relationship (Margulies *et al.*, 1985). This involved cylinders filled with transparent gel containing an embedded orthogonal grid in the plane of interest. Cylinders of three different diameters were used, each given a range of rotational accelerations. High speed film of the grids were analysed to calculate the Lagrangian strain of the grid elements. It was found that the strain produced was proportional to the acceleration magnitude, with different gradients depending on the radius (and hence mass) of the cylinders used. However, plotting the strain versus the *scaled* acceleration magnitude for each of the cylinders produced points which all fell near a single straight line.

The scaling function described above was originally developed to scale tolerance criteria for diffuse axonal injury and cerebral concussion, both of which are injuries to the brain matter thought to be caused by differing levels of strain in the axons (Gennarelli *et al.*, 1982). Subdural haematoma on the other hand is caused by relative motion between the brain surface and the skull which ruptures the parasagittal bridging veins. Therefore while the scaling function may be appropriate for diffuse axonal injury and concussion, it may not be as easily applicable to tolerance criteria for subdural haematoma. The difference between these mechanisms of injury is emphasised by the fact that in the experiments by Gennarelli *et al.* (1982) designed to produce cerebral concussion, coma and diffuse axonal injury in primates by subjecting their heads to a single, high acceleration

(1–2×10^5 rad/s^2) pulse in either the sagittal, oblique or lateral direction, "not one of the animals had a skull fracture, a subdural or intracerebral haematoma..."

When employed to scale tolerance criteria for subdural haematoma in primates, the scaling function has consistently overestimated the conditions required. Research by Meaney and Thibault (1990) amalgamates results from primate experiments, physical model studies and failure criteria for parasagittal bridging veins. The primate experiments involved giving a range of short duration, sagittal plane acceleration to the anesthetised animals producing acute subdural haematoma in some but not all. Points of peak angular acceleration ($\ddot{\theta}_p$) and peak change in angular velocity ($\Delta\dot{\theta}_p$, see below) from each experiment were plotted after being scaled to a human brain mass of 1200 gram. The peak change in angular velocity is a lumped parameter capable of capturing the waveform and magnitude of the applied load and can be defined as (Margulies and Thibault, 1989):

$$\Delta\dot{\theta}_p = \left| \int_{t_2}^{t_1} \ddot{\theta}(t)dt \right| \tag{2.3}$$

where t_1 and t_2 are selected such that $\Delta\dot{\theta}_p$ is maximum.

Physical models were then made from transparent gel cast into a human adult skull cut laterally near the midsagittal plane, with an orthogonal grid embedded into the gel. This model was then given similar accelerations as the primates (using the same equipment), scaled to the gel mass. Hypothetical bridging veins were defined between fixed points on the inner surface of the skull and defined points within the grid. Analysis of the grid point motion during the experiments allowed the estimation of the strain experienced by these veins during the motion. Bridging vein strain was found to be maximal in the frontal region, compared to the parietal and occipital regions. Two studies had previously attempted to determine the ultimate strain of human parasagittal bridging veins (see Section 2.3.1), and these were compared with the strains observed in the physical models. The result of this comparison was that the strains observed in the gel were significantly higher those found by the vein experiments, suggesting that acute subdural haematoma could be caused by conditions far below those derived from the scaled primate

tolerance. It cannot be known if this poor comparison is due to the scaling function itself, or oversimplification of the physical models used in this study.

Furthermore, in his PhD thesis Meaney (1991, pp 98–103) compared his tolerance levels for subdural haematoma with parameter combinations measured by Löwenhielm (1974*b*) in head-on collision tests using cadavers. Bridging vein disruption occurred in 3 of the 9 cadavers tested, yet all conditions used fell well below Meaney's tolerances. Meaney explains that "Since the cadaver heads were not perfused [to] physiological pressure levels before testing, it is possible that the cortical brain surface retracted from the inner skull surface and created a preload on the parasagittal bridging veins. In turn this preload on the veins lowered the inertial loading needed to cause cortical vascular disruption in the cadaver."

2.2.4 Importance of Rotation

Until Holbourn (1943) demonstrated the importance of rotation in head injury, it was assumed that most internal head injuries were caused by impacts and translational accelerations of the head. Holbourn explained that linear acceleration forces tend to produce compressional or rarefactional strains which, because the brain has a much higher bulk modulus compared to its shear modulus, are much less likely to cause injury than rotational accelerations. This was demonstrated by filling a narrow-necked flask with water and adding shredded cotton-wool in order highlight any movement of the water. This approximately represents the cranial contents if one assumes that nerve tissue, blood and cerebrospinal fluid all have approximately the same density as water. When this flask is accelerated purely linearly there is no discernable movement of the water, however when the flask is suddenly rotated the water tends to stay behind and only the flask rotates.

Holbourn went on to investigate the distribution of shear stress in a rotated head by casting a mid-parasagittal cross-section of a skull with 5% gelatin and visualising the shear strains in the section by means of a circular polariscope. When given a sudden forwards rotation this model exhibited regions of high shear strain in two locations, 1) at

the tip of the temporal lobe where the locally convex skull gets a good grip on the brain; and 2) near the vertex which is far removed from any place where the skull can get a grip on the brain to turn it around, hence the brain tends to get left behind in this region and it therefore rubs against the skull more than in other places. Interestingly, this region of high shear strain near the vertex is precisely the location of the delicate parasagittal bridging veins which tear causing subdural haematoma in shaken baby/shaken impact syndrome.

Most of the research since then has acknowledged the importance of separating injuries caused by translation and rotation, and commented upon the relevance of rotation to their results.

Primate experiments (Ommaya and Gennarelli, 1974) specifically designed to test the ability of pure translation and rotation to cause concussion further demonstrated the susceptibility of heads to damage caused by rotation. In these experiments pure rotation was applied to the heads of 12 squirrel monkeys, and pure translation applied to a further 12 monkeys. Peak positive accelerations ranged between 665 G and 1230 G over an angle of 45° or a displacement of 1 inch. All the animals in the rotated group exhibited evidence of cerebral concussion or traumatic unconsciousness, while none of the translated group showed this effect. Also, the rotated groups all suffered subdural and subarachnoid haematoma, compared to only 5 *focal* subdural and 1 focal subarachnoid haematoma in the translated group. This study also compared the integrity of interhemispheric cortical function by monitoring the speed of recorded signals of sensory inputs travelling via the extra-lamensical pathways. The translated group, which showed no signs of concussion, exhibited very little change in cortical function, whereas the cortical function of the rotated group slowed by up to 600% (after return to consciousness) which only reduced to 300% after 80 minutes. It must be noted again, however, that these physical monkey experiments were performed at frequencies of up to 112 Hz (assuming simple harmonic loading), which is very far removed from the 4 Hz achieved in the manual doll-shaking experiments of Duhaime *et al.* (1987).

An earlier report by Ommaya and Yarnell (1969) reported a case of subdural haematoma caused by a road traffic accident where the head probably rotated at a rate equivalent to a frequency of about 3 Hz. In that particular case, the patient was sitting in a stationary vehicle when he was struck from behind by a 10,000 lb truck travelling at about 30 mph. His lap belt limited the initial forwards motion of his body, and he could recall the sudden rotation of his head backwards to the left, without striking any part of the car. He never lost consciousness, but was unsteady on his feet for a short time after. Severe symptoms did not manifest until 3 weeks later and eventually a 2 cm thick middle and high parietal subdural haematoma was discovered. This was evacuated and he returned to work 5 months after the operation. From the details of the incident and experimental work on automobile collisions (Clark and Blechschmidt, 1965) they calculated the peak rotational acceleration of the head to be 1636 rad/s^2 with a time to reach peak velocity of 0.16 s and time to reach peak acceleration of 0.08 s. If this acceleration pulse is assumed to be the first quadrant of a sinusoid then this gives a frequency of 3.125 Hz, a frequency easily achieved in the doll-shaking experiments of Duhaime *et al.* (1987).

Research by May *et al.* (1979) clearly demonstrates the ability of the woodpecker brain to withstand translational accelerations. It was observed that woodpeckers can withstand prolonged repetitive decelerations of the order of 1000 G without suffering any concussion, yet can be knocked unconscious by inadvertently flying head first into a window. Analysis of high speed footage of woodpecker drilling showed that the the strike trajectory of the tip of the beak was straight, and that the trajectories of the vertex and the centre of the head were also essentially translational. The authors remark that "natural selection has favoured the survival of woodpeckers that operate in such a way that the rotational component of their pounding activity is minimised." It may be inferred from the sentence "A rattle of typewriter keys would usually suffice to elicit the pounding" that the drilling behaviour observed in the study was only that used for communication. It may well be possible that when drilling for insects or to tunnel out nesting holes the woodpeckers use even more force and experience much higher decelerations.

2.3 Material Properties

2.3.1 Bridging Veins

The space between the skull and the brain contains cerebrospinal fluid (CSF) and a number of dural layers. Firstly the dura mater is the strong membrane firmly attached to the inside surface of the skull. Below the dura mater is the arachnoid, a delicate membrane resembling a spider's web. The arachnoid is normally closely apposed to the dura, and hence the subdural space between is only a potential space. The bulk of the cerebrospinal fluid lies between the arachnoid and the pia mater—the subarachnoid space. The pia mater is adherent to the cerebral cortex.

Bridging veins pass directly from the surface of the brain to the dura mater, almost at right angles to both, traversing the relatively large subarachnoid space (up to 1 cm in infants), through the arachnoid, across the potential subdural space and finally through dura mater into the venous sinuses. With the majority of the vein occupying the subarachnoid space, one would expect relative motion between the brain and skull to tear the bridging veins in the subarachnoid space causing a subarachnoid haematoma, whereas subdural haematomas are much more commonly found in head injury, especially shaken baby syndrome. The paper "Why do bridging veins rupture into the virtual subdural space?" by Yamashima and Friede (1984) addressed this question by comparing the subdural and subarachnoid portions of the veins microscopically. Seven specimens were obtained from 4 patients, aged 53, 77, 77 and 85 years. Their findings are summarised as follows:

- The thickness of the bridging veins varied remarkably in the subdural portion, ranging from as little as 10 μm to 600 μm. The subarachnoid portion had a fairly constant thickness of 50 μm to 200 μm.
- The walls of the veins had a compact distribution of collagen in the subarachnoid portion, whereas in the subdural portion the collagen fibres were only loosely woven.
- The subdural portion of the bridging veins lacked the tight reinforcement of the

arachnoid trabecular cells, and there were only scattered attenuated dural border cells.

- The arrangements of collagen fibres varies from one portion to the other, but there was always a tendency for circumferential fibres to prevail compared with the longitudinal ones, particularly in the subdural part. This would render the vein's wall more resistant to distension while reducing its resistance to traction.

These differences lead the authors to conclude that "the bridging veins are more fragile in the subdural portion that in the subarachnoid portion... The antero-posterior acceleration or deceleration of the head can easily cause traction of the bridging veins, and they will rupture at their weakest point, that is, in the subdural space."

Löwenhielm (1974*a*)

The first mechanical tests of human parasagittal bridging veins were performed by Löwenhielm (1974*a*). He successfully tested 22 samples taken from 11 persons (7 male, 4 female) aged between 13 and 87 years and who had no previous brain injury. The samples were preserved for up to 6 hours in 0.9% saline at room temperature until the tests were conducted, which was always within 48 hours after death. The veins were held at each end by clips, with one end connected to a rigidly held force transducer and the other end attached to a massive steel cylinder which was free to move axially, with the axis of the cylinder parallel to the axis of the vein. This cylinder was impacted by a second cylinder which was mounted in a tube and accelerated to a steady velocity by compressed air. As the impacted cylinder moved, it broke two circuits which were placed a known distance apart, and these produced two pulses on an oscilloscope, hence allowing the average speed to be calculated. It was shown that the loss of velocity during one trial was less than 4% and the speed was therefore considered constant. In the 22 successful tests the rupture of the bridging veins occurred at random positions, but in about one-quarter of the conducted trials the bridging veins were torn at their insertion at the clip. These trials were considered void and their results discarded.

The vein samples were tested at strain rates between 2 s^{-1} (i.e. the vein would be stretched by twice its original length every second) and 1000 s^{-1} which resulted in ultimate percentage elongations between approximately 83% and 14% respectively, with a negative logarithmic relationship in between (see Figure 2.1). This suggests that the bridging vein properties exhibit a strong strain rate dependence. Converting the percentage elongation into ultimate stretch ratio (the ratio of failure length to initial length) gives ratios between 1.14 and 1.83 and the approximate relationship:

$$\lambda_{ult} = 1.767 - 0.888 \ln \dot{\varepsilon} \tag{2.4}$$

where λ_{ult} is the ultimate stretch ratio at strain rate $\dot{\varepsilon}$ (s^{-1}).

Löwenhielm also calculated the cross-sectional area at one end of each vein and thus discovered that the veins had ultimate stresses from 0.2 MPa when stretched slowly, up to 1.9 MPa when stretched quickly, which implies that for short loading times the veins can withstand higher stresses.

Löwenhielm (1974*b*) also determined the strain tolerances of human bridging veins *in situ* during head-on collision tests with cadavers. Twenty-three cadavers were strapped into a conventional car seat mounted on a test sled along with dashboards and windscreens of various designs. The cadavers were unembalmed and had been kept at a temperature of 14°C so that rigor mortis was not present when the tests were conducted. Marks on the cadavers' heads were filmed by a high-speed stationary camera, and only nine of these films were further analysed to obtain the angular acceleration and velocity of the heads. At autopsy, disruption of several bridging veins along with laceration of the soft cerebral membranes and minor subarachnoid haemorrhage was found in 3 cadavers, a minor subarachnoid haemorrhage was found in 1 cadaver, laceration of the soft cerebral membranes and a subdural haemorrhage were found in another cadaver, and the remaining 4 had no findings. Plotting points of peak angular acceleration ($\ddot{\theta}_p$) versus peak change in angular velocity ($\Delta\dot{\theta}_p$) used in these experiments yielded the conditions of $\ddot{\theta}_p < 4500$ rad/s^2 and $\Delta\dot{\theta}_p < 50$ rad/s, which must both be exceeded to cause bridging vein disruption.

Lee and Haut (1989)

Lee and Haut (1989) also performed mechanical tests to investigate the strain rate dependence of human bridging vein properties, and their results challenge those of Löwenhielm (1974*a*). They tested a total of 139 parasagittal bridging veins from eight unembalmed human cadavers aged between 62 and 85 years old, none of which had noticeable head traumas or cerebrovascular diseases. To extract the veins, the heads were first frozen and a 5 cm thick midsagittal slab was cut, then the slab was thawed at room temperature and the veins carefully removed with their cerebral and dural ends intact. The samples were then bathed in saline at 4°C overnight and tested the next day. They were tested in a servo-controlled hydraulic testing machine at low strain rates of 0.1–2.5 s^{-1} or high strain rates of 100–250 s^{-1} while bathed in saline at 37°C.

The load versus stretch of a bridging vein stretched at 200 s^{-1} is shown in Figure 2.2. The authors report that "no gross damage of the vessel was observed up to the ultimate stretch [1.5], thereafter necking of the specimen appeared." From the plot of ultimate stretch ratio versus strain rate, the ultimate stretch appears to vary between 1.15 and 1.88 at strain rates of 0.2 s^{-1}, between 1.24 and 2.00 at strain rates of 2 s^{-1} and between 1.32 and 2.00 at strain rates of 200 s^{-1}. In the text the ultimate stretch is quoted as 1.51 ± 0.24 at low strain rates and 1.55 ± 0.15 at high strain rates. Ultimate stress was found to be anywhere between 1.0 and 6.5 MPa at all strain rates. This lead to the conclusion that strain rate had no significant effect on the measured failure properties. Lee and Haut criticise Löwenhielm's findings, stating that "strain was measured indirectly and the measurements might be subject to errors due to possible specimen slippage at the clamps... Furthermore, there were only six tests with strain rates less than 70 s^{-1}."

Meaney (1991)

In his PhD thesis, Meaney (1991, Ch. 4) also performed dynamic tests of human bridging veins, mainly due to the disagreement between Löwenhielm (1974*a*) and Lee and Haut (1989), and also because neither of the previous studies investigated the effects of age or

perfusion pressure of the veins. Meaney's testing system consisted of a solenoid connected to the specimen though a linkage which produced strain rates up to 250 s^{-1}. The samples were mounted on stainless steel tubing, which allowed them to be perfused with saline during testing. Parasagittal bridging veins were obtained from unembalmed cadavers which showed no sign of head injury and within 24 hours post mortem. They were then stored in saline at 5°C prior to testing, at most 48 hours post mortem. To examine the effect of strain rate, 59 veins were tested from cadavers ranging in age from 9 to 62 years. Equation 2.5 is the linear regression equation fitted to the results, and indicates a lack of dependency of the ultimate stretch ratio upon strain rate. Further tests showed that bridging vein properties were also insensitive to changes in perfusion pressure and age (minimum age of 3 years).

$$\lambda_{ult} = 1.5127 + 0.000548\dot{\varepsilon} \tag{2.5}$$

The discrepancies between the three mechanical studies above could be due to a number of factors.

1. Lee and Haut suggest that Löwenhielm's tests may have been subject to specimen slippage at the clamps. Löwenhielm does not mention the possibility of slippage, nor does he describe any checks that were in place to ensure the exclusion of results where there was slippage. To minimise slipping, Lee and Haut air-dried the ends of the veins (which strengthened them), wrapped them in sandpaper and gripped them with flat-plate clamps. Furthermore, the tests were filmed at high speed, and the films were carefully checked for evidence of the veins slipping at the clamps, in which case the results from those tests were excluded from further analysis. Meaney's veins were mounted on stainless steel tubes which had circumferential grooves machined near the tip, and medical suture was used to tie the ends of the veins over these grooves. Some of the specimens were photographed before and after testing, and the photographs compared and showed no evidence of slippage at both low and

high strain rates—the majority of samples were merely visually inspected before and after testing.

2. Sample procurement and storage methods varied with each study. Löwenhielm preserved his samples in 0.9% saline at room temperature for up to 6 hours before testing which was always within 48 hours post-mortem. Lee and Haut froze their cadavers' heads at -20°C in order to cut out a midsagittal slab, which were then thawed at room temperature, the veins removed and stored in 4% saline overnight. Meaney stored his samples in 5% saline and tested within 48 hours.

3. Perhaps the most striking difference between the three studies is the method of actuation. Löwenhielm used an impact between a moving and a stationary cylinder connected to one end of the vein, and he found the properties to be strain rate dependent. Meaney's solenoid was directly connected to one end of his samples, and Lee and Haut's servo controlled hydraulic testing machine was probably directly connected to the vein, and both of these studies reported the properties to be strain rate independent. None of the papers present a graph of displacement or speed versus time which would verify that constant strain rates were achieved in each test, although Löwenhielm does specify that "loss of velocity during one trial was less than 4%." When investigating the effect of strain rate it is imperative that the strain rate be constant during each test, and that the steady strain rate is achieved within a negligible strain of each sample. It is possible that the direct drive mechanisms used by the later research was unable to accelerate to the desired speed of up to 2 m/s within a negligible time so that the straining of the vein took place at constant speed, whereas the impact employed by Löwenhielm was more likely to achieve his speeds (perhaps over 5 m/s) almost instantly. An earlier report by Lee (1983) is cited by Lee and Haut (1989) as giving a more detailed description of their equipment. This report does present a graph of load versus strain, with points marked corresponding to the states of four photographs taken at given times

of 0, 24, 36 and 48 ms. At these times the strains are approximately 0, 5.3%, 15.7% and 17.6% respectively, a highly non-linear strain versus time relationship.

One must also question the high degree of scatter in the results of Lee and Haut. The majority of their 63 points of ultimate stretch ratio appear to be spread evenly between 1.2 and 1.9, a range of 0.7 (with two further points at 2.0 and three just below 1.2). Meaney's results are slightly better, with a range of approximately 0.5 for a given strain rate (taking the slight positive gradient of Equation 2.5 into account and ignoring three points of unusually high ultimate stretch ratio). In contrast, Löwenhielm's results appear to be more precise with a range of 0.3 for a given strain rate (i.e. from Equation 2.4, all of his results are encompassed by $\lambda_{ult} = 1.767 \pm 0.15 - 0.888 \ln \dot{\varepsilon}$). This suggests a higher degree of 'repeatability' of Löwenhielm's experiments compared to the later experiments, although the later experiments each used around twice as many points in their analysis. These findings are summarised in Table 2.2.

Author(s)	Year	Samples	Age range	Result	Range
Löwenhielm	1974*a*	22	13–87	$\lambda_{ult} = 1.767 - 0.888 \ln \dot{\varepsilon}$	± 0.15
Lee and Haut	1989	139	62–85	$\lambda_{ult} = 1.5127 + 0.000548\dot{\varepsilon}$	± 0.35
Meaney	1991	59	9–62	$\lambda_{ult} = 1.55$	± 0.25

Table 2.2: Summary of mechanical tests of human bridging veins.

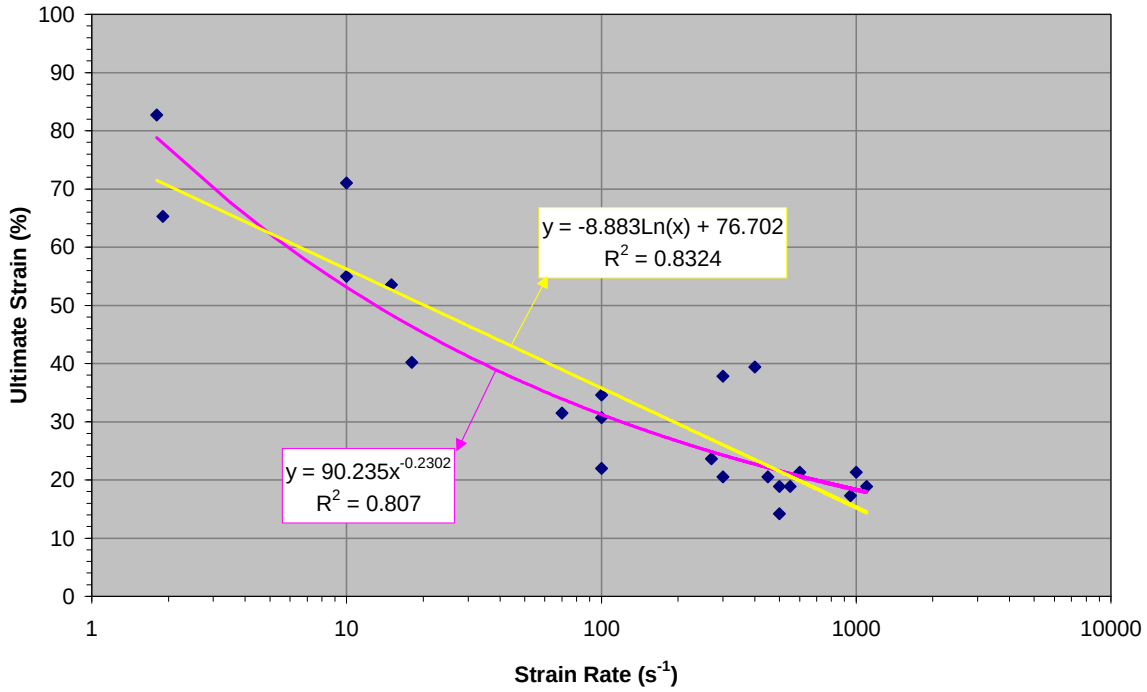

Figure 2.1: Effect of strain rate on the ultimate strain of human bridging veins. From Löwenhielm(1974*a*)

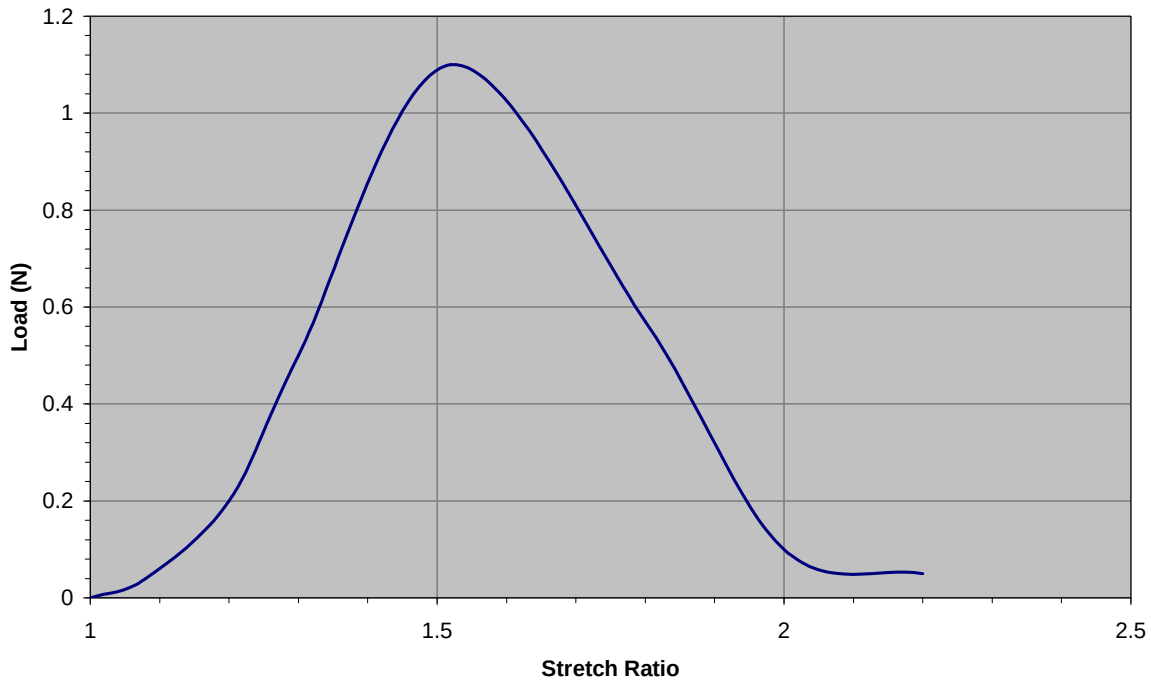

Figure 2.2: A representative load-stretch curve for a human bridging vein stretched at 200 s^{-1}. From Lee and Haut (1989)

2.3.2 Brain

Table 2.3 summarises the mechanical testing of brain tissue, most of which was performed on human brains, but also includes some pig and cow brains. Brain tissue is generally assumed to have a similar bulk modulus to water, as found by McElhaney *et al.* (1973), and since Holbourn (1943) stated that brain tissue is much weaker in shear than it is in compression, most of the mechanical testing of brain tissue has concentrated on its shear modulus.

Most of the results are quoted as the coefficients of the material's complex shear modulus, where $G^* = G' + iG''$. The storage or dynamic elastic modulus (G') is a measure of the spring stiffness of the material, and the dynamic loss modulus (G'') is a measure of the damping ability of the material and represents viscous losses (Fallenstein *et al.*, 1969), hence the coefficients characterise the viscoelastic behaviour of the material. The coefficients are usually determined by applying a dynamic shear stress to the material and monitoring the input force, output strain level and the phase angle between them, in which case the complex shear modulus and its coefficients are all functions of frequency. Instead of using the complex shear modulus, Miller and Chinzei (1997) fit their results to the non-linear viscoelastic Mooney-Rivlin energy function which is commonly used to characterise rubber and can be entered directly into some finite element packages.

The results appear to cover a wide range of values, probably due to the variety of test methods and loading types, however the results of only the shear experiments (Fallenstein *et al.*, 1969, Bilston *et al.*, 1997, Donnelly and Meidge, 1997) are confined to $G' = 0.6$–2.0 kPa and $G'' = 0.35$–0.60 kPa.

The complex shear modulus, unlike the Mooney-Rivlin constants, is not readily applicable to the material models used in finite element packages. The properties actually used by previous finite element models of the human head, and how those properties were derived is discussed in Section 2.4

Author(s)	Year	Loading	Result	
Koeneman	1966	Compression	$G' = 2.7$–5.0	kPa
		80–350 Hz	$G'' = 0.5$–3.2	kPa
Fallenstein *et al.*	1969	Shear	$G' = 0.6$–1.1	kPa
		9–10 Hz	$G'' = 0.35$–0.60	kPa
Galford and McElhaney	1970	Free axial	$E' = 66.7$	kPa
		vibration, 34 Hz	$E'' = 26.2$	kPa
Shuck *et al.*	1970	Torsional Shear	$G' = 0.8$–137	kPa
		2–400Hz	$G'' = 0.3$–83	kPa
Shuck *et al.*	1972	Torsional Shear	$G' = 7.6$–33.9	kPa
		5–350Hz	$G'' = 2.76$–81.4	kPa
McElhaney *et al.*	1973	Compression	$K = 2$	MPa
Miller and Chinzei	1997	Compression		
(using pig brains)		Slow speed	$C_{10\infty} = C_{01\infty} = 81$	Pa
		(0.64 s^{-1})	$C_{20\infty} = C_{02\infty} = 0$	Pa
		Medium speed	$C_{101} = C_{011} = 26$	Pa
		(6.4 ms^{-1})	$C_{201} = C_{021} = 395$	Pa
		Fast speed	$C_{102} = C_{012} = 163$	Pa
		(6.4 μs^{-1})	$C_{202} = C_{022} = 84$	Pa
Bilston *et al.*	1997	Shear	$G' = 1.5$–2.0	kPa
(using cow brains)		1–20 Hz	$G'' = 0.39$–0.51	kPa
Donnelly and Medige	1997	Shear (0–180 s^{-1})	$G' = 1.8$	kPa
Thibault and Margulies	1998	Shear at 20 Hz	$G' = 0.771$	kPa
(using pig brains)			$G'' = 0.222$	kPa
		at 200 Hz	$G' = 1.257$	kPa
			$G'' = 1.042$	kPa
Brands	1999	Torsional Shear	$G' = 0.492$	kPa
(using pig brains)		at 0.1 Hz	$G'' = 0.086$	kPa
		at 10 Hz	$G' = 0.624$	kPa
			$G'' = 0.227$	kPa

Table 2.3: Summary of brain material property testing.

2.4 Finite Element Models

Since the finite element modelling techniques entered the research field of head biomechanics in the early 1970's there have been many attempts to model head injury. The first decade of research is reviewed by Khalil and Viano (1982) and comprises of two- and three-dimensional models. These models consisted mainly of an elastic shell skull completely filled with brain material modelled as an invicid fluid using a bulk modulus $K = 2.19$ MPa or elastic modulus $E = 66.7$ kPa and Poisson ratio $\nu = 0.49$, and density of $\rho = 1040$ kg/m^3. The models were all used to simulate impact response.

The second decade of finite element modelling of head impact is reviewed by Sauren and Claessens (1993). These models consist of both two- and three-dimensional models, generally using a more complex geometry with a greater number of elements than the earlier models, some including dura, falx, tentorium and even CSF, albeit modelled as a soft solid.

Some of the most relevant models included in these two reviews, and some more recent models are discussed in the following pages, with a summary of various models given in Table 2.4. Most of these models employ an isotropic, linear viscoelastic shear model for the brain material with the relaxation function,

$$G(t) = G_\infty + (G_0 - G_\infty)e^{-\beta t} \tag{2.6}$$

where G_0 is the short-term shear modulus, G_∞ is the long-term shear modulus and β is the decay constant.

Lee *et al.* (1987) — 2D; Rhesus Monkey; Inertial Loading

Lee *et al.* (1987) built a 2-D midsagittal finite element model of the head of a rhesus monkey to simulate the experiments of Abel *et al.* (1978) and Gennarelli and Thibault (1982). The brain was treated as an isotropic linear elastic material, with and without structural damping, with the material properties of $G' = 80$ kPa, $G'' = 16$–32 kPa, $\nu = 0.475$ and

$\rho = 1000$ kg/m^3. No fluids, vessels or meningeal membranes were present in the model, hence a no-slip boundary condition existed between the brain and skull. The model was subjected to a triangular acceleration pulse with peak amplitude of 40 krad/s^2 and duration of 6 ms, followed by a constant forward velocity and then a triangular deceleration of 52 krad/s^2 peak amplitude and 3.5 ms duration—a waveform closely following that used in the primate experiments. The shear modulus of 80 kPa was chosen from the upper end of the values given in the review of previous models (Khalil and Viano, 1982), to compensate for the absence of the stiffer tissues.

The results showed that during most of the motion, the area of maximum shear stress was around the vertex where the parasagittal bridging veins are located. The stretch of a hypothetical bridging vein located between a grid point in the vertex and at various locations along the skull was investigated. It was found that a forward draining vein would be stretched to a ratio of 1.05 during the acceleration phase, and a backward draining vein would be similarly stretched during the deceleration phase. By separating the rotational and translational components of their loading, they also found that the rotational component was responsible for over 70% of the stretch of a forward draining bridging vein. Since the brain material was in no-slip contact with the inner skull surface, it is likely that the bridging vein stretch would have been considerably more had slip been allowed, or if a fluid layer had been included.

DiMasi *et al.* (1991) — 3D; Human Adult; Impact; Viscoelastic

DiMasi *et al.* (1991) used a three-dimensional model of a human head to model head impacts during automobile collisions. The model consisted of an elastic skull, viscoelastic brain and elastic dura and falx. The skull/brain interface condition was modelled with an unspecified friction coefficient, so no CSF layer was present. By comparing their results with laboratory data they concluded that the simulated dynamic loadings were representative for the automobile collision environment. They also demonstrate the combined and uncoupled effects of translation and rotation upon the intercerebral shear strains showing

that the rotation causes the majority of the strain, an effect which is unaccounted for in the Head Injury Criterion (HIC) which is only based on translational accelerations.

Ruan *et al.* (1993) — 3D; Human Adult; Impact; Viscoelastic

Ruan *et al.* (1993) built a three-dimensional model of an average adult head, including the scalp, a three-layered skull, CSF, dura mater, falx cerebri and brain. The brain and scalp were considered viscoelastic and the other tissues were assumed to be elastic. Brain material parameters were apparently scaled from Galford and McElhaney (1970). Other material properties were not given, but they were revealed in a later study by the same authors which used the same model for a modal analysis (Ruan *et al.*, 1996). However, this later study appears to use an elastic brain.

No neck was included in the model, and a free boundary condition was used based on the justification that the 6 ms impact was too short to be influenced by a neck restraint. The model was impacted with a moving rigid cylinder to simulate the human cadaver experiments of Nahum *et al.* (1977). For simulations lasting up to 14 ms the intracranial pressure and head acceleration histories showed good agreement with the physical experiments. After validation the model was then used to conduct a parametric analysis to study the effect of impactor directions, speeds and masses.

Chu *et al.* (1994) — 2D; Human Adult; Impact

Chu *et al.* (1994) used a parasagittal two-dimensional finite element model of an average human head to investigate theories for the mechanism of cerebral contusion under impact conditions. The model consisted of linearly elastic brain and skull, with common brain and skull interface nodes (except at the foramen magnum to produce a force-free opening there) producing a no-slip boundary between the brain and skull with no fluid gap. The head was constrained to rotate around the neck. They report high shear stress at the vertex and suggest that this may be responsible for the rupture of parasagittal bridging veins. Their results suggest that shear stress (as opposed to cavitation theory) produce

cerebral contusions, however, their shear stresses are likely to be over-estimated due to the no-slip condition between the brain and skull. Presence of the force-free opening at the foramen magnum appeared to make little difference to their results.

Kuijpers *et al.* (1995) — 2D; Human Adult; Impact; Viscoelastic

Kuijpers *et al.* (1995) investigated the importance of skull-brain interface conditions, boundary conditions at the head-neck junction and brain material properties when modelling the response of the human head to transient loading. They used a two-dimensional plane strain model of a parasagittal section of a human head. The skull-brain interface was either completely coupled or a free interface without friction, sometimes coupled just at the head-neck junction. Some models included a force-free opening at the foramen magnum. The skull was modelled as linearly elastic, and the brain was either linearly elastic or viscoelastic, with the parameters chosen as the average from those presented in the review by Sauren and Claessens (1993). In some models the head was constrained to rotate about a pivot towards the base of the neck. They simulated and compared their results with the primate experiments of Nahum *et al.* (1977). Their conclusions were as follows:

- The free skull-brain interface condition produced pressure histories more comparable with the experimental results than the coupled interface, and suggest that the presence of a CSF layer would produce even better results.
- The influence of the foramen magnum was negligible for the coupled model, as was found by Chu *et al.* (1994), but had a substantial effect on the free-interface models.
- Imposing a kinematic constraint at the head-neck junction appears to be an important modelling assumption, especially for the free interface model.
- The results obtained using different time-dependent deviatoric material parameters did not significantly change the model's response to impact. This indicates that

the response of the brain material to the impact is dominated by the short-term (elastic) phenomena.

Zhou *et al.* (1996) — 3D; Human Adult; Rotation

Zhou *et al.* (1996) refined the 3D finite element model used by Ruan *et al.* (1993). The model was of a 50th percentile male human head, consisting of scalp, skull, dura, falx, tentorium, pia, CSF, venous sinuses, ventricles cerebrum (gray and white matter), cerebellum, brain stem and bridging veins. They converted the complex shear moduli from the shear experiments of Shuck *et al.* (1972) to achieve their brain material parameters, as did Kang *et al.* (1997) albeit with slightly different results. They loaded the model with an impulsive angular acceleration in both the sagittal and lateral planes, scaled from the monkey experiments of Abel *et al.* (1978). The stress and strain in the brain and the stretch of bridging veins were compared during rotation in the sagittal and lateral planes, and the effect of modifying the material parameters was also investigated.

Their bridging vein elements experienced strains up to 38.3% during sagittal rotation (forwards–backwards) and only 8.1% during lateral rotation (side to side). Shear stress in the genu was 8.81 kPa for sagittal rotation and only 1.97 kPa for lateral rotation. Reduction of the decay constant β from 700 s^{-1} to 70 s^{-1} decreased the maximum bridging vein strain to 33% but increased the peak shear stress to 18.5 kPa. Increasing the shear modulus of the brain also decreased the strain of the bridging veins. The results of the elastic and viscoelastic analyses showed a similar trend.

Kang *et al.* (1997) — 3D; Human Adult; Impact

The 3D finite element model used by Kang *et al.* (1997) included elastic skull, scalp, CSF, facial bones, tentorium, falx and a viscoelastic brain (scaled from Shuck *et al.*, 1972). The model was validated against the experimental results of Nahum *et al.* (1977) and showed good correlation in the results for impact force, head acceleration and various intracranial pressures. The model was then used to investigate head injury in a motorcycle accident

(peak linear and angular accelerations of 1940 m/s^2 and 13153 rad/s^2), and predicted high shear stress regions in good correspondence with the sites of contusion in the right temporal lobe and subarachnoid haematoma over the occipital lobes.

Huang *et al.* (1999) — 3D; Human Adult; Impact; ASDH

Huang *et al.* (1999) built a three-dimensional finite element model of a human adult head to determine tolerance criteria for subdural haematoma. The model comprised a three-layer skull, brain, dura mater, tentorium and falx, all modelled as linear elastic materials with some parameters given in Table 2.4. The model was given a simulated impact similar to that of Nahum *et al.* (1977) and constrained to either rotate about the neck, rotate about the centre of mass or move only with pure translation.

They estimated the strain of bridging veins at the vertex by monitoring the distance between several pairs of adjacent nodes on the brain and skull surface. However, since CSF was not included in this model, it is unclear what could be between the brain and skull, except for the dura mater. If it was indeed the case that only the dura existed between the brain and skull, then considering the stiffness of the dura (200 times that of the brain) this would have imposed an unrealistically stiff connection between the brain and skull.

Nevertheless, they found that veins that drain forward into midsagittal superior sinus at an angle of 130° incurred the maximal strain of 10.4% during rotation about the neck, 14.4% during rotation about the centre of mass, and only 2.5% during pure translation. This leads to their first conclusion that rotational accelerations, as opposed to translational accelerations) seem to be the most important factor in causing acute subdural haematoma.

They went on to estimate thresholds of angular and translational accelerations by scaling their modelled accelerations with the ratio of maximum strain (10.4%) and the ultimate strain (55%) as measured by Lee and Haut (1989). This lead to thresholds of $\alpha = 71.2$ krad/s^2 and $a = 3.9\times10^3$ m s^{-2}.

Al-Bsharat *et al.* (1999) – 3D; Human Adult; Impact

Al-Bsharat *et al.* (1999) were understandably concerned that the relative motion between the brain and skull was being underestimated in previous finite element models, even in those which employed a solid of low shear modulus to represent the CSF. They modified the model of Zhou *et al.* (1996) (which included a low shear modulus CSF but is reported to only predict relative motions of up to 0.5 mm) and added a sliding interface between the CSF and the pia mater with a zero coefficient of friction. As well as verifying their models against the experiments of Nahum *et al.* (1977), they performed occipital impact experiments on an inverted disarticulated cadaver head (87 year old male) with radio-opaque, neutral-density targets implanted in the brain so that the relative motion of the brain could be measured using a high-speed x-ray system. Peak displacement between the targets and the skull was 3.5 mm, and the finite element simulation produced results of comparable trend and magnitude.

This research acknowledges its own shortcomings which are threefold. Firstly, impact speeds were limited to 4 m/s due to the frame rate of the high-speed x-ray equipment. Secondly, the cadaver head motion was mostly translational so the applicability of this CSF modelling technique has not yet been verified with rotational motions. Finally, the cadaver experiments were performed using a single specimen and so the response may be attributed to the anthropometry specific to this subject and repeated testing of the same specimen may have an effect on the results.

Author(s)	Year	2D/3D	Brain model	CSF model	Comments
DiMasi *et al.*	1991	3D	$G_0 = 34.45$ kPa $G_\infty = 17.225$ kPa $\beta = 100$ s^{-1} $K = 0.0689$ MPa		Human adult Impact loading $K_{dura} = 6890$ MPa
Ruan *et al.*	1993	3D	$G_0 = 528$ kPa $G_\infty = 168$ kPa $\beta = 35$ s^{-1} $\rho = 1040$ kg/m^3 $K = 127.9$ MPa	$E = 148.5$ kPa $\nu = 0.485$ $\rho = 1040$ kg/m^3	Human adult Impact Analysis $E_{dura} = 31.5$ MPa $\nu_{dura} = 0.45$ $\rho_{dura} = 1130$ kg/m^3
Chu *et al.*	1994	2D	$E = 250$ kPa $\nu = 0.49$ $\rho = 1000$ kg/m^3		Human adult Impact Analysis
Kuijpers *et al.*	1995	2D	$E = 1{\times}10^3$ kPa $\nu = 0.48$ $\rho = 1040$ kg/m^3 $G_0 = 338$ kPa $G_\infty = 169$ kPa $\beta = 50$–$1{\times}10^4$ s^{-1}		Human adult Impact Analysis
Zhou *et al.*	1996	3D	$G_0 = 34$–41 kPa $G_\infty = 6.3$–7.6 kPa $\beta = 700$ s^{-1} $K = 2.19$ GPa	$E = 148.5$ kPa $\nu = 0.485$ $\rho = 1040$ kg/m^3	Human adult Impulsive rotation
Kang *et al.*	1997	3D	$G_0 = 49$ kPa $G_\infty = 16.7$ kPa $\beta = 145$ s^{-1} $K = 1.125$ GPa	$E = 12$ kPa $\nu = 0.48$ $\rho = 1040$ kg/m^3	Human adult Impact Analysis $E_{dura} = 31.5$ MPa $\nu_{dura} = 0.23$ $\rho_{dura} = 1140$ kg/m^3
Huang *et al.*	1999	3D	$E = 250{\times}10^3$ kPa $\nu = 0.49$ $\rho = 1000$ kg/m^3		Human adult Impact $E_{dura} = 50$ MPa $\nu_{dura} = 0.45$ $\rho_{dura} = 1130$ kg/m^3

Table 2.4: Summary of material properties used in previous finite element models.

2.5 Conclusions

This review of the current literature has demonstrated many points. Firstly, although a large number of studies have attempted to determine the incidence of acute subdural haematoma without any evidence of head injuries, Table 2.1 shows a wide range of results. This could be due to a number of factors, especially the care with which even the smallest evidence of scalp bruising was identified. Furthermore, even in cases of acute subdural haematoma with minor scalp bruising one cannot be certain whether the bridging veins were ruptured during the shaking or the battering.

The evidence against shaken baby syndrome is practically limited to or based on the report by Duhaime *et al.* (1987) which started from a discovery of low incidence of acute subdural haematoma without any evidence of impact and then compared doll shaking experiments with previous primate experiments (using questionable scaling methods) to develop tolerance criteria for acute subdural haematoma. The conclusions of this research are debatable, nevertheless it is often quoted as *proving* that impact is necessary to cause acute subdural haematoma in children and frequently used in criminal proceedings against suspected baby 'batterers' to suggest that more violence was used than is claimed by the accused.

From the values in Table 2.1 and the other studies reviewed in Section 2.2.1, it certainly seems that there is plenty of evidence to support the hypothesis that it is possible to cause acute subdural haematoma just by shaking a baby, although the debate is still ongoing. However, the question still remains as to how much you might have to shake a baby to cause acute subdural haematoma and whether such levels of shaking might arise accidentally or must obviously be caused by violent, vigourous shaking, or perhaps only occur after a blunt impact. One point on which many of the previous modelling attempts agree is that rotation of the head causes high shear stress at the vertex (in models where the brain is connected to the skull) or moderate relative displacement between the brain and skull (in models with a specific CSF gap or a sliding interface between the brain and skull). These results suggest that if these unrealistic boundary conditions were replaced

with a properly modelled fluid between the brain and skull, significant motion of the brain within the skull would occur and hence bridging veins may undergo catastrophic strains.

This review has shown that this question has still not been properly addressed using finite element modelling techniques. Most finite element models of head injury are concerned with adult impact injuries, usually from road traffic accidents. Also all of the modelling work to date has ignored the cerebrospinal fluid layer altogether, or modelled it as a soft solid.

Therefore this review has shown that there is a shortage of knowledge on the actual biomechanics of acute subdural haematoma caused by shaken baby syndrome. Hence a finite element model specifically designed to model the complex fluid/solid interactions that occur when a baby's head is shaken would provide and much needed insight into shaken baby syndrome.

To this end the review of bridging vein and brain mechanical properties has shown that there is still much disagreement on the properties of these materials. While there have been many attempts to model brain matter using a wide range of elastic and viscoelastic material properties, it is believed that the range of properties could be used in this research and their results compared to produce general conclusions on shaken baby syndrome tolerances and the relative importance of the brain model. The uncertainty about the type and values of the bridging vein properties was probably due to the differences in the testing methods employed for each study. Hence a fresh investigation into the tensile failure properties of bridging veins, using a testing rig specifically designed to overcome the problems of the previous research would be of great benefit to this and future brain modelling attempts.

BRIDGING VEIN TESTING

3.1 Introduction

As discussed in Chapter 2, current research into the material properties of bridging veins is limited to three studies (Löwenhielm, 1974*a*; Lee and Haut, 1989; Meaney, 1991). These studies not only disagree on the ultimate tensile stress and strain of bridging veins, but also on whether or not the properties are dependent on the rate of strain. Since the current research is to use the finite element method to develop tolerance criteria for acute subdural haematoma caused by shaking a baby, then reliable failure properties of the bridging veins will be required. Hence a testing rig was designed and built specifically to determine the strain rate dependence of human infant bridging veins.

This chapter describes the design of the testing rig, gives details of the human infant and porcine vein samples obtained and the results acquired from these samples. Unfortunately, several external circumstances arose which made it difficult to obtain sufficient human or porcine vein samples. Hence only a limited number of samples were successfully tested and these were insufficient to achieve statistically robust conclusions.

3.2 Testing Rig Design

The testing rig has to fulfill three main design criteria:

1. It is to stretch human bridging veins at a wide range of speeds (strain rate) whilst providing force and displacement data;

2. The strain rate during each test should be as constant as possible

3. This constant strain rate should be reached before the vein has undergone any significant extension.

Author(s)	Year	Strain Rates
Löwenhielm	1974*a*	1–1000 s^{-1}
Lee and Haut	1989	0.1–250 s^{-1}
Meaney	1991	0.4–241 s^{-1}

Table 3.1: Strain rates used in previous mechanical tests of human bridging veins.

The strain rates used in the previous studies are listed in Table 3.1. Lee and Haut (1989) quote their average vein length of 6.2 mm, resulting in stretch speeds between 0.62 mm/s and 6.2 m/s.

Early calculations showed that a DC servo motor would not be able to reach such high speeds within a small displacement, and also that at the low speeds an impact driven rig would decelerate significantly due to friction and bridging vein elasticity. Therefore it was decided to design the rig such that it could be driven either by a DC motor or an impact so that the motor could drive the rig at the low speeds, and the impact could drive it for the high speeds, preferably with an overlap at the mid-range speeds. To this end, a basic rig base was designed consisting of four steel blocks which could be arranged and connected differently for actuation by a motor or an impact as shown in Figures 3.1 and 3.2. For connection to a DC motor only three blocks are used with the two outer blocks fixed and the moving block mounted between them on linear bearings running on two fixed shafts. The moving block is connected to the DC servo motor via a ball screw and nut. To be impacted with a moving mass, the two moving blocks are rigidly connected by the shafts which run on linear bearings within the two fixed blocks. One moving block is positioned between the two fixed blocks providing the mounting point for the vein, and the second moving block is on the other side of a fixed block, providing an impact surface for the moving mass. Figure 3.3 shows a photograph of the rig assembled for actuation by the DC servo motor.

Veins were attached between mounting points on a stationary and a moving block. The mounting point on the stationary block was connected via a Kistler 9207 force transducer (range ± 50 N) to measure the tensile force within the vein sample. Strain of the samples was measured using a linearly variable differential transformer (LVDT, RS Components Ltd catalogue number 646-498) with a range of ± 15 mm connected between the moving and stationary blocks. Mounting points were initially made of hypodermic tubing around which the vein ends could be tied using suture. This would allow the samples to be perfused with saline if enough samples became available to also study the effect of perfusion pressure as did Meaney (1991). Unfortunately it quickly became apparent that it was very difficult to tie the veins to the tubing adequately, so that they would not slip off under load. Therefore the mounting points were replaced with small stainless steel clamps.

For the selection of a DC servo motor to drive the rig, it was specified that the motor should accelerate the rig to its final, steady speed within only 10% strain (a distance of approximately 1 mm for a 10 mm vein). This lead to the selection of an Electrocraft BRU Y3023-2 brushless DC servo motor, driving the rig with an SKF SFB16×5R ball screw which is able to accelerate the rig to 0.1 m/s within 1 mm. For impact actuation, a pendulum was designed to be 0.5 m long with a cylindrical steel mass of 5.5 kg at the end. When released from horizontal, this would give the rig speeds of up to 3 m/s.

The DC servo motor could be programmed to produce the required movement via software supplied by Electrocraft running on a Pentium Pro WindowsNT PC. A ComputerBoards Inc. CIO-DAS801 100kHz data acquisition card with eight 16 bit analogue inputs and 7 digital input/output channels was used with custom written software to provide the data logging, triggered either by a digital start signal provided by the DC motor driver or an optical beam sensor placed in the path of the pendulum bob.

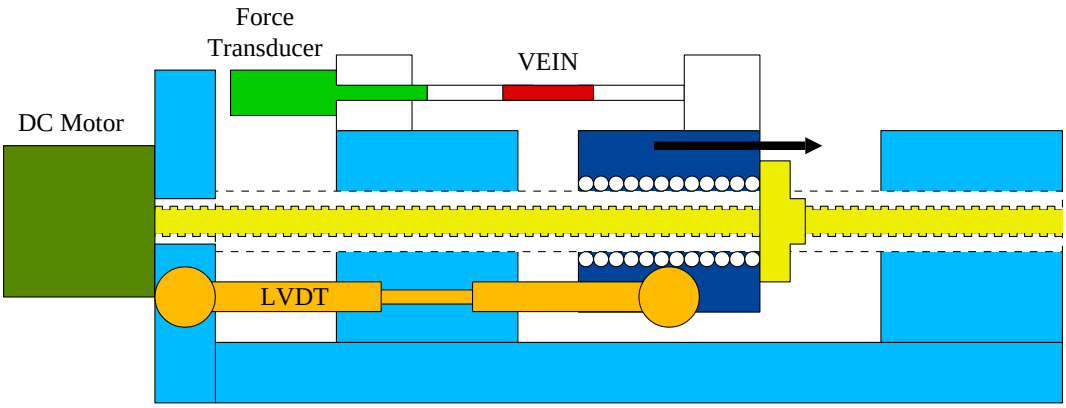

Figure 3.1: Diagram of the testing rig, connected to the DC servo motor.

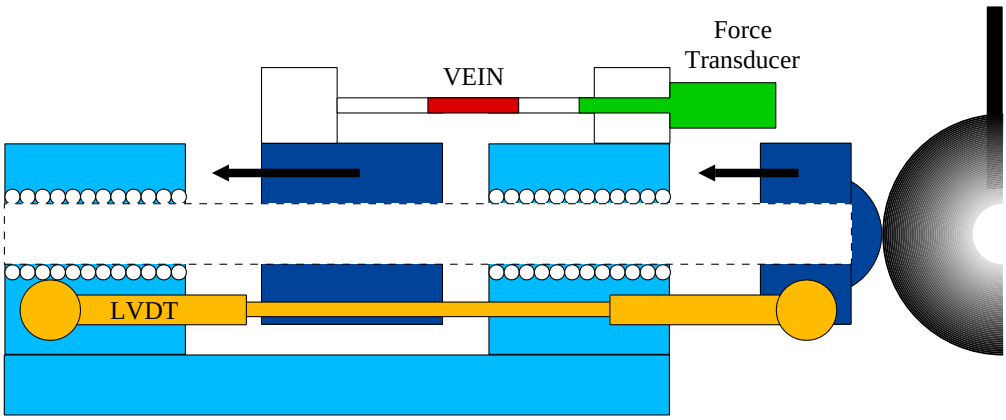

Figure 3.2: Diagram of the testing rig, connected to the pendulum.

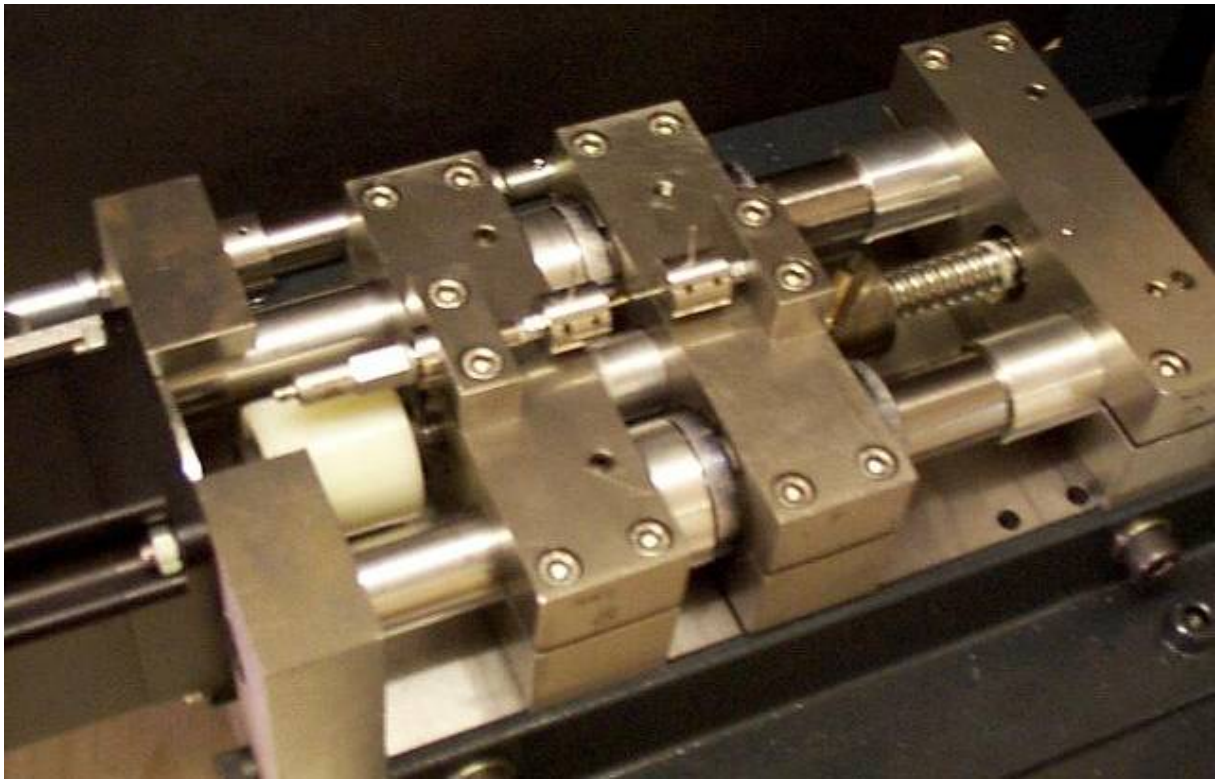

Figure 3.3: Bridging vein testing rig, connected to the DC servo motor.

3.3 Bridging Vein Samples

Ethical approval was given for the experiments, with human infant bridging veins to be supplied from Birmingham Women's Hospital, Birmingham Children's Hospital and Birmingham Coroner's Court. Unfortunately the timing of these experiments coincided with the organ retention scandal at Alder Hey Children's Hospital. The local Ethics Committee determined that an additional consent form should be presented to the parents giving them details of the experiments, why they are necessary, exactly what would be taken from their child during the post mortem examination (a maximum of 4 bridging veins) and how they would be disposed of afterwards. Parents proved to be very unwilling to give their consent, perhaps because of the negative publicity surrounding the Alder Hay scandal and the explicit consent form, resulting in access to only 3 cadavers from which 7 samples were successfully excised.

During the wait for human bridging vein samples various local butchers were asked if they could provide cow, sheep or pig heads from which bridging veins could be taken. Sup-

plies were constrained by the introduction of a series of public health directives responding to concerns about Bovine Spongiform Encephalopathy (BSE), swine fever, scrapies and finally foot and mouth disease. Eventually a suitable butcher was found but only two pig heads were obtained before they could no longer be provided. From these two pig heads 21 pia or arachnoid veins and 6 bridging veins were excised. Vein samples were stored in sterile saline solution and tested within a few hours, with the exception of the the large number of samples from the first pig from which there were tested over two days and so some were refrigerated overnight. Details of the two pig and three human donors are given in Table 3.2

Veins from the first pig and first human baby were mounted to the rig using the original method of tying them around hypodermic tubing with suture. It was hoped that the ends of the veins would be threaded over the tubing to enable them to be filled with saline. Unfortunately the veins were so small and moist that they were very difficult to manipulate and just lying them flat over the ends of the tubing while suture was tied around them was difficult in itself. Therefore the clamps were built and samples from the second pig and second and third human baby were mounted in the clamps. The clamps were still not a perfect mounting mechanism as some samples did pull out of a clamp rather than break between them, and many broke very close to the clamp. This may in part have been due to the difficulty in tightening the left hand side clamp screw without applying a dangerous bending moment to the force transducer it was connected to. Samples that were pulled out of the clamps were remounted and tested again. Whilst remounting it was evident that the samples had lengthened and had also become drier and stiffer.

Prior to being mounted, each sample was placed in a petri dish with a small amount of sterile saline solution. The dish was then placed on the the movable stage of a microscope equipped with vernier scales capable of measuring with a 1 μm precision. The outer diameter of the samples was easily visible on all but a few samples which were contained amongst other tissues (such samples were only used for practising with the equipment),

and the transparency of most of the veins also allowed their inner diameters to be measured. Once each sample was mounted the distance between the knots or end of the clamps was measured with vernier calipers. Force and displacement data for the samples which were successfully tested sometimes showed no force during the initial displacement as the slack in the vein was taken up. For the purpose of strain calculations these initial displacements were added to the initial vein lengths. Stretch ratio was calculated as the ratio of extended length to initial length, hence a stretch ratio of 2 implies that a vein has been stretched to twice its initial length.

Donor	Age (weeks)	Comments
Pig 1	16-17	Veins removed approximately 24 hours after slaughter.
Pig 2	16-17	Veins removed approximately 24 hours after slaughter.
Human 1	0	Still birth (34 weeks gestation), Veins removed and tested 4 days postmortem.
Human 2	10	Suspected shaken baby syndrome, Subdural haematoma on left hand side
Human 3	12	Skull abnormalities in left parietal area, Vein supplied already broken.

Table 3.2: Details of bridging vein donors.

3.4 Results

Dimensions of all pig and human samples are given in Table 3.3. Only some of the samples produced adequate results due to the difficulty of mounting them properly, and most of those which did eventually produce results had to be remounted, perhaps more than once. Table 3.4 gives a detailed testing history of all samples for which further results are quoted. Samples marked with an asterisk (*) were either pia or arachnoid veins, others were bridging veins.

Sample	Length (mm)	Diameter Inner (mm)	Diameter Outer (mm)	Area (mm^2)
P/1/1*	11.53		0.493	
P/1/2*	17.31			
P/1/3*	10.13			
P/1/4*	17.14	0.520	0.761	0.2425
P/1/5*	10.81	0.512	0.678	0.1551
P/1/6*	10.10	0.418	0.539	0.0905
P/1/7*	15.38	0.058	0.195	0.0272
P/1/8*	10.61	0.489	0.618	0.1117
P/1/9*	18.76		0.766	
P/1/10*	13.48	0.404	0.514	0.0790
P/1/11*	13.35	0.352	0.436	0.0521
P/1/12*	10.94			
P/1/13*	14.61			
P/1/14*	16.16			
P/1/15*	14.37	0.293	0.397	0.0560
P/1/16*	14.01	0.350	0.474	0.0796
P/1/17*	10.60	0.271	0.362	0.0450
P/1/18*	9.21	0.363	0.452	0.0570
P/1/19*	18.43			
P/1/20*	12.58	0.330	0.405	0.0433
P/1/21	9.98	0.197	0.312	0.0450
P/1/22	9.94	0.250	0.340	0.0417
P/1/23	7.06	0.254	0.408	0.0795
P/1/24	7.42	0.108	0.223	0.0298
P/2/1*	5.90	0.229	0.341	0.0508
P/2/2*	11.04	0.328	0.489	0.1033
P/2/3*	8.79	0.122	0.224	0.0278
P/2/4*	8.85			
P/2/5*	10.51			
P/2/6*	9.24	0.220	0.341	0.0528
P/2/7	13.23	0.490	0.643	0.1361
P/2/8	5.02	0.334	0.484	0.0979
H/1/3	13.94	0.052	0.146	0.0145
H/1/4	11.70	0.052	0.140	0.0129
H/2/1	2.80		0.315	
H/2/2	3.06	0.278	0.402	0.0645
H/3/1	6.79	0.387	0.515	0.089
H/3/2	6.05		0.718	

* = pia or arachnoid vein.

Table 3.3: Bridging vein dimensions.

Test ID	Mounted Length (mm)	Comments
P/1/4*	17.14	Came out of RHS knot.
4b*	13.09	Came out of LHS knot.
4c*	**14.08**	**Vein slightly dry but broke in middle.**
10*	**12.69**	**Broke in middle.**
14*	**16.16**	**Frayed arachnoid vein, broke in middle.**
18*	9.12	Came out of RHS knot.
18b*	**8.55**	**Broke in middle.**
23	7.14	Came out of RHS knot.
23b	**7.06**	**Broke near the end of RHS tube.**
P/2/1b*	**5.90**	**Broke near LHS clamp.**
3*	**8.79**	**Vein very dry but broke in middle.**
7	**13.23**	**Broke in middle.**
8	3.91	Came out of LHS clamp.
8b	**4.80**	**Vein quite dry but broke in middle.**
H/1/3	**13.94**	**Broke in middle.**
4	**11.70**	**Broke in middle.**
H/2/1	5.67	Broke in middle, but large force overloaded charge amplifier.
1b	**2.80**	**Broke very near RHS clamp.**
2	**3.06**	**Broke very near LHS clamp.**
H/3/1	6.27	Stretched, thinned near RHS but came out of LHS clamp.
1b	**6.79**	**Vein very dry, broke near RHS clamp.**

LHS = left hand side; RHS = right hand side; * = pia or arachnoid vein.

Table 3.4: Test history of pig and human bridging veins samples which were (eventually) successfully tested.

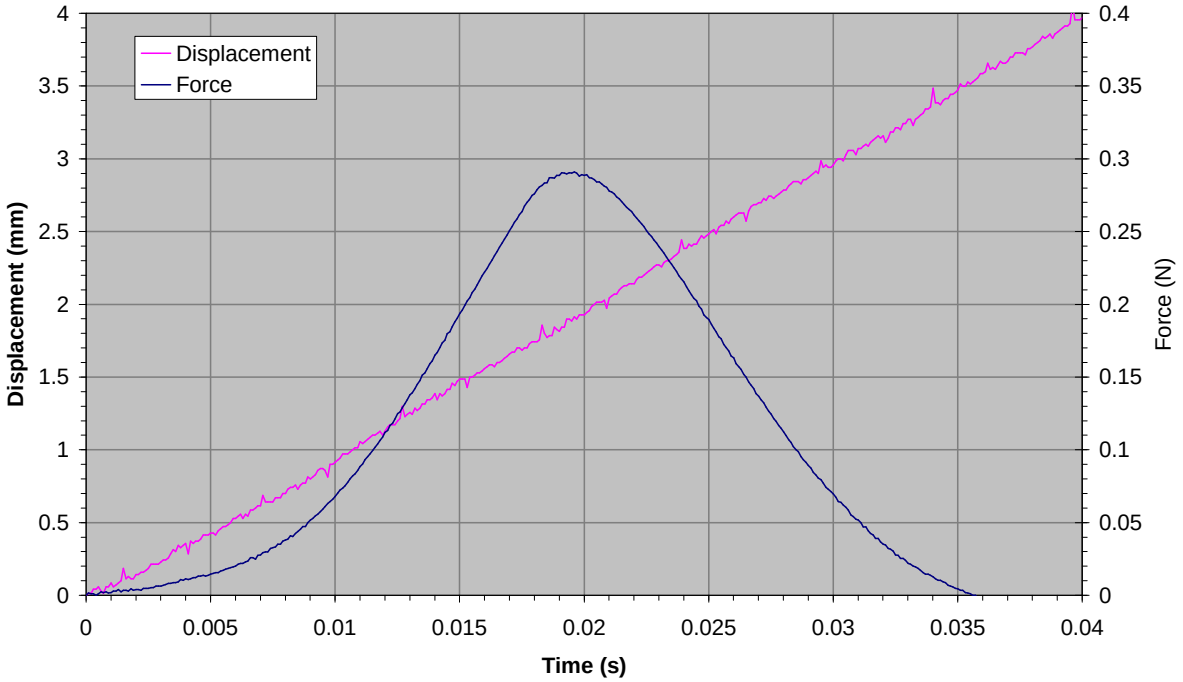

Figure 3.4: Force and displacement histories for test H/2/2.

Due to the limited number of samples, it was decided to test them all at a relatively low speed of 100 mm/s which given the range of vein lengths corresponds to strain rates between 5.8 and 32.7 s^{-1}. Figure 3.4 gives example force and displacement histories of test H/2/2, which proves that the test speed was constant throughout the test.

Figures 3.5 and 3.6 show all the stress versus stretch curves for the pig and human samples respectively, compared against the representative load versus stretch curve from Lee and Haut (1989). Lee and Haut do not quote the area of the sample for which the load/stretch curve is shown, but they do report a relationship between bridging vein thickness (T) and circumference (C) of $T = 0.021 + 0.0061C$ (where T and C are both in mm) and a mean vein circumference of 4.4 mm, resulting in a mean area of approximately 0.203 mm^2 which was used to convert their load/stretch curve of Figure 2.2 into the stress/stretch curve shown in Figures 3.5 and 3.6.

Figure 3.7 shows a good relationship between vein cross-sectional area and outer diameter and Figure 3.8 shows a less obvious linear relationship between vein thickness and outer diameter. The relationship between vein area (A, mm^2) and outer diameter (D,

mm) is shown in Figure 3.7 to be approximately:

$$A = 0.5106D^2 - 0.1516D + 0.0346 \tag{3.1}$$

Unfortunately the outer diameter of sample H/2/1 and neither diameter of sample P/1/14* were clearly visible under the microscope. Therefore Equation 3.1 was used to estimate the area of sample H/2/1 and the area of sample P/1/14* was assumed to be the mean of the areas of the other pia veins from the same pig.

Table 3.5 shows the range of ultimate stresses and strains for the pig and human veins. Also shown in Table 3.5 are the range of results reported by the previous research for strain rates between 5.8 and 32.7 s^{-1}.

Result set	Stretch ratio			Ultimate Stress (MPa)		
	Median	Mean	Range	Median	Mean	Range
Pig	1.469	1.430	1.429 ± 0.181	1.748	1.565	1.380 ± 0.636
Human	1.190	1.311	1.433 ± 0.308	4.820	4.130	3.440 ± 1.960
All	1.315	1.394	1.433 ± 0.308	1.854	2.354	3.072 ± 2.328
Löwenhielm(1974*a*)			1.556 ± 0.154			1.05 ± 0.85
Lee and Haut (1989)			1.575 ± 0.425			3.71 ± 2.84
Meaney (1991)			1.5 ± 0.2			6.35 ± 3.65

Table 3.5: Range of ultimate stresses and strains from this and earlier studies.

3.5 Conclusions

Unfortunately the great difficulty in obtaining parental consent for the extraction of human bridging veins was compounded by the difficulty in obtaining pig heads. This meant that very few samples were available making it impossible to examine the effect of strain rate. Instead all the samples were tested at a constant, relatively low speed to determine whether or not the equipment was capable of producing consistent results over a very low range of strain rates.

Even though the graphs in Figures 3.5 and 3.6 appear to be spread over a wide range

of ultimate stresses and stretches, Table 3.5 shows that the results fall well within the ranges reported by the previous research. It is also apparent that the results from samples from individual donors are more closely clustered than the results as a whole, especially if you further separate the results for the pig pia veins (thin lines) from the bridging veins (thick lines) in Figure 3.5. The wide range of results between donors, especially noticeable for the human donors in Figure 3.6 may partly be a product of the different circumstances surrounding each donor. Ideally, for a study such as this all samples should come from fatalities in which there was no head trauma to ensure that the veins are in a good condition, however, two of the human donors had significant head trauma and the third was an extremely small premature baby. Furthermore, sample H/3/1 was supplied already broken and was extremely dry by the time it was mounted for the second and final test which may explain the relatively low failure properties for this sample.

One point these experiments have clearly demonstrated is that bridging veins are very small and extremely delicate, and their properties can vary significantly between individuals. This makes it very difficult to rely on tolerance criteria quoted in previous research which are themselves just the averages of a wide range of values. The results of this and previous research shown in Table 3.5 indicates that for some veins stretches of as little as 1.15 (ie. strains of only 15%) may be enough to cause failure, therefore shaken baby syndrome tolerance criteria based on the commonly quoted average ultimate stretch of 1.5 may be significantly over-estimated. It must also be remembered that shaken baby syndrome is usually caused when bridging veins fail, but is most likely to occur when the *weakest* veins fail.

Any future experiments which are to determine the effect of strain rate, age, location or other variables upon the failure properties of bridging veins would require a very large number of good quality samples in order to have any confidence in the results. Even so, just like this and the previous research, they would probably still suffer from a large scatter due to the inherent variability of biological tissue samples.

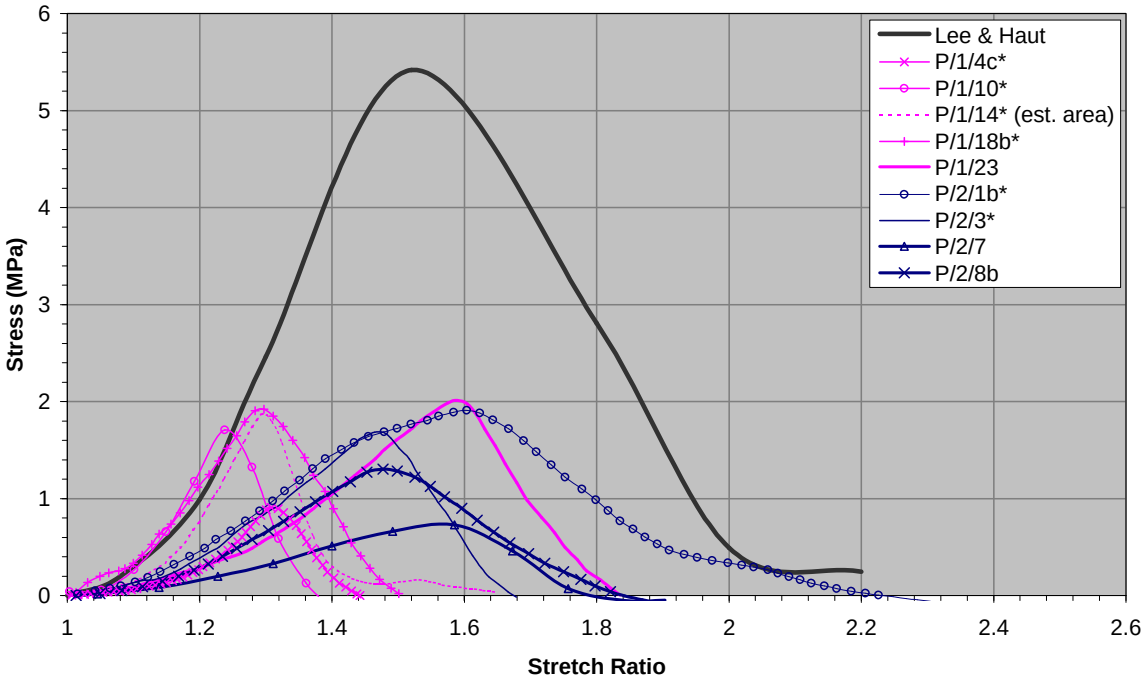

Figure 3.5: Results of pig vein testing.

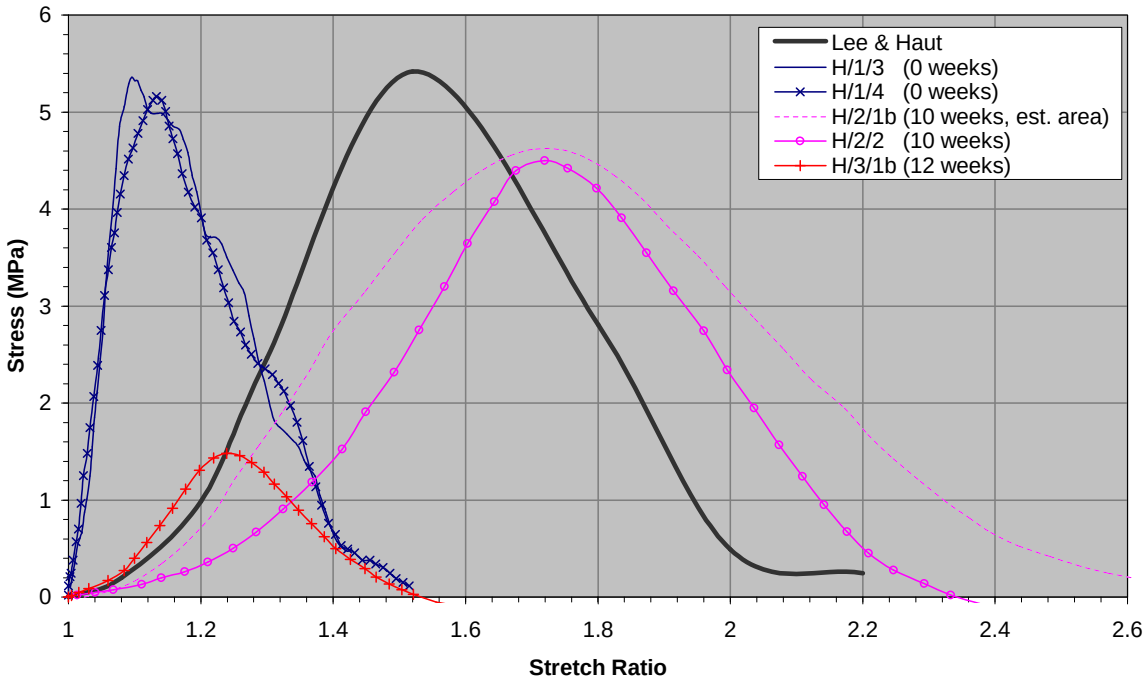

Figure 3.6: Results of human vein testing.

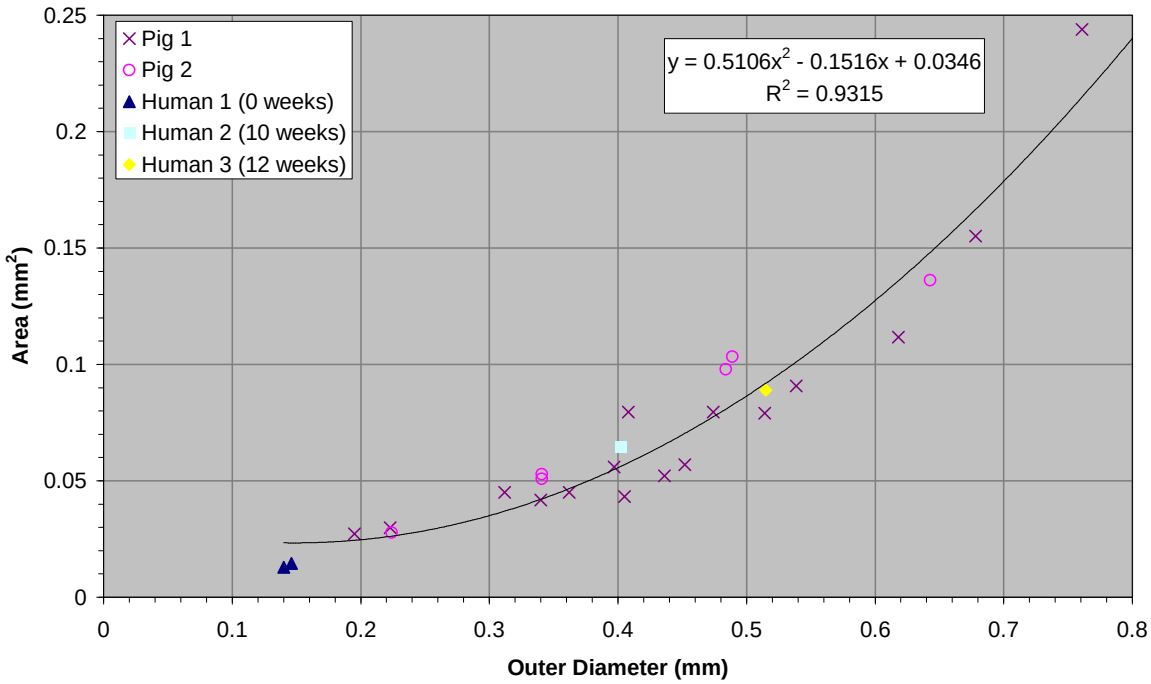

Figure 3.7: Relationship between bridging vein area and outer diameter.

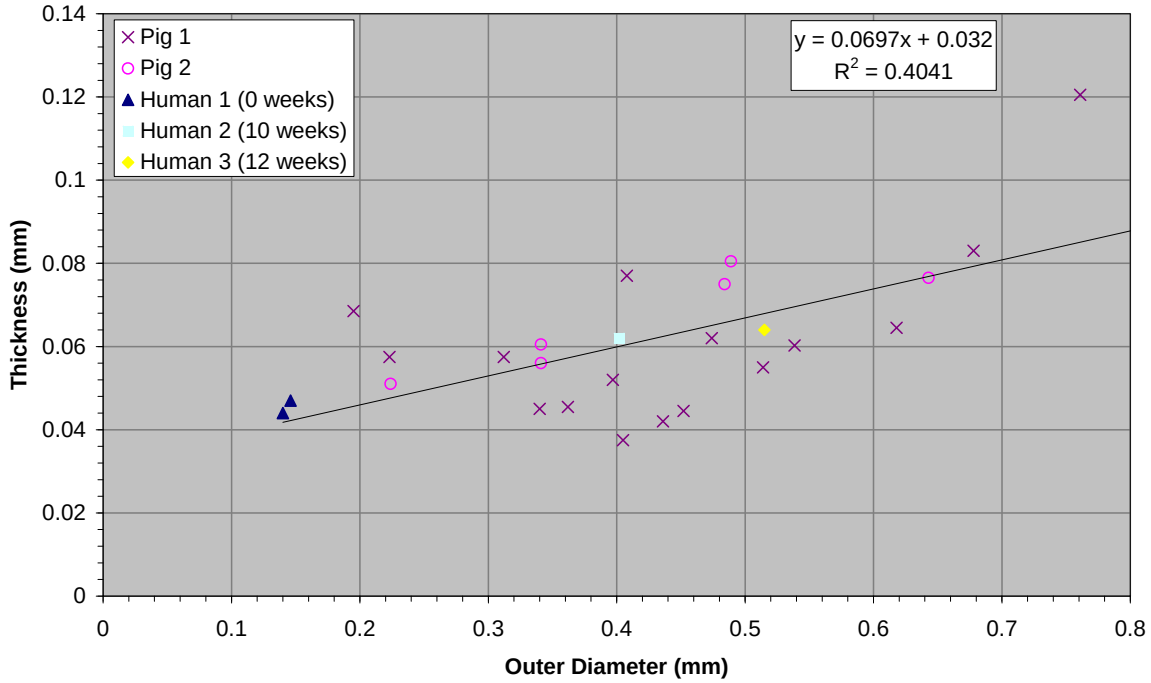

Figure 3.8: Relationship between bridging vein thickness and outer diameter.

PROTECTIVE ROLE OF THE CEREBROSPINAL FLUID

4.1 Introduction

Since Guthkelch (1971) and Caffey (1974) started highlighting similarities between the injuries caused by 'battered child syndrome' and those caused by severe whiplash, the medical community has started to appreciate the vulnerability of the infant brain to rotational accelerations. The earlier work of Holbourn (1943) seemed to provide an adequate explanation for this discovery by stating that brain material is more likely to be injured by rotational rather then translational accelerations due to its relatively low shear modulus compared to its bulk modulus.

Despite this hypothesis the effect that the cerebrospinal fluid might have on the motion of the brain has been largely ignored or perceived to be merely a 'shock absorber'. In nearly all previous finite element models of the head, the cerebrospinal fluid has either been totally ignored or modelled as a solid with low shear modulus. This is not surprising considering the difficulty of modelling the complex interactions between fluids and solids during dynamics analyses, and previous researchers did the best they could given the limitations of the modelling software available at the time.

However, finite element software has recently become available which claims to be able to combine the governing equations of fluid and solid materials in the same analyses, and thus model the interactions between them. If the current research is to successfully model shaken baby syndrome, whilst paying particular attention to the cerebrospinal fluid, then

the dynamic fluid/solid interactions need to be understood and the ability of the chosen modelling software to accurately account for these interactions needs to be demonstrated. The lack of adequate physical experiments against which the final finite element model of shaken baby syndrome can be verified makes this especially important. Verification that the software is accurately modelling the physics of dynamic interactions between fluids and solids will add confidence to the results of more complex models which cannot otherwise be verified.

This chapter will briefly present the forces which act on a submerged body, namely Archimedes' force (or buoyancy), acceleration reaction force and viscous drag. The software package used to perform the finite element modelling will then be described and used to model simple fluid/solid interaction problems. In this way the software can be validated by comparing its predictions with known theoretical results.

4.2 Forces Acting on a Submerged Body

4.2.1 Archimides' Force (Buoyancy)

Archimedes' principle states that a body immersed in a fluid is buoyed up by a force equal to the weight of the displaced fluid. This can be inserted into Newton's Second Law of motion for the body (neglecting fluid resistance) shown in Figure 4.1a as the final term in the equation,

$$m_s \ddot{y} = -m_s g + m_f g \tag{4.1}$$

Equation 4.1 can be rewritten as,

$$\ddot{y} = -g\left(1 - \frac{\rho_f}{\rho_s}\right) \tag{4.2}$$

where m_s and m_f are the masses of the submerged body and displaced fluid respectively

ρ_s and ρ_f are the densities of the body and fluid respectively

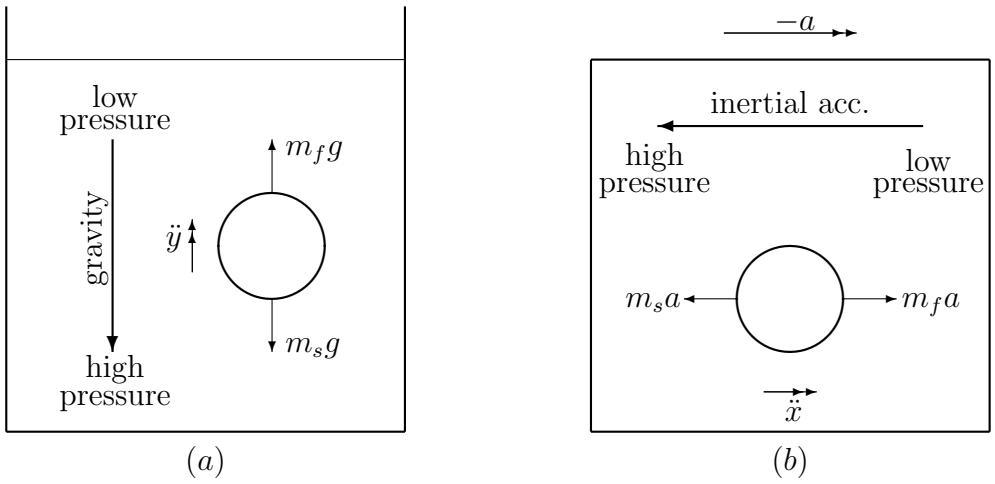

Figure 4.1: Inertial and buoyancy forces acting on submerged bodies.

g	is the gravitational acceleration (downwards)
$\ddot{y}$	is the vertical acceleration of the submerged body

This buoyancy force is present because the gravitational field produces a pressure gradient in the fluid with a high pressure below the submerged body and a lower pressure above it resulting in a net vertical force on the body. Equation 4.2 shows that if the solid is denser than the fluid ($\rho_s > \rho_f$) then its acceleration will be negative and it will sink. Conversely if the solid is less dense than the fluid then it will rise, and if the solid and fluid have equal densities then the solid will remain stationary within the fluid.

'Buoyancy' forces will exist in any fluid which contains a pressure gradient, whether or not it's caused by gravity. Figure 4.1b shows a container completely filled with a fluid in which a sphere is submerged. If the container is accelerated to the right then a high pressure will be produced in the fluid to the left of the body graduating to a low pressure to the right of the body. Viewing the contents of the container from a frame of reference moving with it, every particle of matter within the container will experience an *inertial* acceleration to the left. This inertial acceleration is equivalent to the gravitational acceleration in Figure 4.1a, and hence Equations 4.1 and 4.2 can be modified to give,

$$m_s \ddot{x} = -m_s a + m_f a \tag{4.3}$$

$$\ddot{x} = -a\left(1 - \frac{\rho_f}{\rho_s}\right) \tag{4.4}$$

where a is the inertial acceleration experienced within the moving container

$\ddot{x}$ is the horizontal acceleration of the body relative to the moving container

Therefore, if the solid is denser than the fluid ($\rho_s > \rho_f$) then its acceleration (relative to the moving container) will be negative and it will move to the left within the container. Viewing from a fixed (inertial) frame of reference, the container will be moving to the right with acceleration a and the solid will also be moving to the right but with the reduced acceleration $a + \ddot{x}$ (where $\ddot{x}$ is negative). Again, if the solid and fluid have equal densities then the solid will remain stationary relative to the container.

This perfectly explains the 'cushioning effect' of the cerebrospinal fluid on the brain during translational accelerations, as was pointed out by Hodgson, Shippen and Sunderland (2001). An accelerated head can be simplified to the system in Figure 4.1b, with the skull, brain and CSF represented by the rigid container, the submerged solid and the fluid respectively. As the skull is accelerated backwards as a rigid body in pure translation (eg. after an impact to the forehead with a padded surface), the brain will accelerate forwards within the skull by an amount given by Equation 4.4. If the brain and CSF were to have equal densities then the acceleration of the brain within the skull would be zero and bridging veins would not be stretched at all. Unfortunately the brain is slightly more dense than the CSF, however their densities are quite close, with a mean brain density of 1040 kg/m^3 (Ruan *et al.*, 1996) and CSF density of 1005 kg/m^3 (Saladin, 1998). From Equation 4.4 this gives a relative brain acceleration of,

$$\ddot{x} = -a\left(1 - \frac{1005}{1040}\right) = -0.0337a \tag{4.5}$$

Hence, the buoyancy force produced by the CSF would have the effect of reducing the acceleration of the brain within the skull by about 96.6% compared to an unsupported brain with no CSF, and it does so without applying any high localised forces to any part

of the brain. Unfortunately, this buoyancy force offers no protection against rotational accelerations, and as the container is rotated around the solid the solid would remain stationary (neglecting viscous drag forces).

Every aspect of the design of the human body has been optimised over millions of years of evolution and the protection of the brain against inertial accelerations would be a powerful evolutionary force in the human environment. Therefore despite the fact that both brain and CSF are largely made of water, evolution will probably have ensured that their densities remain as close as possible whilst still providing their physiological functions.

4.2.2 Acceleration Reaction Force

As a submerged body accelerates it also has to accelerate the surrounding fluid, by pushing the fluid in front of it and 'sucking' the fluid in behind it. This requires the body to apply a force on the fluid, which by Newton's Third Law will apply an equal and opposite reaction force on the body. Hence this force is known as the *'acceleration reaction force'*. It has been shown (Milne-Thompson, 1968, p. 246) that this force is proportional to the acceleration of the body, and hence has the effect of increasing the inertia of the solid. Therefore, it is convenient to quote this force in terms of an added mass coefficient (α) whereby the effective inertial mass (m'_s) is given by,

$$m'_s = m_s + \alpha m_f \tag{4.6}$$

The added mass coefficient is dependent on the shape of the submerged body, the shape of the fluid reservoir and the direction of motion. Milne-Thompson (1968, pp. 418–446) gives the added mass of a sphere in an infinite fluid reservoir as $\alpha = \frac{1}{2}$, and for a sphere of radius a in a spherical fluid reservoir of radius b the added mass is given by,

$$\alpha = \frac{2a^3 + b^3}{2b^3 - 2a^3} \tag{4.7}$$

which tends to the infinite fluid value of $\frac{1}{2}$ as $b \to \infty$, and has been verified experimentally by Ackerman and Arbhabhirama (1964) and also McConnell and Young (1965).

4.2.3 Viscous Drag

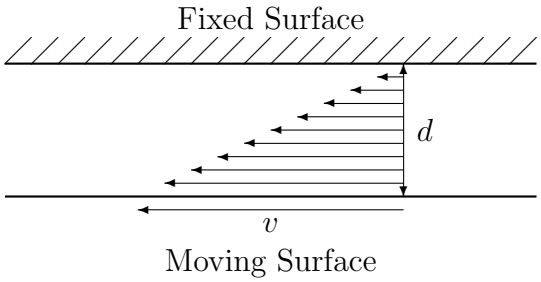

Figure 4.2: Fluid velocity gradient between moving and fixed surfaces.

If two objects which are moving relative to each other are separated only by a layer of viscous fluid then the fluid will apply a *viscous drag* force to each object. Figure 4.2 shows the case where an infinite flat plate is moving with velocity v parallel to a fixed plate which is a height d above it. The viscosity of the fluid will cause the particles of fluid immediately next to each plate to move with the same velocity as the plates, with a linear velocity gradient between them. The constant deformation of the fluid will apply a shear force on each plate, which for a Newtonian fluid is proportional to the velocity gradient in the fluid. The constant of proportionality is known the *viscosity coefficient* (μ) of the fluid, which gives rise to Equation 4.8 relating the force (F) acting on a given area (A) of plate.

$$F = \mu \left(\frac{v}{d}\right) A \tag{4.8}$$

4.3 Modelling Fluid/Solid Interactions with Dytran

MSC.Dytran is a three-dimensional analysis code for analysing the dynamic, nonlinear behaviour of solid components, structures and fluids. It uses explicit time integration and incorporates features that simulate a wide range of material and geometric nonlin-

earity. Lagrangian and Eulerian solvers are available to enable the modelling of both structures and fluids, and meshes within each solver can be coupled together to analyse fluid-structure interactions, although the current version of MSC.Dytran is unable to model viscous forces.

The Lagrangian solver requires a mesh defined with elements of constant mass, whereby the nodes of each element are fixed to locations on the solid body and thus the mesh is distorted as the body deforms. However, the Eulerian solver requires a mesh defined with elements of constant volume so that the grid points are fixed in space and the mesh provides a fixed frame of reference through which the fluid flows, transporting the mass, momentum and energy from element to element.

The coupling of the Lagrangian and Eulerian meshes is performed using a coupling surface between them and can be controlled in one of two ways: general coupling or Arbitrary Lagrange Euler (ALE) coupling. Under general coupling the surface is only connected to the Lagrangian mesh and acts as a boundary to the flow of material in the Eulerian mesh, while the pressures in the Eulerian material exerts forces on the surface thus causing the Lagrangian mesh to distort. Under ALE coupling the same forces are transferred through the coupling surface but the surface is also connected to nodes in the Eulerian mesh, so the Eulerian mesh can distort with the Lagrangian mesh while the Eulerian material flows through it. Each method has its advantages and disadvantages which will be discussed during the development of each model in this and the following chapter.

The majority of finite element programs use implicit solution methods, normally using Newmark schemes to integrate with respect to time, whereas the explicit method employed by MSC.Dytran uses the central difference scheme. Implicit methods can be made unconditionally stable regardless of the time step by performing successive approximations until a solution is converged upon, whereas to ensure a stable solution with the explicit method the time step must be smaller than the time taken for a stress wave to cross the smallest element in the mesh. This means that explicit time steps are typically

thousands of times smaller than those used with implicit methods, however they can still be competitive with implicit methods since each iteration does not involve the costly formation and decomposition of matrices required for the Newmark scheme.

4.3.1 Modelling Buoyancy

The ability of MSC.Dytran to accurately model buoyancy was determined by making a simple model of a 1 m radius rigid sphere within a 6 m^3 cube of fluid. General coupling was employed so that the Euler mesh wouldn't deform as the Lagrangian mesh moved through it, therefore the cube of fluid was defined by a complete regular Euler mesh and the Lagrangian mesh was surrounded by a coupling surface. As well as transferring forces and displacements between the Euler and Lagrangian elements, the coupling surface was also defined to disable any Euler elements that fell within its enclosed volume. A gravity field was applied to the whole model using the global `GRAV` option. The system closely represents that shown in Figure 4.1a, for which — taking the added mass of the sphere into account — Equation 4.1 gives,

$$m'_s \ddot{y} = -m_s g + m_f g \tag{4.9}$$

substituting Equation 4.6 for the added mass of the sphere gives,

$$(m_s + \alpha m_f)\, \ddot{y} = -m_s g + m_f g \tag{4.10}$$

$$\ddot{y} = -g \left(\frac{m_s - m_f}{m_s + \alpha m_f} \right) \tag{4.11}$$

and since the sphere and displaced fluid are of equal volume,

$$\ddot{y} = -g \left(\frac{\rho_s - \rho_f}{\rho_s + \alpha \rho_f} \right) \tag{4.12}$$

Density (kg/m^3)		Acceleration (m/s^2)		
Sphere	Fluid	Gravity	Theoretical	Model
2000	1000	20	-8	-7.66
1000	1000	20	0	-0.31
500	1000	10	5	5.51
500	1000	20	10	11.03
100	1000	10	15	16.03
100	1000	20	30	31.72
100	1000	200	300	271.28

Table 4.1: Theoretical and FEM results of modelling buoyancy for various parameters.

Various MSC.Dytran input files were created with the combinations of parameters shown in Table 4.1. As expected, the displacement history of the sphere was a smooth parabola, from which the acceleration was calculated from the second differential. This resulted in the accelerations in the final column of Table 4.1, which are compared against the theoretical values (given by Equation 4.12) in the table and also in Figure 4.3. Since the fluid volume is significantly larger than submerged sphere the value of $\alpha = \frac{1}{2}$ (corresponding to an infinite fluid) was chosen for the added mass coefficient, which proved to be a fair approximation. MSC.Dytran has produced results which correlate very well with theory, which verifies that MSC.Dytran can accurately model buoyancy forces, and the acceleration reaction force for a sphere within an infinite fluid.

4.3.2 Modelling Acceleration Reaction Forces

Although Section 4.3.1 goes some way to verifying that MSC.Dytran can accurately model the acceleration reaction force (at least for a sphere within an infinite fluid) further verification with geometries more similar to a human head was sought. The closest model of a brain surrounded by CSF that can still be compared against known results is a rigid sphere within an enclosed, spherical volume of fluid. The theoretical result for such models is given by substituting the added mass coefficient from Equation 4.7 into Equation 4.12 giving,

$$\ddot{y} = -g\left(\frac{\rho_s - \rho_f}{\rho_s + \frac{2a^3+b^3}{2b^3-2a^3}\rho_f}\right) \tag{4.13}$$

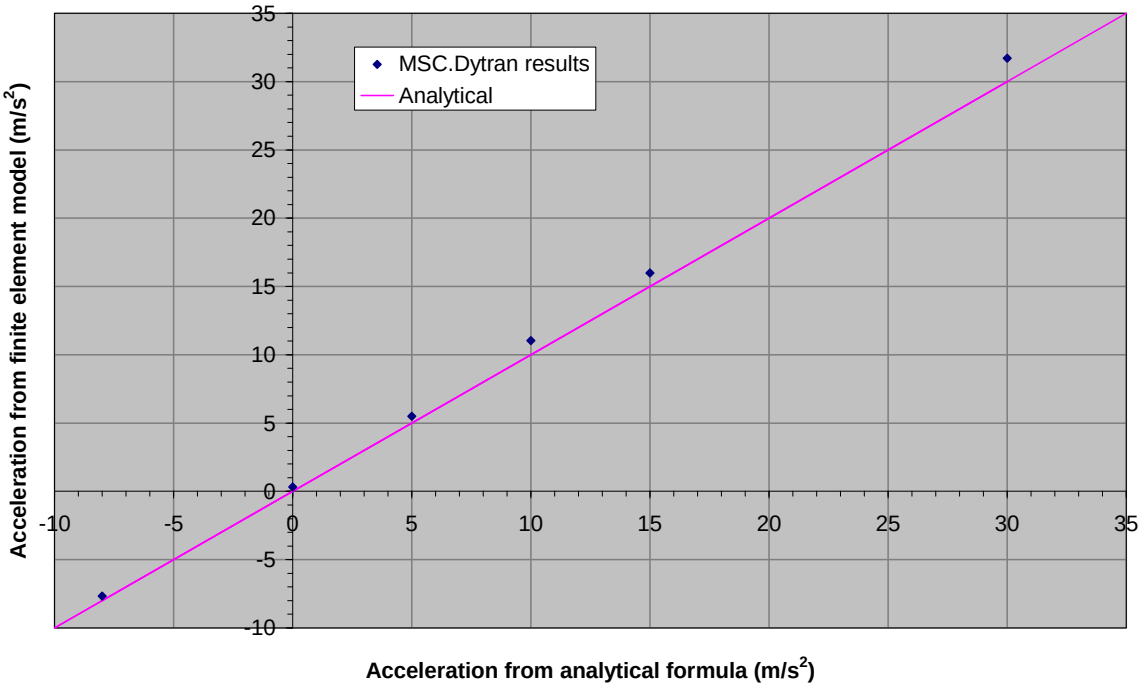

Figure 4.3: Comparison of Analytical and FEM results of modelling buoyancy with various parameters.

For these models, the inner sphere was given a radius a of 5 cm, similar to that of the brain of a human baby. The fluid envelope was given various radii between $5.1 \leq b \leq 7$ cm. The fluid was given the properties of CSF, i.e. a density of 1005 kg/m^3 and bulk modulus of 2.25 GPa. The rigid sphere was originally given the brain tissue density of 1040 kg/m^3 and was later given densities of 1005 kg/m^3 and 2000 kg/m^3 to investigate the poor results initially achieved. A horizontal gravitational acceleration of 63 m/s^2 was applied, which is approximately the peak horizontal acceleration of a child's head as it is shaken through a $\pm 60°$, 10 cm arc at 4 Hz. Models were built employing both general and ALE coupling, producing effectively identical results.

Table 4.2 shows the results for the ALE coupling models. Figure 4.4 shows that MSC.Dytran produces reasonably accurate results when the sphere is considerably more dense than the fluid. However, the square points in Figure 4.5 show poorer results when the brain is only slightly more dense than the fluid. The results for when the sphere and fluid have equal densities clearly demonstrates, and also helps to explain this problem. When $\rho_s = \rho_f$ the sphere should be neutrally buoyant because the inertial force

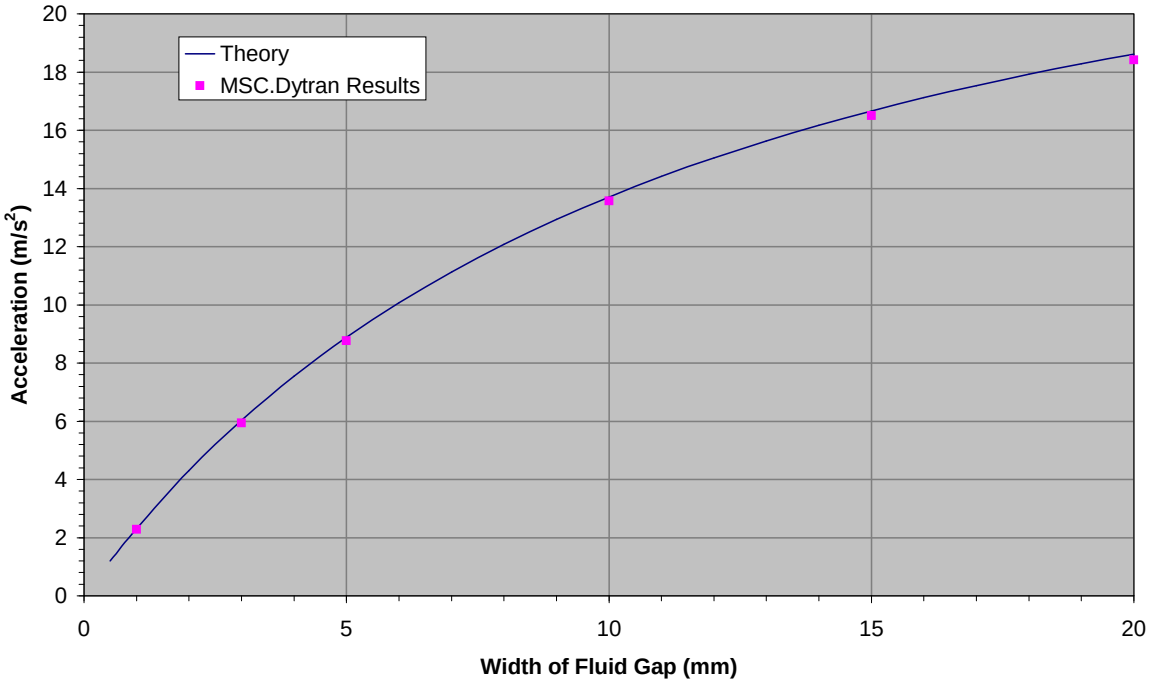

Figure 4.4: Modelling results for a sphere with density 2000 kg/m^3 accelerating within a sphere of fluid.

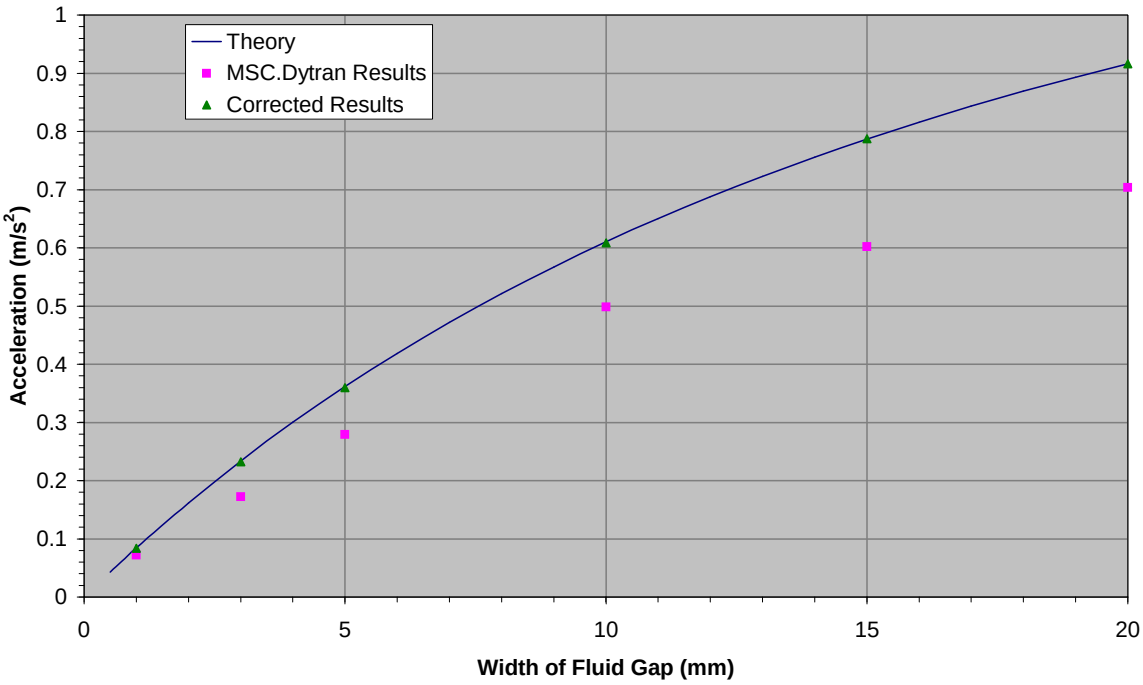

Figure 4.5: Modelling results for a sphere with density 1040 kg/m^3 accelerating within a sphere of fluid.

CSF gap width (mm)	Model $\rho_s = \rho_f$	Model $\rho_s = 1040$ kg/m^3	Theory $\rho_s = 1040$ kg/m^3	Model $\rho_s = 2000$ kg/m^3	Theory $\rho_s = 2000$ kg/m^3
1	-0.012	0.072	0.084	2.285	2.310
3	-0.061	0.172	0.234	5.939	6.031
5	-0.080	0.237	0.280	8.736	8.760
10	-0.110	0.499	0.610	13.560	13.707
15	-0.186	0.602	0.787	16.496	16.663
20	-0.212	0.704	0.916	18.421	18.618

Table 4.2: Acceleration results (m/s^2) from theory and FEM for a rigid sphere within a spherical volume of fluid

should be cancelled out by the buoyancy force and Equation 4.13 gives an acceleration of zero. However, Table 4.2 shows increasingly negative accelerations for increasing CSF gap widths. Adding the magnitude of these negative accelerations to the incorrect results for $\rho_s = 1040$ kg/m^3 and $\rho_s = 2000$ kg/m^3 gives values almost exactly equal to the theoretical values, as shown by the triangular points in Figure 4.5.

Rigid bodies can be defined in MSC.Dytran in one of two ways: 1) two-dimensional elements can be defined as the surface of the rigid body; the body's mass, centre of mass, principal axes of inertia, etc., can then be entered manually; 2) three-dimensional elements can directly define the rigid body, in which case its mass and other properties are computed from geometry and the given density. Although more computationally expensive, method (2) was chosen for these models in the hope that the computed mass of the actual geometry (defined with 4032 elements) would give better results than the entered mass of a perfect sphere. However, examining the MSC.Dytran output file for the 1005 kg/m^3 models shows that MSC.Dytran computed an actual mass of the sphere as 0.51985 kg, compared to 0.5262 kg for a perfect 5 cm radius sphere. This is to be expected since a sphere made of discrete elements will have less volume than a perfect sphere which *should* cause an equal reduction in the inertial and buoyancy forces and hence have no net effect, but this does not appear to be the case with MSC.Dytran. The errors are probably due to the calculation of pressure forces on complex geometries since models consisting of a rigid cube within a cube of fluid can achieve almost perfect neutral buoyancy.

The effect of this discrepancy is still relatively small when the the fluid gap is thin and the acceleration reaction force dominates over the buoyancy force, so it is unlikely to have much impact on a model of a baby's head. Increasing the sphere density by about 8 kg/m^3 in all of the models appears to compensate for this error, and so the sensitivity of the final model to this phenomenon compared to other variables such as the brain material properties can easily be investigated.

4.3.3 High Frequency Oscillations

If the concentric sphere models are re-run so as to concentrate on only the first few tenths of a millisecond, then the displacement histories shown in Figure 4.6 are produced. It is apparent that high frequency oscillations are superimposed upon the steady acceleration of the inner sphere, with higher frequencies caused by thinner fluid layers. This can perhaps be explained by comparing this system to a piston compressing an enclosed volume of fluid as shown in Figure 4.7.

The Bulk Modulus (K) of a material is defined as the ratio of pressure (p) to volumetric strain ($\delta V/V$) such that,

$$K = -\frac{p}{\delta V/V} \tag{4.14}$$

For a piston of constant cross-sectional area,

$$\frac{\delta V}{V} = \frac{x}{l} \tag{4.15}$$

and hence,

$$p = -K\frac{x}{l} \tag{4.16}$$

Newton's second law applied to the piston gives,

$$m\ddot{x} = pA \tag{4.17}$$

where m is the mass of the piston and A is its cross-sectional area. Substituting Equation 4.16 gives,

$$\ddot{x} = -\frac{KA}{ml}\,x \tag{4.18}$$

Equation 4.18 describes simple harmonic motion with angular frequency,

$$\omega^2 = \frac{KA}{ml} \tag{4.19}$$

and frequency,

$$f = \frac{1}{2\pi}\sqrt{\frac{KA}{ml}} \tag{4.20}$$

Figure 4.8 shows this theoretical frequency and the frequencies from the modelling results plotted against the fluid gap width. To evaluate Equation 4.20 the bulk modulus of water ($K = 2.55$ GPa) was used, A was set to the projected area of the sphere, m was the ideal mass of the sphere and l was set to the width of the fluid gap. The good agreement between the theory and the modelling results confirms that the piston model adequately explains the displacements shown in Figure 4.6 and is another good verification that MSC.Dytran is modelling interactions between fluids and solids reliably.

Incidentally, it is also evident from Figure 4.6 that during the first few microseconds the spheres in each model all have the same initial acceleration, and that this initial condition persists for longer when the gap is wider. The value of this initial acceleration is in fact 63 m/s^2 — the inertial acceleration applied to the whole model. For the first microsecond or so the sphere is moving as if there were no fluid present. This is because it takes time for the pressure gradient to establish itself in the fluid and to oppose the motion of the sphere.

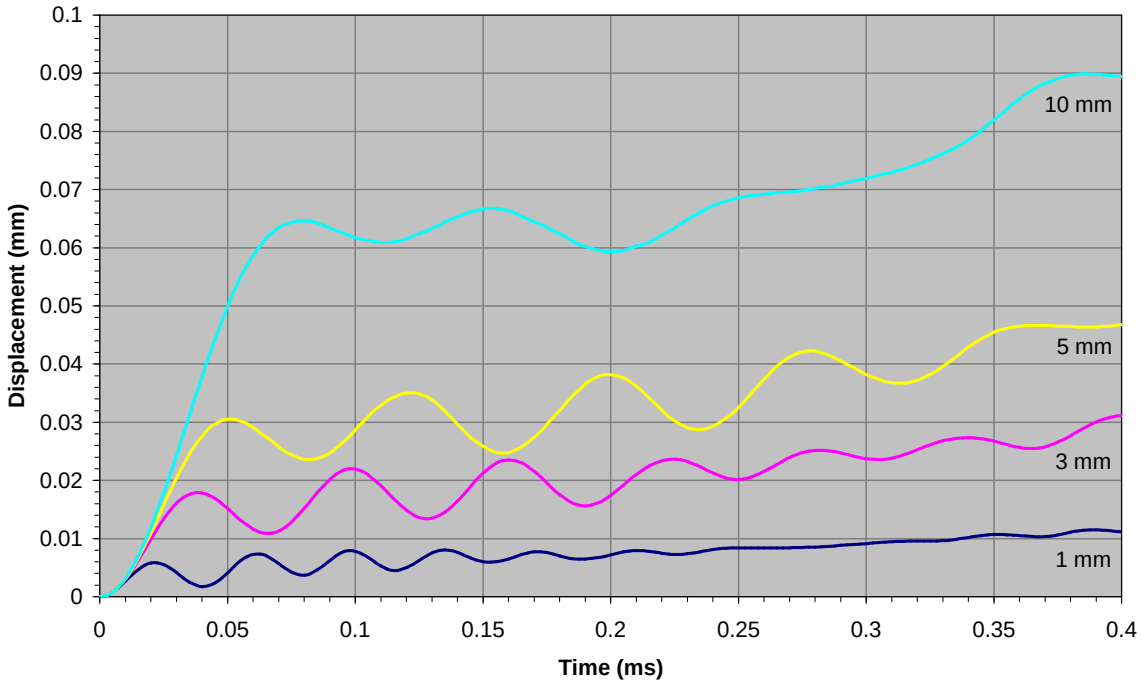

Figure 4.6: Short-term displacement histories for the concentric sphere models, $\rho_s = 1040$ kg/m^3.

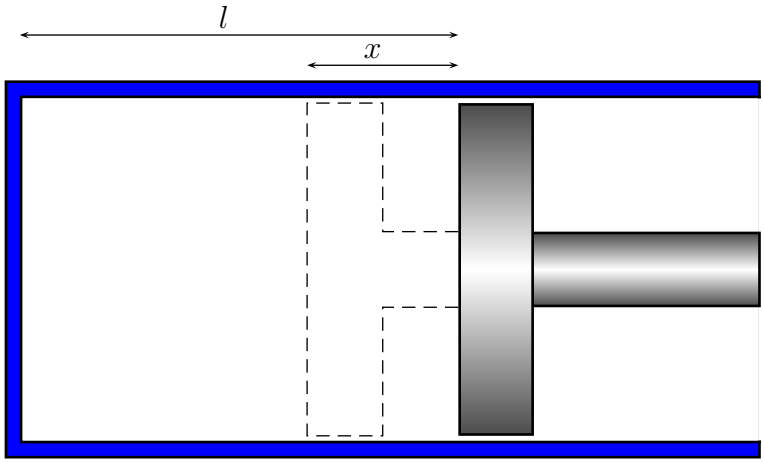

Figure 4.7: Compressing an enclosed volume of fluid.

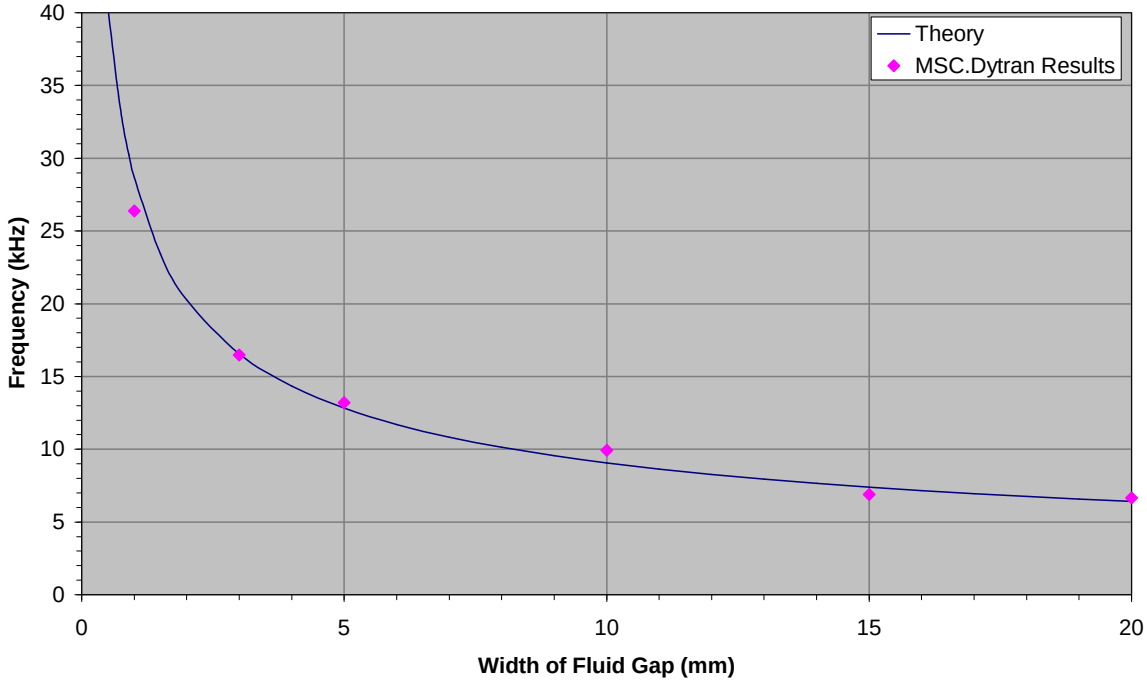

Figure 4.8: Frequency of oscillations for the concentric sphere models.

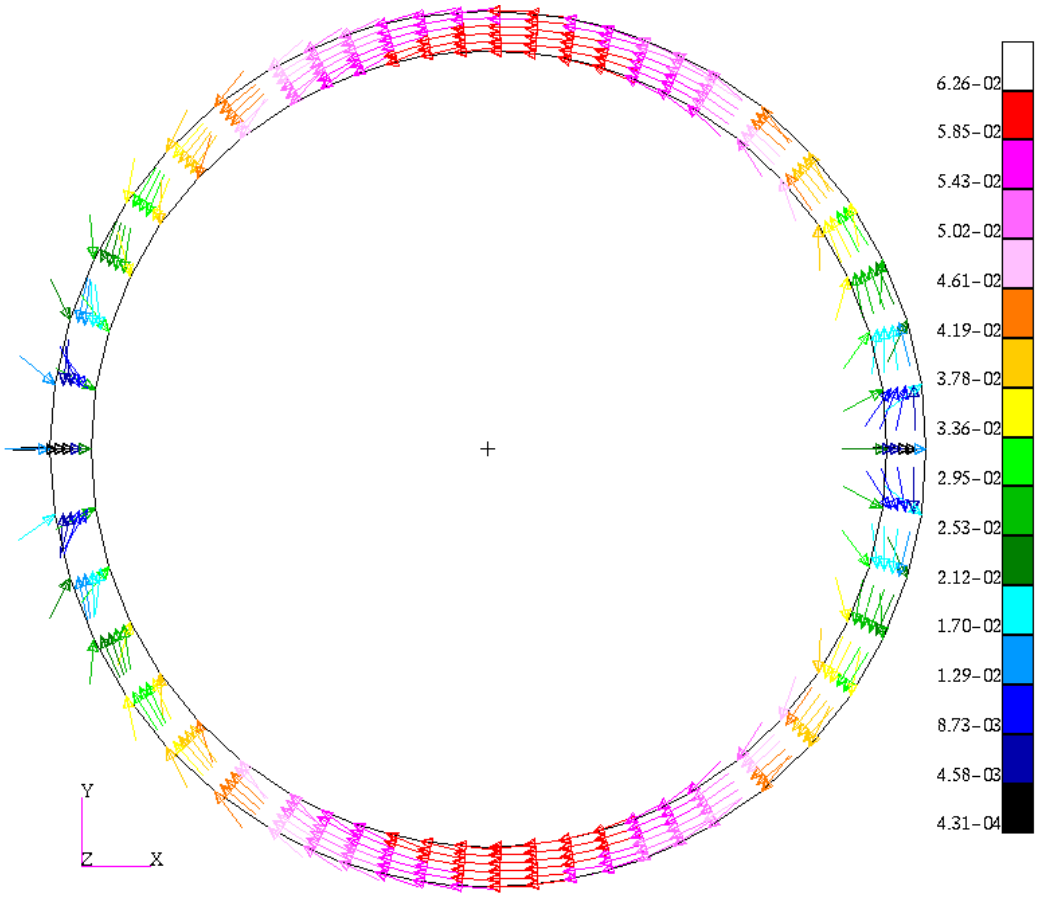

Figure 4.9: Fluid flow around the rigid sphere with a 5 mm thick envelope of fluid.

4.3.4 Effect of Viscosity

MSC.Dytran cannot model viscosity in models that employ ALE coupling. This is because MSC.Dytran has two Eulerian solvers, the standard solver and a ROE solver (which is based on the Riemann solvers developed by Professor Philip Roe, 1981). Viscosity is available only in the ROE solver, but the ROE solver can be used only with general coupling. Some models were created using general coupling and the ROE solver, with viscosity coefficients between $1{\times}10^{-6} \leq \mu \leq 1{\times}10^{6}$ ($\mu_{water} = 1 \times 10^{-3}$) but this had no effect on the results. Communication with support personnel at MSC Software revealed that although there is support for the viscosity coefficient in the input file it is not yet actually implemented in the code in MSC.Dytran version 4.7.

Nevertheless, the possible effect of viscosity for the models discussed in the previous section can be estimated from the velocity of fluid flow around the rigid sphere. Figure 4.9 shows a typical fluid flow with a peak fluid velocity of about 0.06 m/s, a value which is representative of all the other models with different thicknesses of the CSF layer. This system is dissimilar to the system shown in Figure 4.2, because the sphere is moving in one direction and the fluid is being forced to flow in the other direction round it, but an estimate of the viscous drag force acting on the rigid sphere can still be estimated from Equation 4.8. Assuming that the peak velocity of the fluid would be increased to 0.12 m/s^2 if there were a velocity gradient across the gap, and that this high pressure gradient exists over the entire surface instead of just at the edges furthest from the axis of translation gives an upper estimate of,

$$
\begin{aligned}
F_{drag} &= \mu \left(\frac{v}{d}\right) A \qquad (4.8)\\
&\approx 1 \times 10^{-3} \times \frac{0.12}{d} \times 4\pi(0.05)^2\\
&\approx \frac{4 \times 10^{-6}}{d}\\
&\approx 0.004 \text{ N when } d = 1 \text{ mm}
\end{aligned}
$$

The net result of the inertial and buoyancy forces produces a motive force of,

$$\begin{aligned} F_{motive} &= g(m_s - m_f) \\ &= 63 \times \frac{4}{3}\pi(0.05)^3 \times (1040 - 1005) \\ &= 1.15 \text{ N} \end{aligned} \tag{4.21}$$

The acceleration reaction force acting on the sphere surrounded by a 10 mm layer of fluid accelerating at 0.6 m/s^2 (from Figure 4.5) is smaller than the force acting on the sphere surrounded by a 1 mm layer of fluid accelerating at 0.08 m/s^2 and is given by,

$$\begin{aligned} F_{reaction} &= \alpha m_f \ddot{x} \\ &= \left(\frac{2 \times 0.05^3 + 0.06^3}{2 \times 0.06^3 - 2 \times 0.05^3} \right) \times \frac{4}{3}\pi(0.05)^3 \times 1005 \times 0.6 \\ &= 0.81 \text{ N} \end{aligned} \tag{4.22}$$

Therefore the viscous drag force is considerably smaller than the other forces acting on the sphere, and hence its omission should not significantly affect the accuracy of the current models.

4.4 Modelling the Fluid as a Solid

This chapter has so far presented the fluid forces that might act on the brain by the CSF as the skull is accelerated, and thus demonstrated the importance of including these forces in finite element models of heads. However, to date all previous FE models of heads have modelled the fluid as a solid or even ignored it altogether, so how accurately can these models represent the simple submerged body examples described above?

To answer this question a concentric sphere model was modified so that the rigid sphere was surrounded by a 10 mm layer of an isotropic elastic solid with various combinations of material properties. The densities of the rigid sphere and 'fluid' were 2000 and 1005 kg/m^3 respectively, and a horizontal inertial acceleration field of 63 m/s^2 was applied. Table 4.2 shows that this should result in a constant horizontal acceleration of the rigid sphere of 13.7 m/s^2.

The elastic material properties given to the 'fluid' are shown in Table 4.3. The elasticity of a material can be defined with any two of the four elastic material constants: Young's modulus E, Poisson's ratio ν, bulk modulus K, and shear modulus G, where,

$$G = \frac{E}{2(1+\nu)} \tag{4.23}$$

$$K = \frac{E}{3(1-2\nu)} \tag{4.24}$$

The first set of models were defined with the bulk modulus of water (2.25×10^9 kPa) and a range of Poisson's ratios. The second set of models were those employed in the previous FE models of Ruan *et al.* (1993) and Kang *et al.* (1997) as shown in Table 2.4, and also the Young's modulus of brain tissue as used by many of the earlier models. The results of the first set of models are shown in Figure 4.10, which demonstrates that the rigid sphere is oscillating with a very high frequency and low amplitude. The results from the second set of models are shown in Figure 4.10, along with the constant acceleration displacement history achieved from the equivalent Eulerian model. This set of results

shows lower frequency, higher amplitude oscillations.

The results clearly demonstrate that these substitute fluid models are extremely unrepresentative of the original fluid/solid system. This is to be expected because unlike the fluid, the solid material cannot flow to relieve stress and absorb energy. Hence as the rigid sphere accelerates to the right, the elastic material in front of and behind it is compressed and extended respectively until the spring energy it acquires is enough to bounce the sphere back to its initial position, at which point the cycle repeats. Incidentally, the frequency of the oscillations is still a function of the bulk modulus as given by Equation 4.20 and shown in Table 4.3.

Name	ν	E (Pa)	G (Pa)	K (Pa)	Frequency Model (Hz)	Frequency Theory (Hz)
Water	**0.48**	180.0×10^6	60.8×10^6	$\mathbf{2.25\times10^9}$	8200	6538
Water	**0.49**	90.0×10^6	30.2×10^6	$\mathbf{2.25\times10^9}$	7600	6538
Water	**0.499**	9.0×10^6	3.0×10^6	$\mathbf{2.25\times10^9}$	6382	6538
Ruan	**0.485**	$\mathbf{148.5\times10^3}$	50.0×10^3	1.65×10^6	214	177
Kang	**0.48**	$\mathbf{12.0\times10^3}$	4.1×10^3	100.00×10^3	55	44
Brain	**0.499**	$\mathbf{66.7\times10^3}$	22.2×10^3	11.12×10^6	447	460

Bold numbers are given, others are calculated.

Table 4.3: Elastic material properties used for substitute fluid material.

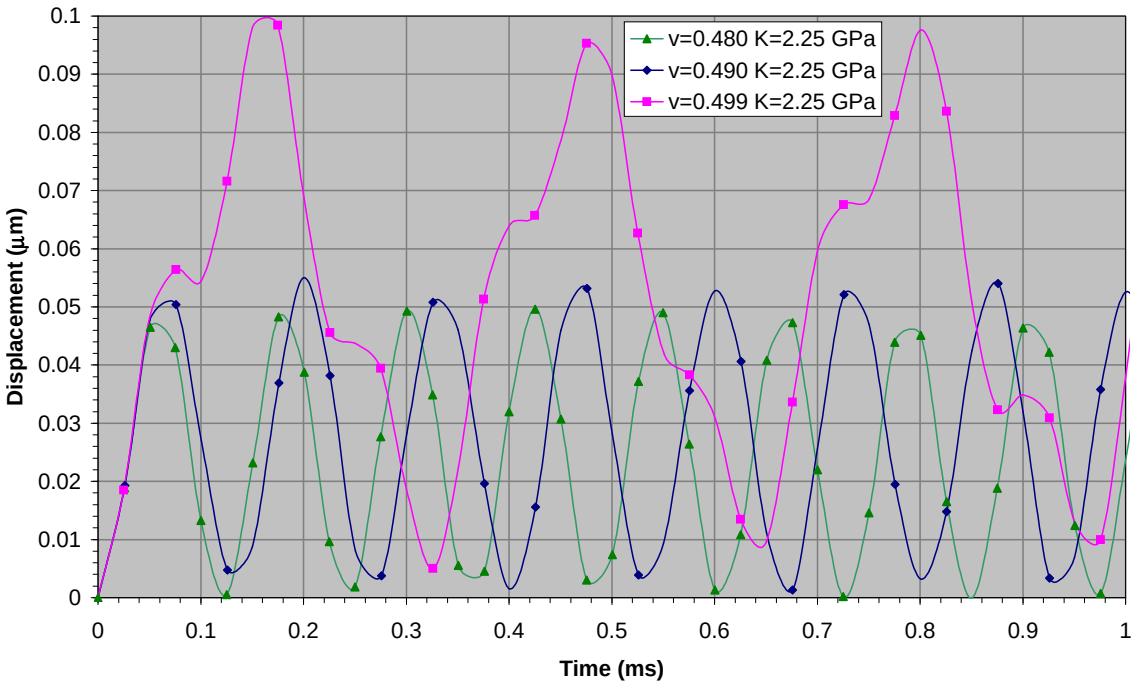

Figure 4.10: Displacement history of sphere surrounded by a solid with the same bulk modulus as fluid.

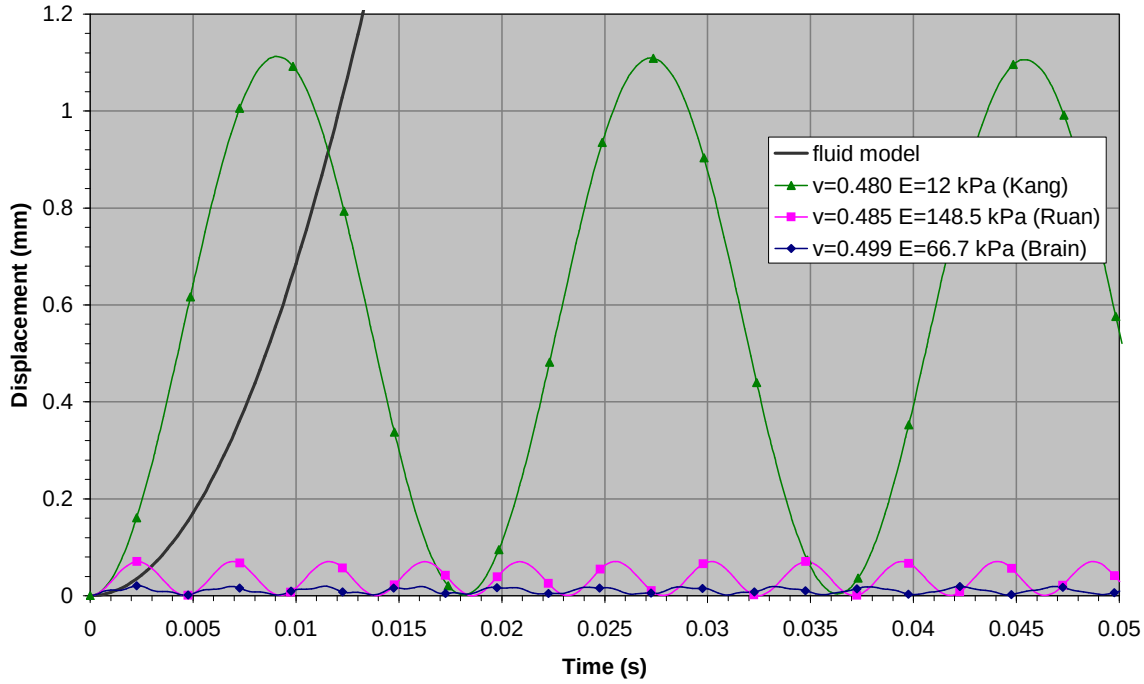

Figure 4.11: Displacement history of sphere surrounded by various fluid substitute elastic materials.

4.5 Conclusions

This chapter has presented the fluid forces that act on the brain as it accelerates within the skull. The buoyancy force alone will reduce the acceleration of the brain within the skull to only 3.3% of the acceleration of the skull. In addition the acceleration reaction force produced by the layers of fluid between 1 mm and 10 mm thick will increase the inertial mass of the brain by factors of approximately 25 to 2.5 respectively, further reducing the relative acceleration of the brain to perhaps only 0.13–1.00% of the skull acceleration. Furthermore, both these forces are evenly distributed over the entire brain surface, and hence will cause no large localised stresses on the brain.

This explains why humans (and all animals for that matter, notably woodpeckers) are extremely resistant to head injury caused by translational accelerations. The fact that none of these forces help reduce the relative rotational acceleration of the brain explains our vulnerability to injuries caused by head rotation, especially subdural haematoma which is primarily caused by movement of the brain within the skull.

The significant effect of these forces means that any finite element model which is to model the motion of the brain within the skull with any reliability *must* take them into account. Unfortunately finite element software has only recently become sophisticated enough to allow the modelling of fluid/solid interaction forces, and hence all earlier models which ignore the fluid or modelled it as a soft solid must be regarded with caution. While these earlier models may still be useful in some applications, for example to determine areas of relatively high stress concentration under impact, etc., there is no way they can accurately predict the motion of the brain within the skull.

Most importantly, this chapter had demonstrated that MSC.Dytran is capable of modelling buoyancy and acceleration reaction forces and hence the first known model of a human head which accurately models the cerebrospinal fluid can be produced. Unfortunately there are small discrepancies in the buoyancy force cause by uneven geometry which become significant as the density of the solid approaches that of the fluid, but the impact of this error can and will be assessed in the next chapter.

MODELLING SHAKEN BABY SYNDROME

5.1 Introduction

This chapter describes the development of a finite element model of an infant's head and its application to modelling shaken baby syndrome. The geometry is derived from a series of magnetic resonance images (MRI) of sagittal sections of the child's head, and includes the brain, cerebrospinal fluid (CSF), tentorium cerebelli and rigid skull.

The model was initially used to determine the added mass coefficients of the complex geometry by simulating constant acceleration of the skull in pure vertical, lateral and sagittal translation, with an artificially dense rigid brain and no tentorium. The model was then used to simulate the combined rotation and translation representative of shaken baby syndrome and the effects of various elastic and viscoelastic combinations of brain material models were investigated.

The strain of several bridging veins was then investigated with the different material models, vein locations, input amplitude and frequency to estimate the effect of these variables on the likelihood of bridging vein failure as discussed in Chapter 3.

5.2 Model Development

The geometry of the brain and inner skull surfaces was derived from a series of 11 MRI scans of sagittal sections of the right-hand half of the head of an 11 week old male infant.

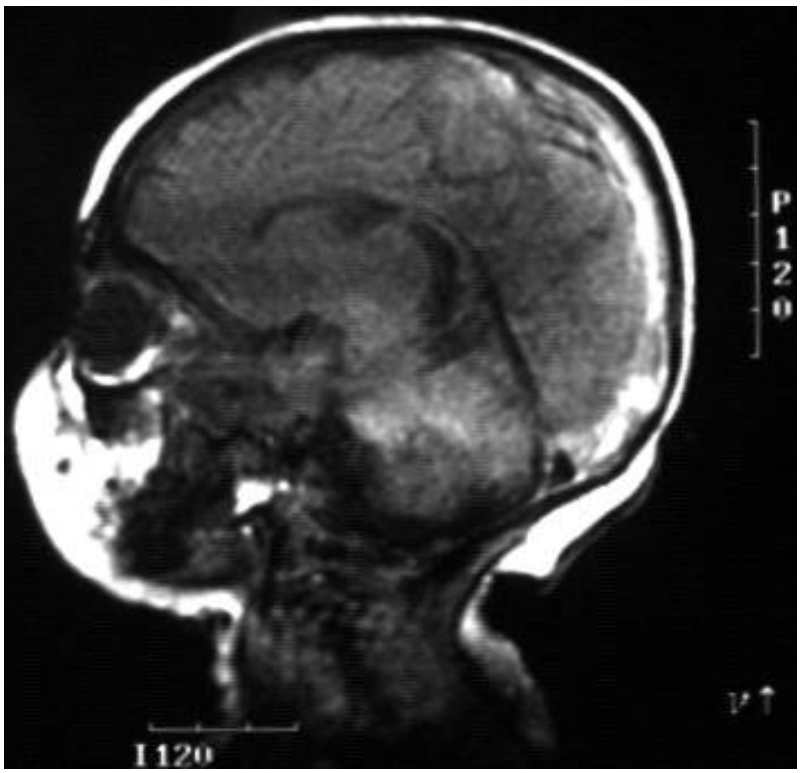

Figure 5.1: Sample magnetic resonance image of the child's head.

A sample image is shown in Figure 5.1. The images were captured from the film using a digital video camera and imported into Matlab.

Software was written in Matlab to display each image in a window and for the coordinates of points on the brain and inner skull surface to be determined simply by clicking on the image. The ability to magnify the image allowed accurate placement of the points, and the horizontal and vertical calibration marks on each image allowed the origin and rotation of each image to be accounted for. The inner cavity of the skull is subdivided into three cavities by the falx cerebri which runs fore and aft, and the tentorium cerebelli which runs side to side across the back of the head. The anterior cavities are occupied by the left and right cerebral hemispheres, the posterior cavity by the cerebellum, all joined by the brain stem. For the purposes of this model however, the two cerebral hemispheres and the cerebellum were considered to be one continuous body, which greatly simplified the geometry digitisation and mesh generation processes and should not have a great impact on the results of the model since it will mainly be used to investigate relative fore/aft

(sagittal) brain movement at the vertex (the highest point of the brain).

A Matlab function was then written which returned the brain and skull radii for given angles of azimuth and elevation about an assumed origin. This function was used to create an MSC.Patran (MSC.Dytran's pre- and post-processor) session file which when played by MSC.Patran automatically creates sets of points, curves and surfaces which define the brain and skull geometry. Unfortunately, the doubly-convex nature of the brain at the sphenoid ridge (shown in Figure 5.2) caused MSC.Patran's automatic hex mesher to produce inverted elements in this region, hence the complete brain solid had to be subdivided into 6 exterior solids and one central cube which could all be successfully meshed. The exterior faces of the elements on the surface of the brain were then extended to the skull surface and subdivided radially to produce the CSF mesh.

The exterior faces of the the CSF elements were then duplicated to create a surface mesh to represent the skull rigid body. Arbitrary Lagrange Euler (ALE) coupling surfaces were also defined at the interfaces of the brain/CSF and CSF/skull meshes. Eight of the CSF elements at the mid-sagittal line and the base of the brain were duplicated to create brain stem elements, and the two-dimensional tentorium elements were created manually between existing brain and CSF nodes to resemble the actual tentorium geometry as closely as possible. Brain stem and tentorium nodes were merged with coincident brain and skull nodes. Sliding contact between the brain and skull was made possible by defining the surfaces already defined for the brain ALE coupling and the skull rigid body as contact surfaces.

The falx cerebri was not included in the model because it was assumed that it would have little effect on the translation or rotation of the brain in the sagittal plane. This assumption was based on the fact that the falx is not in direct contact with the sides of the brain hemispheres, instead it is separated by a thin layer of fluid which, in the absence of viscosity, would provide little resistance to the motion of the brain parallel to it. Conversely the tentorium cerebelli is effectively perpendicular to the sagittal plane and hence will apply direct forces to the surrounding brain tissue as it moves normal to

Region	Element Type	Elements	Nodes
Brain	3D Lagrangian	3584	3873
CSF	3D Euler	993	1542
Skull	2D Rigid	512	514
Spine	3D Lagrangian	8	27
Tentorium	2D Lagrangian	128	153

Table 5.1: Number of elements and nodes used in the finite element model.

it. If lateral motion were to be included then the effect of the falx cerebri would be more significant and it thus it should be included in such models.

The resulting mesh is shown in Figure 5.2, with half of the brain and one-quarter of the CSF removed to reveal the tentorium. The volume of the brain elements was 466 cm^3, giving a brain mass of 0.485 kg for a density of 1040 kg/m^3. A summary of the type, and number of elements used in the model is given in Table 5.1.

Nine bridging veins were included in the model by placing non-linear spring elements between nine pairs of nodes on the brain and skull surface near the vertex in the mid-sagittal plane. The springs were programmed with the force/displacement behaviour from Figure 3.4. The strain of the bridging veins was estimated using a user-defined subroutine which calculates the distance between these node pairs and writes these distances and the elapsed time to a simple text file. The location and numbering of the veins is shown in Figure 5.2.

5.2.1 Added Mass Coefficients of the Model

The complex geometry of the brain and CSF will mean that it will have slightly different added mass coefficients for translation in every direction. To determine the added mass coefficients in the sagittal (x), vertical (y) and lateral (z) directions the brain was defined as a rigid body with density $\rho_s = 2000\ kg/m^3$, the CSF was given density $\rho_f = 1005\ kg/m^3$ and a gravity field (g) of 100 m/s^2 was applied in each of the three directions in separate models. All six degrees of freedom of the skull rigid body were fixed to avoid movement of the skull. An unrealistically large brain density was used to avoid MSC.Dytran's problems

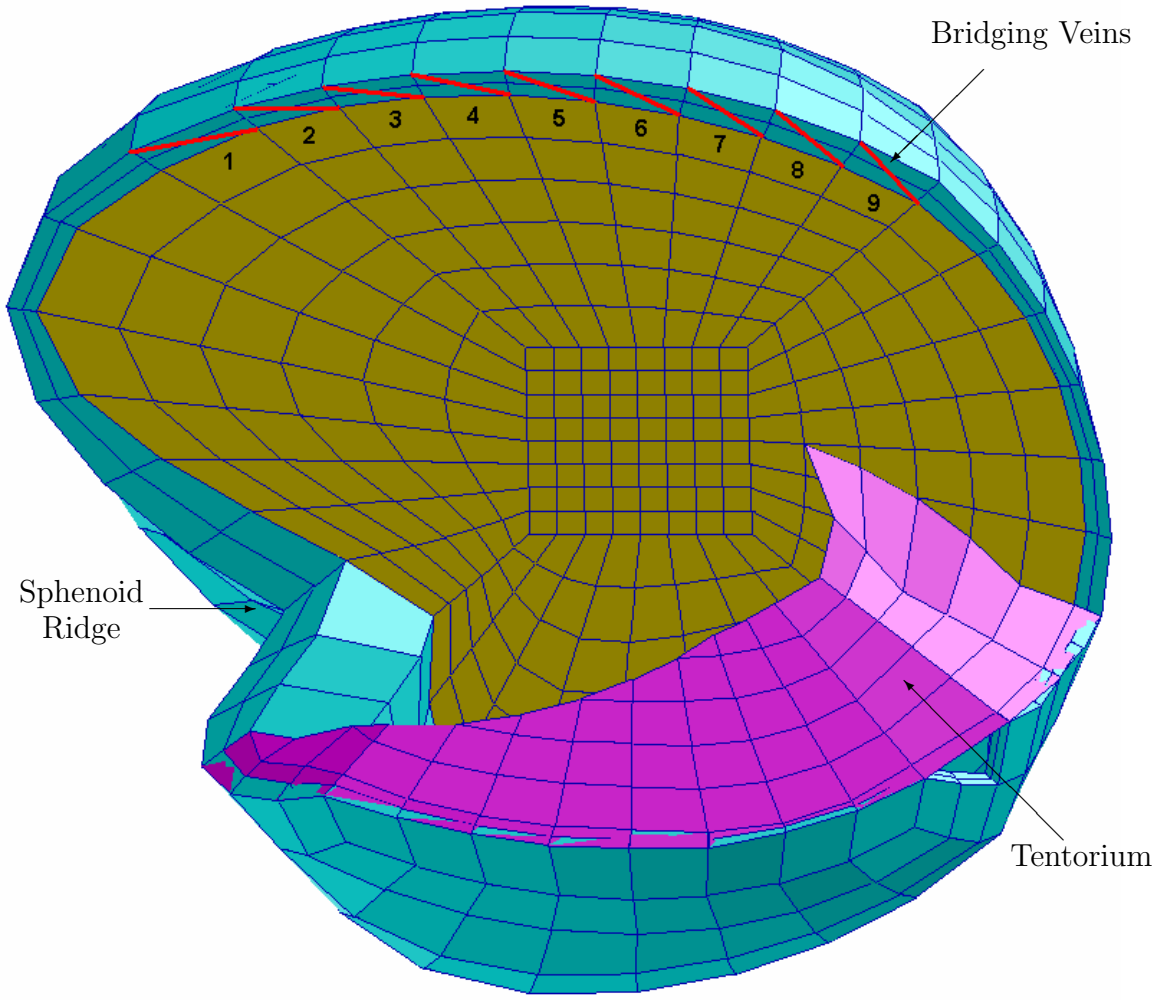

Figure 5.2: The finite element model showing the brain, CSF, tentorium cerebelli and bridging veins.

of modelling buoyancy forces when the relative density is low (as reported in Section 4.3.2) and to produce more displacement and hence more accurate results within shorter model durations. The added mass coefficient (α) in each direction was then calculated from the acceleration reported by the model using the equation,

$$\ddot{x} = g_x \left(\frac{\rho_s - \rho_f}{\rho_s + \alpha_x \rho_f} \right) \tag{5.1}$$

The results for the three models are in Table 5.2, with added mass coefficients within the expected range for that of a perfect sphere surrounded by a 1–10 mm fluid layer. Assuming a mean added mass coefficient of $\alpha = 14.54$, the expected relative acceleration of a brain with density 1040 kg/m^3 would be,

$$\begin{aligned} a &= 100 \left(\frac{1040 - 1005}{1040 + 14.54 \times 1005} \right) \\ &= 0.22 \text{ m/s}^2 \end{aligned} \tag{5.2}$$

This shows that the combined effect of the buoyancy and acceleration reaction forces on the brain is to reduce its relative translational acceleration to only 0.22% of the translational acceleration applied to the skull.

Direction	Axis	Acceleration (m/s^2)	Added Mass Coefficient
Sagittal	x	6.34	13.62
Vertical	y	6.80	12.56
Lateral	z	5.10	17.43
Mean			14.54

Table 5.2: Added mass coefficients for the final model.

5.3 Boundary Conditions

All previous models discussed in this and the previous chapter have employed frames of reference moving with the outer container, sphere or skull which simplifies the visualisation

of the movement of the submerged body relative to it. This was done by completely fixing the outer container and applying inertial acceleration fields via the `GRAV` option. This was only possible because the applied acceleration field did not change direction.

When a baby is held by its torso and shaken back and forth, the movement of its head will be similar to simple harmonic oscillations about a pivot in the neck. This motion includes both translational and rotational components, and the resultant acceleration of the head will be continually changing direction. Furthermore, the inertial acceleration experienced by each particle within the head will vary according to its position vector from the centre of rotation. Therefore the `GRAV` option cannot be used. MSC.Dytran also provides the option `RFORCE` which defines a rotational force field and would be ideal for this situation, however the centrifugal forces produced by this option are applied only to Lagrangian elements and rigid surfaces. This means that the force field would not produce a pressure gradient in the fluid and hence buoyancy forces would not be effective. Therefore, in order to apply a realistic motion to the model a fixed frame of reference had to be used and the skull moved through it. To verify that MSC.Dytran still models the fluid/solid interaction forces correctly in a fixed frame of reference some of the previous models were re-run with equivalent results.

Therefore, the only boundary condition that needs to be applied to the model is the rigid body motion of the skull. This was done using the `EXFUNC` user-defined function to describe the translational and rotational velocities of the skull rigid body. These functions were based on purely sinusoidal sagittal (forwards–backwards) translation and rotation of the skull about a pivot at the base of the neck. It was decided to start the motion of the skull from the fully forward position, since in this position the skull would have zero initial velocity and hence no initial velocity conditions needed to be applied to the model. Therefore the oscillation of the skull, as shown in Figure 5.3 was programmed into the user-defined function as equations 5.4, 5.7 and 5.10, where θ_0 is the amplitude of the oscillations, ω is their frequency and r is the distance of the centre of mass of the skull from the neck pivot.

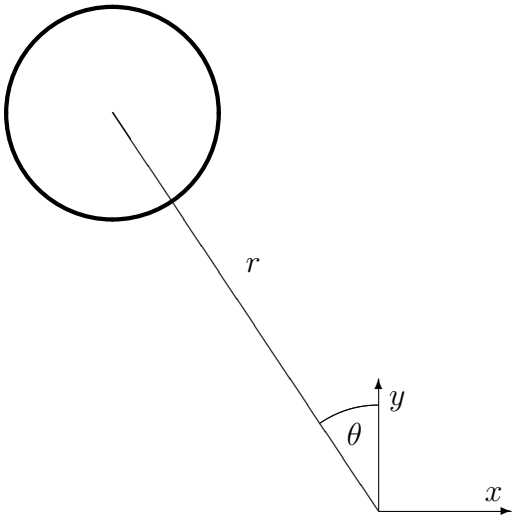

$$\theta = \theta_0 \cos(\omega t) \tag{5.3}$$
$$\dot{\theta} = -\omega\theta_0 \sin(\omega t) \tag{5.4}$$

$$x = -r \sin\theta \tag{5.5}$$
$$\dot{x} = -r\dot{\theta}\cos(\theta) \tag{5.6}$$
$$= \omega r\theta_0 \sin(\omega t)\cos(\theta_0 \cos(\omega t)) \tag{5.7}$$

$$y = r\cos(\theta) \tag{5.8}$$
$$\dot{y} = -r\dot{\theta}\sin(\theta) \tag{5.9}$$
$$= \omega r\theta_0 \sin(\omega t)\sin(\theta_0 \cos(\omega t)) \tag{5.10}$$

Figure 5.3: Motion of skull

5.4 Material Properties

The skull surface was defined as a rigid body and hence needed no material properties. The CSF was given a density of $\rho_{csf} = 1005$ kg/m^3 and bulk modulus $K_{csf} = 2.25$ GPa. The tentorium cerebelli was given a density of $\rho_{tent} = 1130$ kg/m^3, Young's modulus $E_{tent} = 31.5$ MPa and Poisson's ratio $\nu_{tent} = 0.45$, taken from Table 2.4 and similar to that of McElhaney *et al.* (1973). The brain and brain stem were given a density of $\rho_{brain} = 1040$ and each of the isotropic, linear viscoelastic properties listed in Table 5.3. These are taken from Table 2.4 but also includes others from Sauren and Claessens (1993). Models were run with each set of material properties, using an input oscillation with frequency of 4 Hz and amplitude of 60°.

Figure 5.4 shows the stretch ratio of the bridging vein which experiences the largest strain for each model using the brain material properties in Table 5.3. The peak stretch ratio (λ) for each model is also listed in Table 5.3. These results show that the large range of material properties are causing peak stretch ratios between 1.015 and 1.3, demonstrating the importance of the choice of the brain material properties, and the lack of agreement on these properties in the literature. However, investigating the source of the properties used in the models reveals that:

Author	Year	G_0 (kPa)	G_∞ (kPa)	β (s^{-1})	K (GPa)	λ
Galbraith	1988	11.02	5.512	200	2.19	1.300
Zhou	1996	38	7	700	2.19	1.243
Kang	1997	49	16.7	145	1.125	1.127
DiMasi	1991	34.45	17.225	100	2.19	1.098
Kuijpers	1995	338	169	100	2.19	1.022
Ruan	1993	528	168	35	2.19	1.015

Table 5.3: Brain material properties tried in the model.

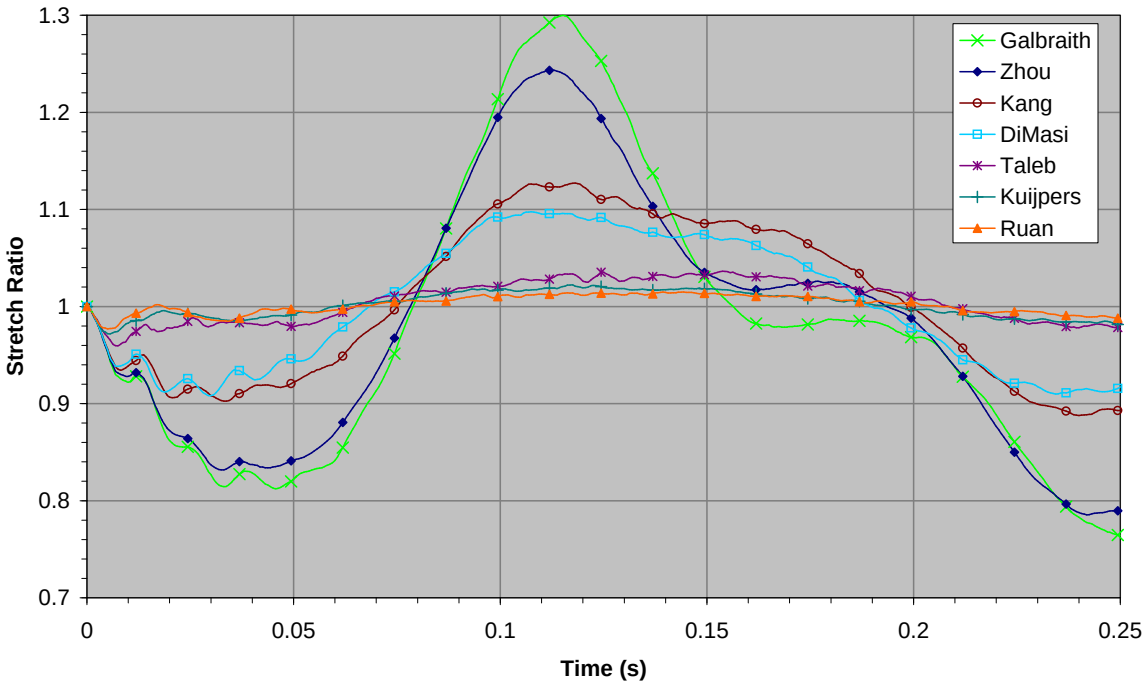

Figure 5.4: Maximum bridging vein stretch ratio due to different material properties.

- Ruan *et al.* (1993) reports that his material properties were scaled from the results of the experiments performed by Galford and McElhaney (1970). These experiments consisted of creep, relaxation and free-vibration tests performed in compression, resulting in a complex Young's modulus for human brain tissue. It is unclear how these results were converted into the long- and short-term shear moduli by Ruan *et al.* but the fact that they were compression moduli and not shear moduli may explain the very low brain deformation produced by this material model.

- Kuijpers *et al.* (1995) claims to have achieved their material properties by using the average of those reported in the review of Sauren and Claessens (1993). This review includes the models of Galbraith *et al.* (1988), DiMasi *et al.* (1991), another identical to Kang *et al.* (1997) and a fourth model, resulting in actual average values of $G_0 = 46.3$ kPa, $G_\infty = 11.96$ kPa and $\beta = 123$ s^{-1}. Therefore the average properties used by Kuijpers *et al.* appear to be incorrect.

- Galbraith *et al.* (1988) used a physical model consisting of a silicone gel as a substitute for brain matter, and the properties used in the finite element model were determined from mechanical tests on the gel and modified to replicate the results of the physical model. Hence the material model is of a gel, not brain tissue.

- DiMasi *et al.* (1991) do not quote the original source of their material properties.

This leaves the models of Zhou *et al.* (1996) and Kang *et al.* (1997), who both converted their model from the torsional shear experiments of Shuck and Advani (1970), in which the variation of the complex shear moduli with frequency is clearly tabulated to facilitate the conversion of these properties into other representations of viscoelastic properties. Zhou *et al.* used the interconversion equations of Christensen (1982) while Kang *et al.* do not explain how they arrived at their converted values which are slightly different from those of Zhou *et al.*. The interconversion equations of Christensen (1982) relate the complex

shear modulus,

$$G^* = G'(\omega) + iG''(\omega) \tag{5.11}$$

to the shear relaxation modulus,

$$G(t) = G_\infty + \hat{G}(t) \tag{5.12}$$

where,

$$\hat{G}(t) = (G_0 - G_\infty)e^{-\beta t} \tag{5.13}$$

using the equations,

$$G'(\omega) = G_\infty + \omega \int_0^\infty \hat{G}(t)\sin(\omega t)dt \tag{5.14}$$

$$G''(\omega) = \int_0^\infty \hat{G}(t)\cos(\omega t)dt \tag{5.15}$$

$$\hat{G}(t) = \frac{2}{\pi}\int_0^\infty \frac{G'(\omega) - G_\infty}{\omega}\sin(\omega t)d\omega \tag{5.16}$$

$$\hat{G}(t) = \frac{2}{\pi}\int_0^\infty \frac{G''(\omega)}{\omega}\cos(\omega t)d\omega \tag{5.17}$$

where, $G'(\omega)$ and $G''(\omega)$ are the real and imaginary parts of the complex shear modulus, and, G_0 and G_∞ are the short- and long-term shear moduli respectively.

Equations 5.16 and 5.17 were used to convert the complex shear moduli from the data of Shuck and Advani (1970) into the time domain, as shown in Figure 5.5. This figure also shows the shear moduli of Zhou *et al.* (1996) and Kang *et al.* (1997) plotted against time using Equations 5.12 and 5.13. Clearly the moduli of Zhou *et al.* produce a better fit to the experimental data, however the limited frequency range of the experimental data means that the integrals fail to converge causing the oscillatory nature of the converted moduli.

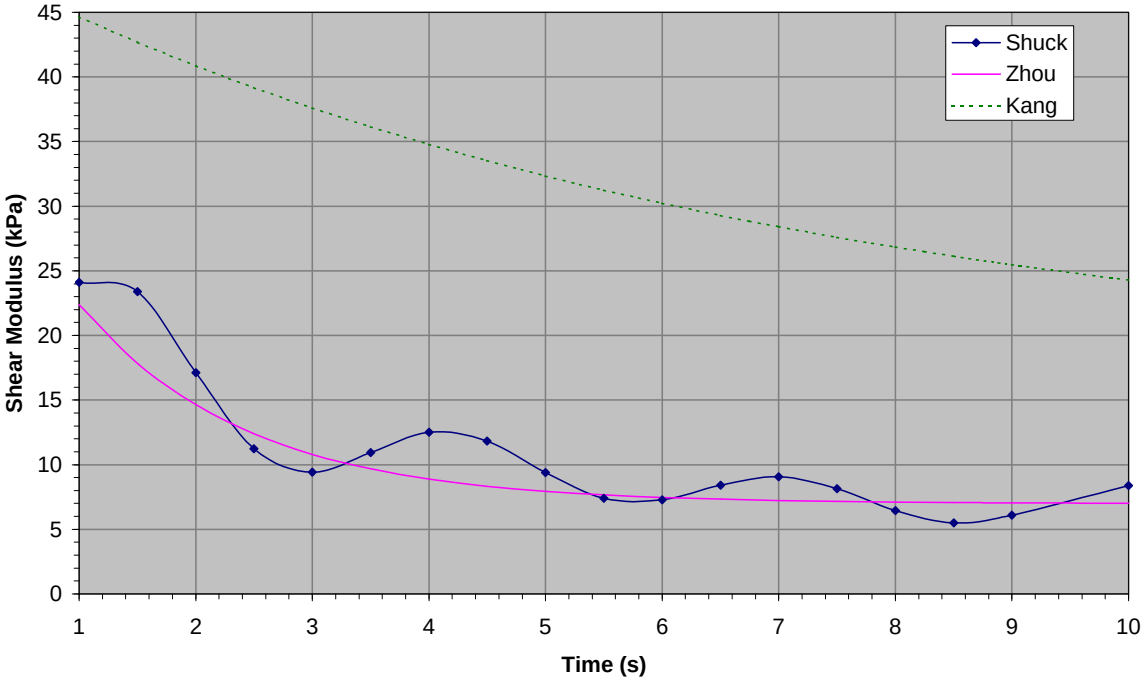

Figure 5.5: Shear modulus of Shuck and Advani (1970) converted into the time domain and compared to the moduli of Zhou *et al.* (1996) and Kang *et al.* (1997).

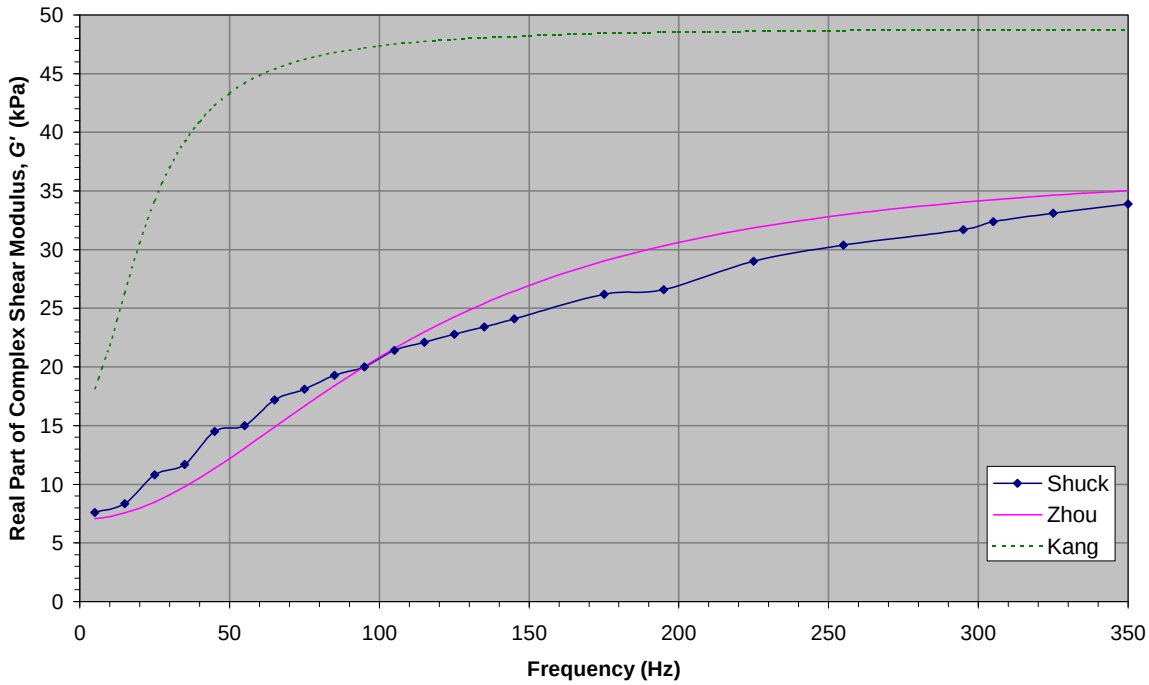

Figure 5.6: Shear moduli of Zhou *et al.* (1996) and Kang *et al.* (1997) converted into the frequency domain and compared to the experimental data of Shuck and Advani (1970).

A more accurate method of assessing the properties of Zhou *et al.* (1996) and Kang *et al.* (1997) is to use Equation 5.14 to convert their properties into the real part of the complex shear modulus and then comparing these with the actual tabulated data of Shuck and Advani (1970). Because these moduli result in a continuous function of time, the integration in Equation 5.14 can be performed over a much longer time range to ensure convergence. Figure 5.6 shows the results of this, and again the model of Zhou *et al.* (1996) produces a much better fit to the experimental data, at least when using the method of Christensen (1982).

Therefore it was decided to adopt the material properties of Zhou *et al.* (1996) in all subsequent models, since these are the only properties for which the sources of both the physical experiments and the method of conversion is known to be reliable, and also because the model was verified favourably against experimental data.

5.5 Results

The previous section has already shown the effect of the material properties on the maximum strain of the bridging veins. Figure 5.7 shows the motion of the brain within the skull using the chosen properties of Zhou *et al.* (1996), an input frequency of 4 Hz and amplitude of 60°. The choice of 4 Hz as the input frequency was taken from Duhaime *et al.* (1987) in which the angular acceleration histories of the baby doll shaking experiments are plotted. The input amplitude of ±60° was determined to be representative of the maximum range of passive motion of 20 infants' heads, as measured using a goniometer by Dr Sunderland, Consultant Paediatrician at Birmingham Children's Hospital (personal communication).

Figure 5.7a shows the position of the brain and skull as the head moves backwards during the first half of the first cycle, and Figure 5.7b shows the head moving forwards during the rest of the cycle. The motion of the brain and the extension of the bridging veins goes through several stages:

1. As the skull starts translating and rotating backwards the brain lags forward since it is more dense than the CSF. Since the bridging veins drain forwards from the brain into the midsagittal sinus they are relaxed as the brain moves forwards within the skull producing a stretch ratio less than 1.

2. Then as the skull decelerates towards the rear extremity of its motion the brain continues accelerating backwards until the back of the brain approximates with the skull and the brain is compressed against it. It is at this point in the motion that Figure 5.4 shows the peak stretch ratio.

3. As the skull rotates forwards the brain begins to move forwards reducing the strain of the bridging veins.

4. The skull starts to decelerate as it rotates forwards while the brain continues moving forwards, further relaxing the bridging veins.

5.5.1 Multiple oscillations

Figure 5.8 shows the stretch of the nine bridging veins during four complete oscillations at 4 Hz and amplitude 60°. It is evident that after the first transient oscillation all subsequent oscillations are effectively identical, and cause slightly less stretch of the bridging veins. This is because at the start of the subsequent oscillations the brain is compressed against the front of the skull instead of in the centre of the head as it is before the first oscillation, hence the brain can move further backwards during the first oscillation. Although a consequence of the initial conditions used in the model, it is likely that under real shaking conditions brain compression against the front of the skull after the first shake will reduce bridging vein strain in subsequent shakes and hence the first shake could be considered the most dangerous.

Figure 5.9 shows the peak stretch of each of the nine veins during each cycle. This distribution is typical of all the previous models, with vein 4 consistently experiencing the highest stretch ratio.

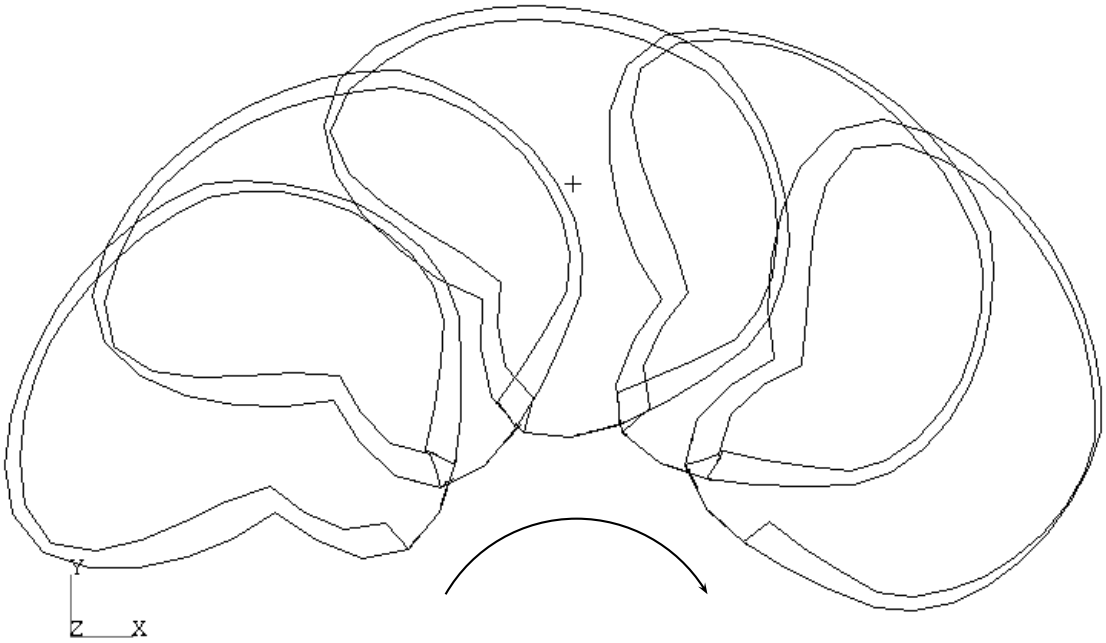

(a) Backwards motion of the head, $0 \leq t \leq 0.125$ s.

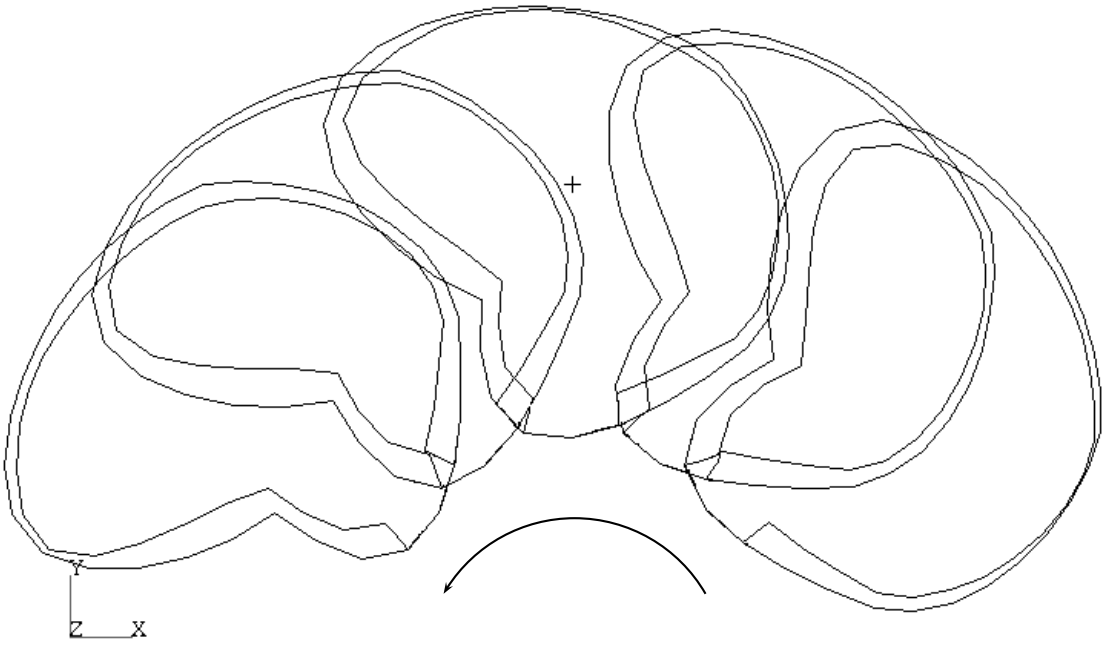

(b) Forwards motion of the head, $0.125 \leq t \leq 0.25$ s.

Figure 5.7: Backwards and forwards motion of the head for one cycle.

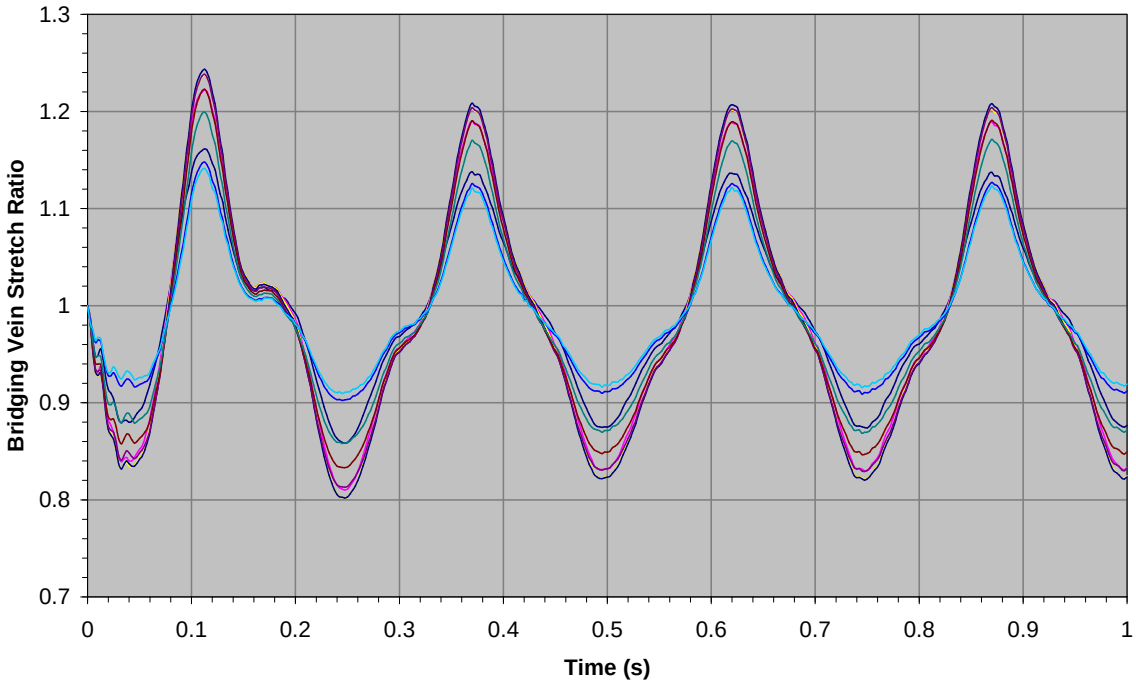

Figure 5.8: Stretch ratio of the nine bridging over 4 oscillations at 4 Hz.

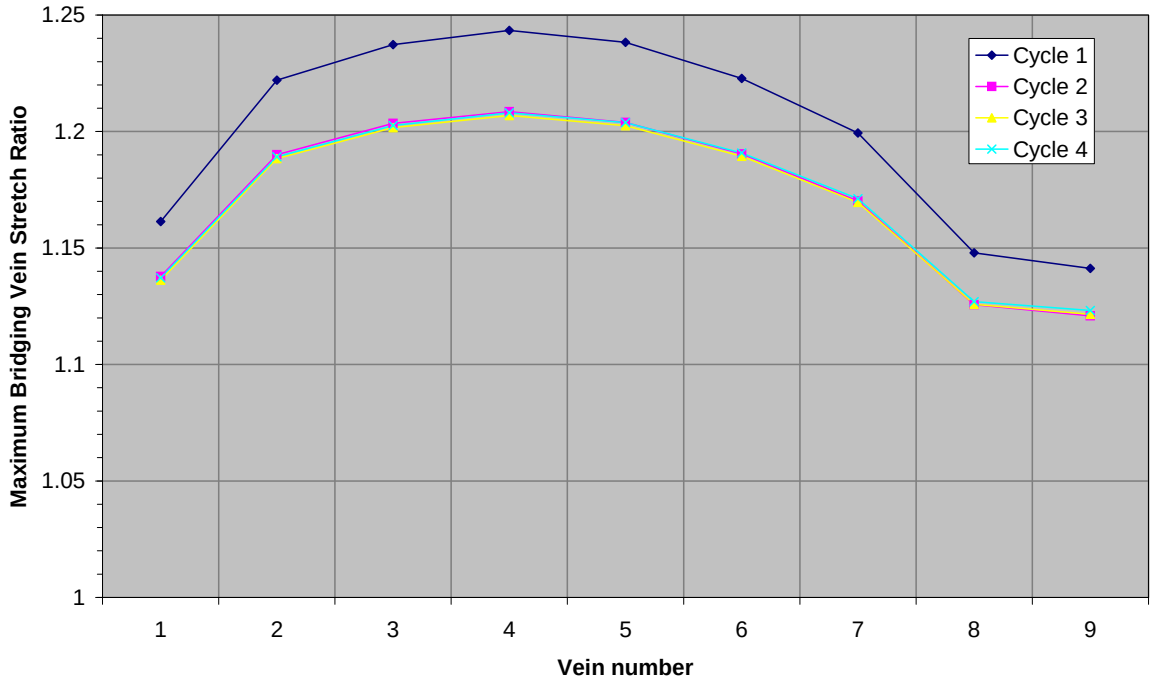

Figure 5.9: Comparative stretch ratio of the nine bridging veins for each oscillation.

5.5.2 Effect of Bridging Vein Elasticity

Figure 5.10 compares the standard results with those achieved when the nine bridging vein spring elements are removed from the model. This shows that the bridging vein elasticity causes a reduction in stretch ratio from 1.256 to 1.243, a 5% reduction in strain.

5.5.3 Effect of the Tentorium Cerebelli

Figure 5.11 shows the effect of running the model with and without the tentorium cerebelli during one oscillation at a frequency of 4 Hz and amplitude 60°. The tentorium has the dramatic effect of reducing the maximum stretch ratio from 1.608 to 1.243, a 60% reduction in strain. Therefore it is of great importance that the tentorium cerebelli is included in finite element models of heads, especially when there is movement in the sagittal plane. Similarly, if lateral or oblique motions are to be modelled then the falx cerebri will have a significant effect.

5.5.4 Translation vs. Rotation

Figure 5.12 shows the stretch ratio caused by isolated translation, isolated rotation about the skull centre of mass, and the full combined rotation and translation (i.e. rotation about the neck pivot). This clearly demonstrates the influence of the fluid forces acting to protect the brain from translational accelerations, since the isolated translational components of the motion cause stretch ratios of only 1.016 compared to 1.243 for the full motion at a frequency of 4 Hz and amplitude 60°. Thus the rotation is responsible for over 93% of the bridging vein strain.

5.5.5 Effect of the Brain Density

Section 4.3.2 described a small discrepancy when using MSC.Dytran to model buoyancy when the density of the fluid and submerged solid are very close, as are the densities of CSF and brain tissue. It was discovered that this discrepancy could be compensated for

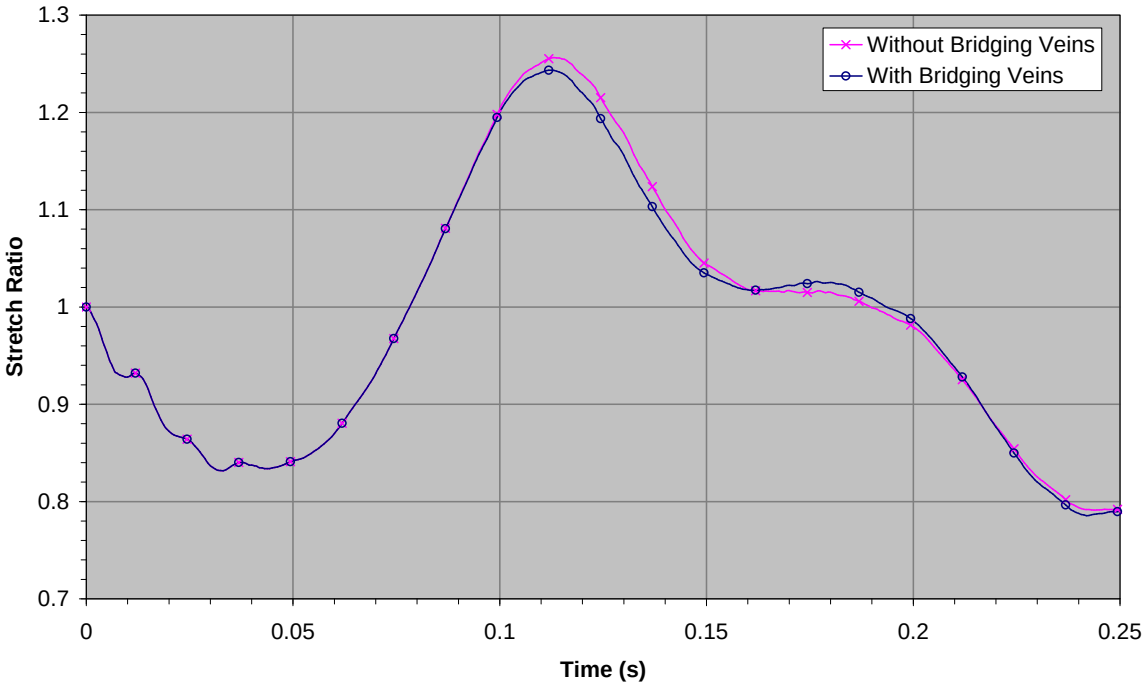

Figure 5.10: Effect of bridging vein elasticity on the bridging vein strain.

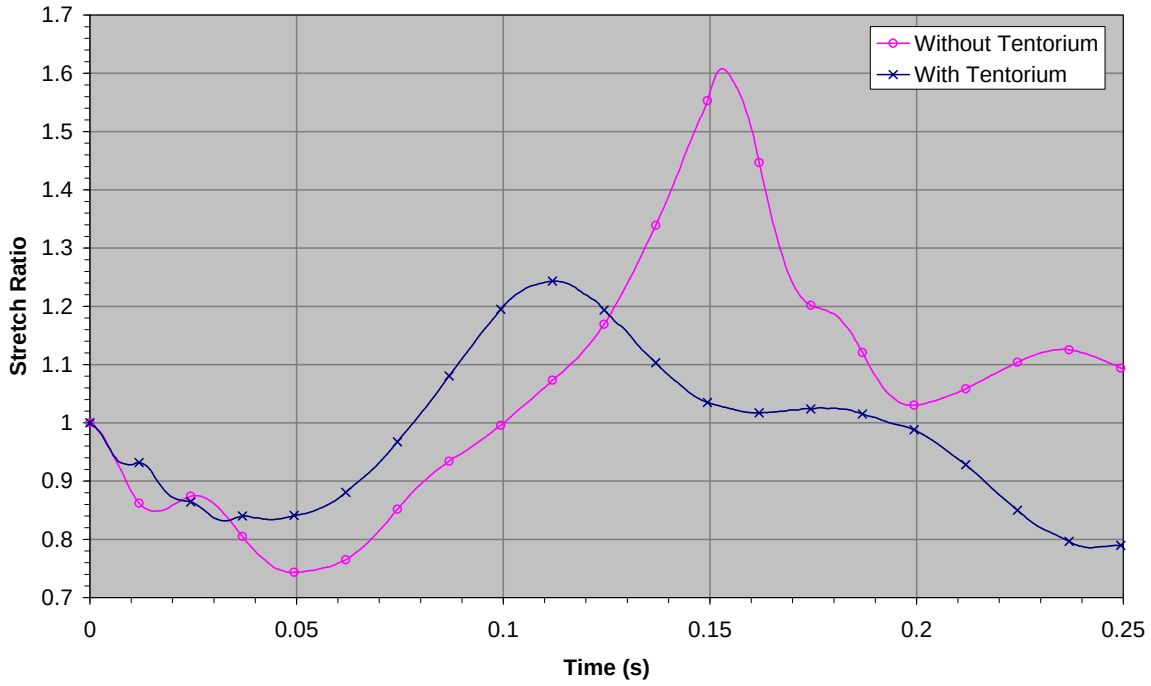

Figure 5.11: Effect of the tentorium cerebelli on the bridging vein strain.

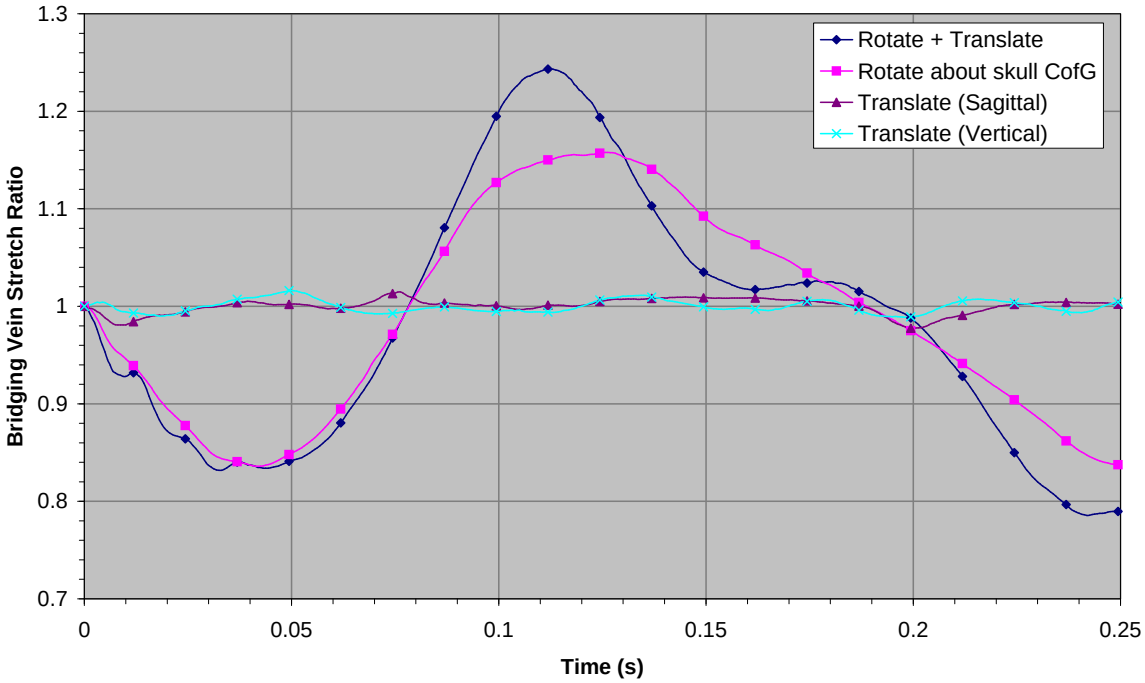

Figure 5.12: Effect of isolated translation and rotation.

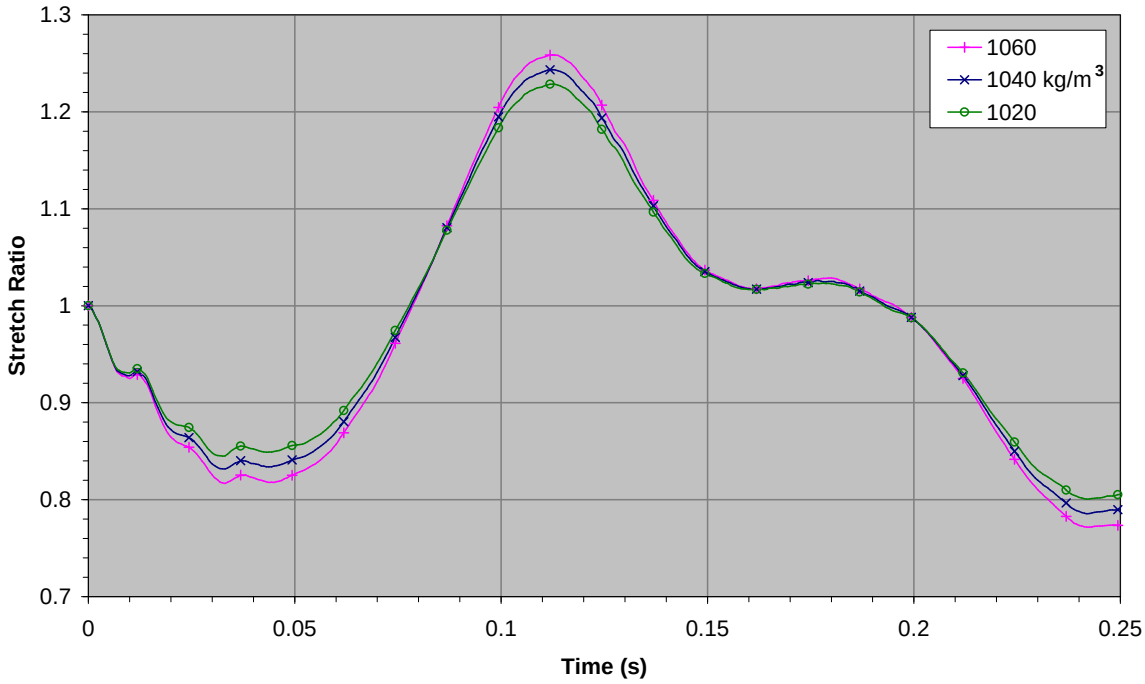

Figure 5.13: Effect of the brain density on the bridging vein strain.

by increasing the density of the submerged sphere by just 8 kg/m^3. The effect of this problem on the model of a baby's head was investigated by comparing the results obtained when using the correct density of 1040 kg/m^3 with those for 1020 kg/m^3 and 1060 kg/m^3.

This is shown in Figure 5.13, and it is evident that a significant change in density of $\pm$20 kg/m^3 causes relatively little change in the stretch ratio of the bridging veins, and hence MSC.Dytran's 'neutral buoyancy' problem can safely be ignored. The insensitivity of the model to this error follows from Section 5.5.4 which showed that the translational component of the shaking motion is responsible for only 7% of the bridging vein strain. The small errors in the buoyancy force calculations will only have an effect on the translation of the brain within the skull, which in itself is much less significant than the rotation of the brain.

5.5.6 Effect of Input Frequency and Amplitude

Figure 5.14 shows the stretch ratio of vein 4 (which was stretched the most in all models) during the first cycle for an amplitude of 60° at frequencies of 2–10 Hz. Figure 5.15 shows the maximum of all these stretch ratios plotted against frequency, along with those for oscillations of 20° and 40°.

As expected, oscillations of higher amplitude or frequency produce higher stretch ratios, with a high degree of sensitivity between frequencies of 2–6 Hz and with lower sensitivity at higher frequencies. The curves seem to flatten out consistently at stretch ratios of around 1.5. This is because the initial vein strain is caused by movement of the brain as a whole, but at higher frequencies or amplitudes the brain comes into contact with the skull and further vein strain can only caused by brain compression against the back of the skull.

These curves can be plotted against peak angular acceleration, $\ddot{\theta}_p$ (rad/s^2) instead of frequency by taking the maximum of the derivative of Equation 5.4 to give:

$$\ddot{\theta}_p = \omega^2 \theta_0 \tag{5.18}$$

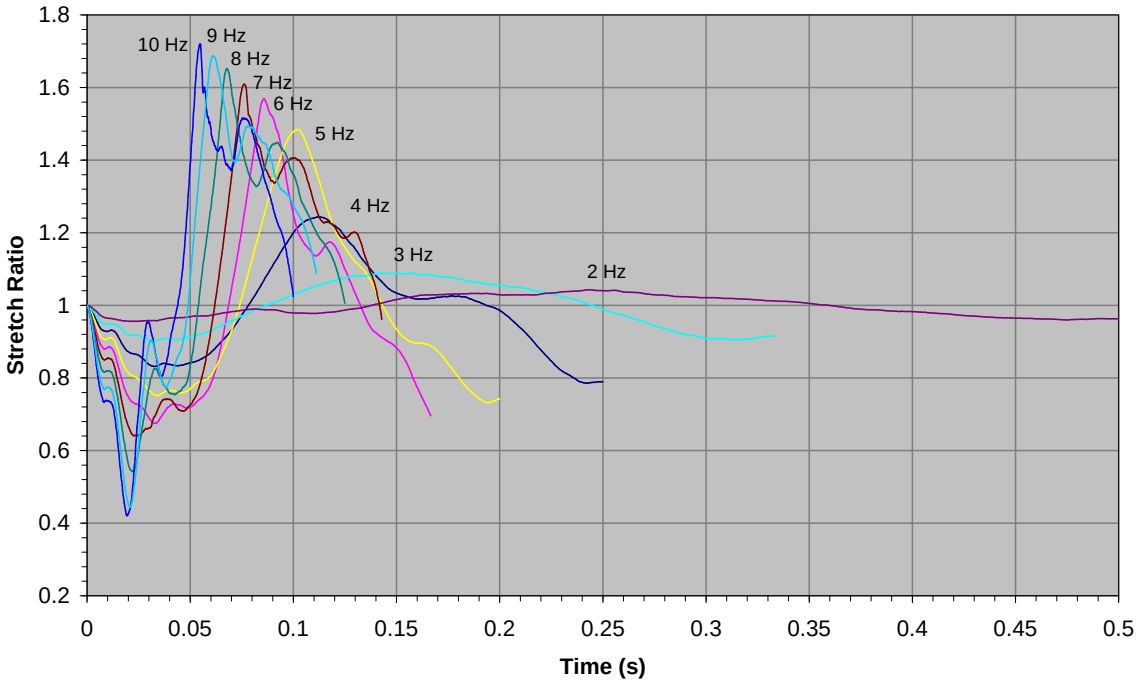

Figure 5.14: Effect of shaking frequency on the bridging vein stretch ratio for an amplitude of 60°.

This gives Figure 5.16 which shows that the stretch ratio is roughly proportional to the peak angular acceleration below approximately 1234 rad/s^2, and linearly related above 1234 rad/s^2. This relationship is represented approximately by:

$$\lambda \approx \begin{cases} 1 + 4.5 \times 10^{-4}\,\ddot{\theta}_p & \text{for} \quad 0 \le \ddot{\theta}_p \le 1234 \text{ rad/s}^2, \\ 1.476 + 6.3 \times 10^{-5}\,\ddot{\theta}_p & \text{for } 1234 \le \ddot{\theta}_p < 4000 \text{ rad/s}^2. \end{cases} \tag{5.19}$$

5.5.7 Strain Rate

The strain rate of the bridging veins was calculated directly from the rate of change of the strain vs. time data. This gives Figure 5.17 with the strain rate plotted against frequency, and Figure 5.18 with the stain rate plotted against peak angular acceleration. This shows that the bridging veins are stretched at speeds up to 105 mm/s for shaking frequencies up to 4 Hz, which gives strain rates of about 10 s^{-1} given the average model bridging vein length of 11 mm.

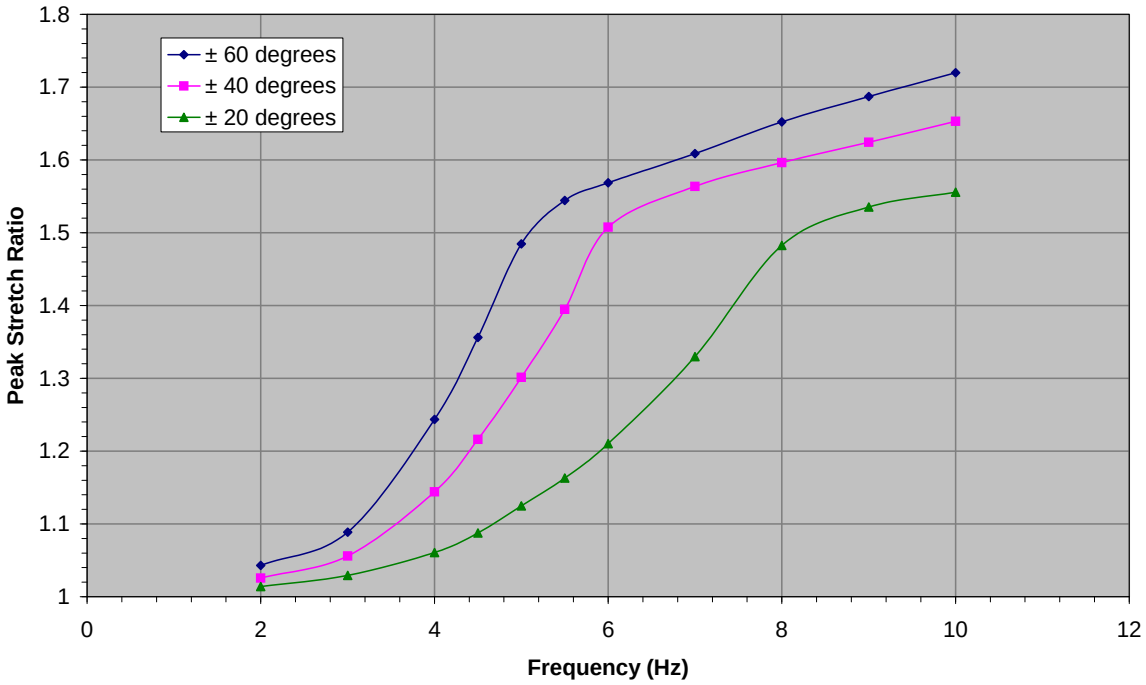

Figure 5.15: Effect of shaking frequency and amplitude on the bridging vein stretch ratio.

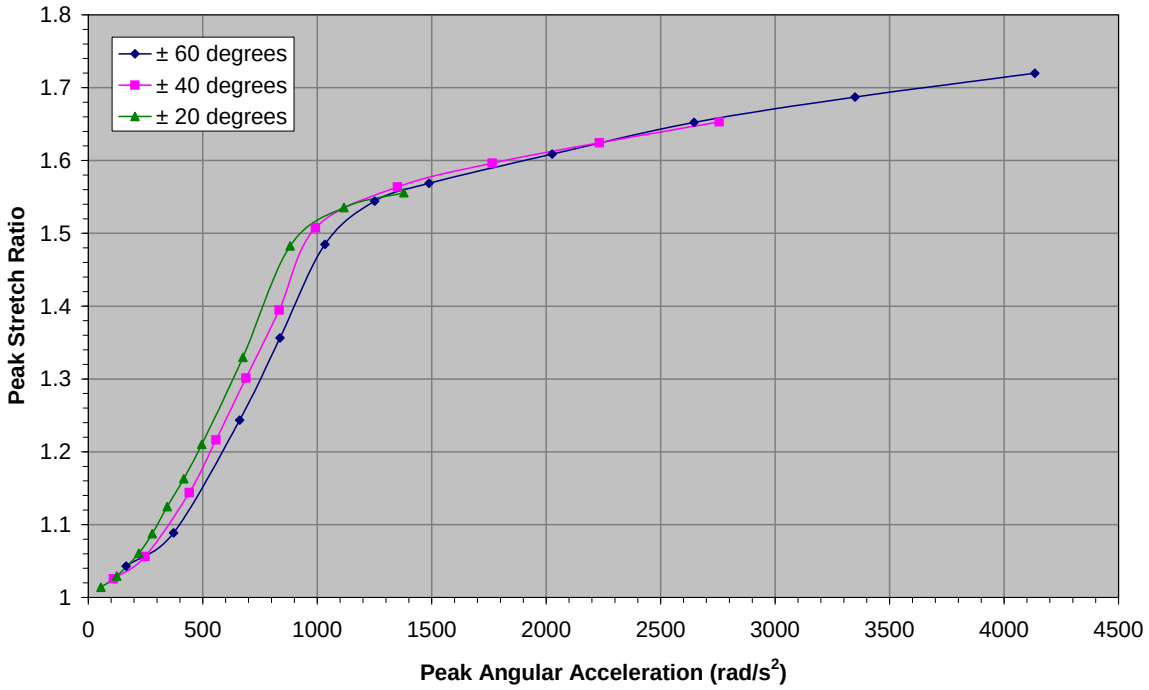

Figure 5.16: Effect of peak angular acceleration on the bridging vein stretch ratio.

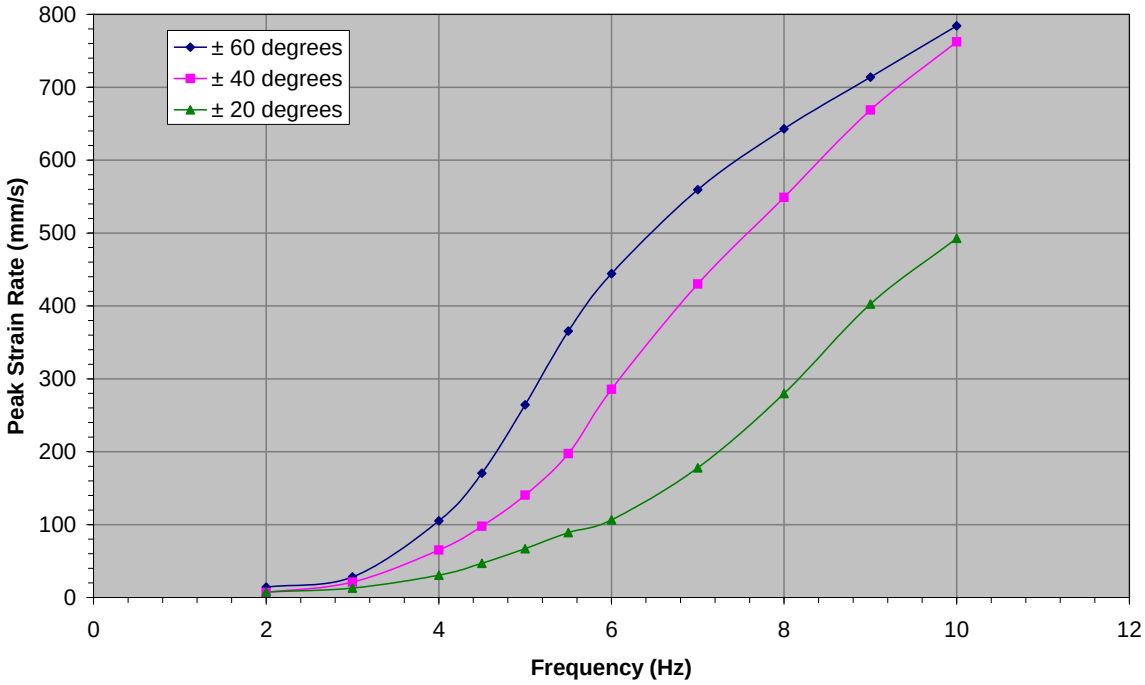

Figure 5.17: Effect of shaking frequency and amplitude on the bridging vein strain rate.

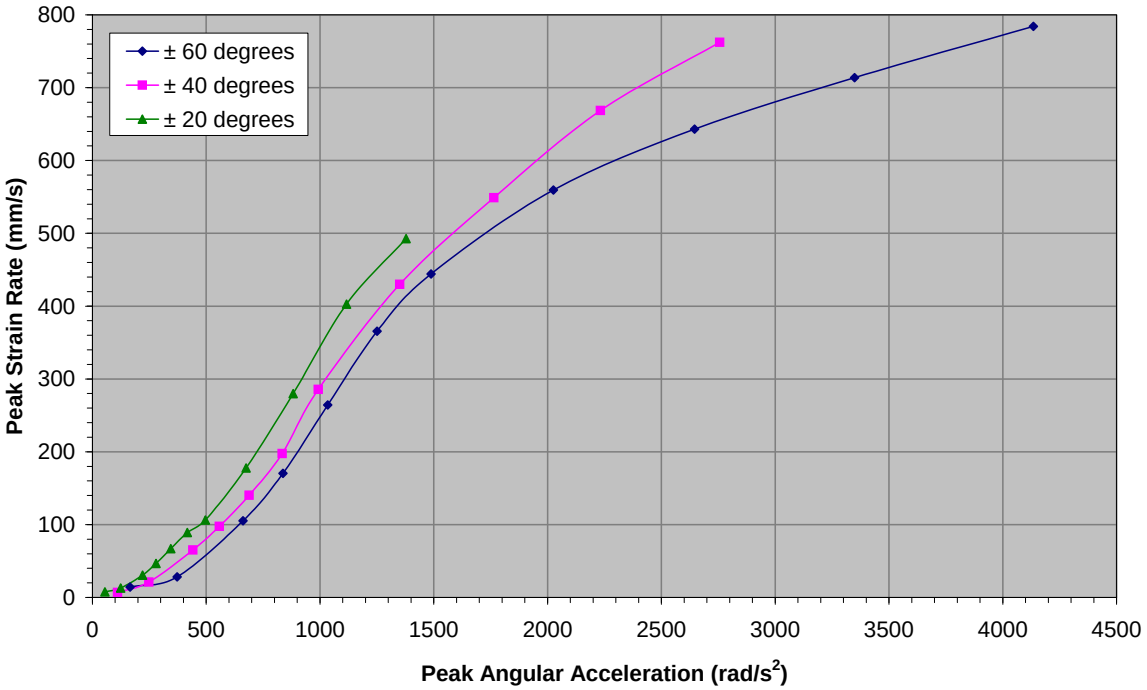

Figure 5.18: Effect of peak angular acceleration on the bridging vein strain rate.

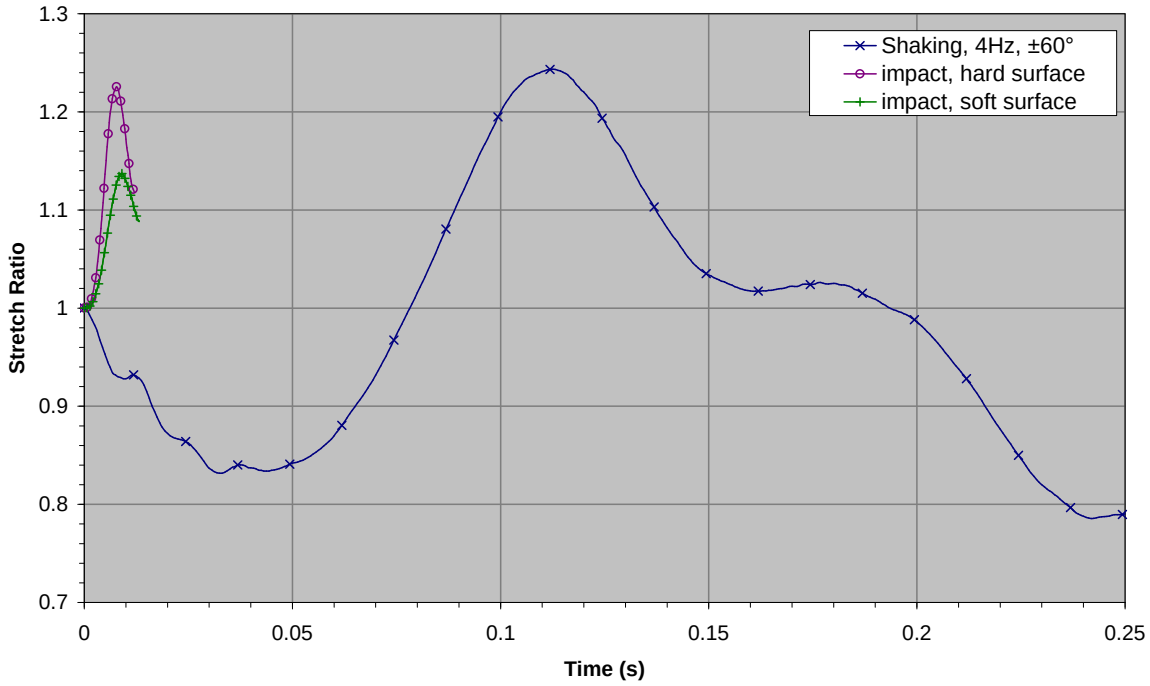

Figure 5.19: Bridging vein strain caused by hard and soft impacts compared to shaking.

5.5.8 Modelling Impacts

Impacts of the head against both hard and soft surfaces were also modelled. Since the skull is a rigid body in this model, any impact has to be applied either through the modelling of the resulting inertial forces or as enforced motion of the skull. The acceleration histories presented by DiMasi *et al.* (1991) were used as the inputs, and consisted of effectively half-sine wave accelerations with amplitude 300 G and duration 8 ms for the hard impact and amplitude 160 G, duration 10 ms for the soft impact. These translational accelerations were converted to angular accelerations about the neck pivot, with the head rotating in the more dangerous forwards direction representing an occipital impact. Figure 5.19 shows peak stretch ratios of 1.226 and 1.137 for the hard and soft impacts respectively, and 1.243 for the shaking. This suggests that shaking can be just as dangerous as hard impacts, and considerably more dangerous than soft impacts.

5.5.9 Brain Stresses

Figure 5.20 shows the Von Mises stress distribution in the brain at the instant of maximum stress for shaking at 4 Hz and all three amplitudes. As expected they show the stress increasing from the brain stem to the vertex, up to almost 800 Pa, however the steep stress gradients around the widest section are unexpected.

Figure 5.21 shows the stress distributions for the hard and soft impacts, with peak coup stress occurring shortly after impact and peak contrecoup stress occurring shortly after the angular acceleration input is removed. In these models the peak stresses are approximately 2 kPa and 1.6 kPa respectively for the coup and contrecoup stresses during the hard impact, and 1.2 kPa and 0.8 kPa respectively for the coup and contrecoup stresses during the soft impact.

Previous finite element models of head injury (see Section 2.4) report brain stresses in the order of 80 kPa, considerably higher than those found in this research, however this is to be expected for several reasons:

- Shaking was expected to produce more whole brain movement and hence less brain stress because there is more time for the brain to move as a whole.
- All previous models failed to model the cerebrospinal fluid, and hence the stresses are transferred directly from the skull to the brain tissue.
- The accurate inclusion of the cerebrospinal fluid in this model allows for fluid flow and whole brain movement, both of which would relieve internal brain stress and absorb energy.
- Previous models may have modelled the impacts more accurately and paid more attention to the boundary conditions involved - either by applying the impact as an enforced displacement instead of a prescribed acceleration, or by providing more restraint to the movement of the head. Since this new model was not specifically designed to model impacts it does not include any resistance to movement at the neck pivot.

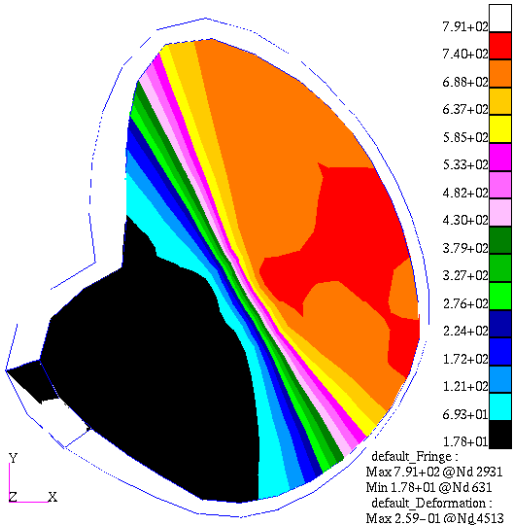

(a) Instant of maximum stress for ±60°.

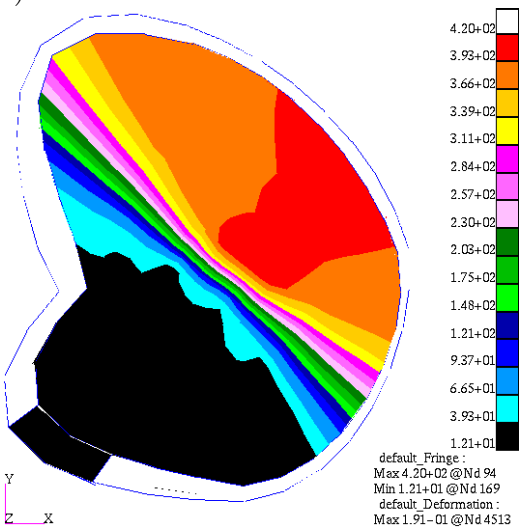

(b) Instant of maximum stress for ±40°.

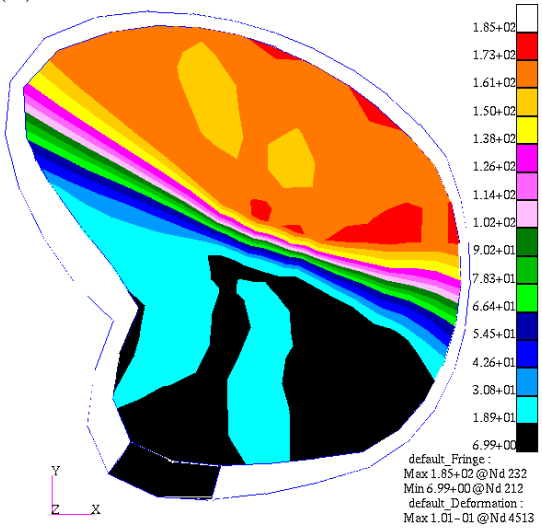

(c) Instant of maximum stress for ±20°.

Figure 5.20: Von Mises stress distributions during shaking at 4 Hz and ±60°, ±40° and ±20°.

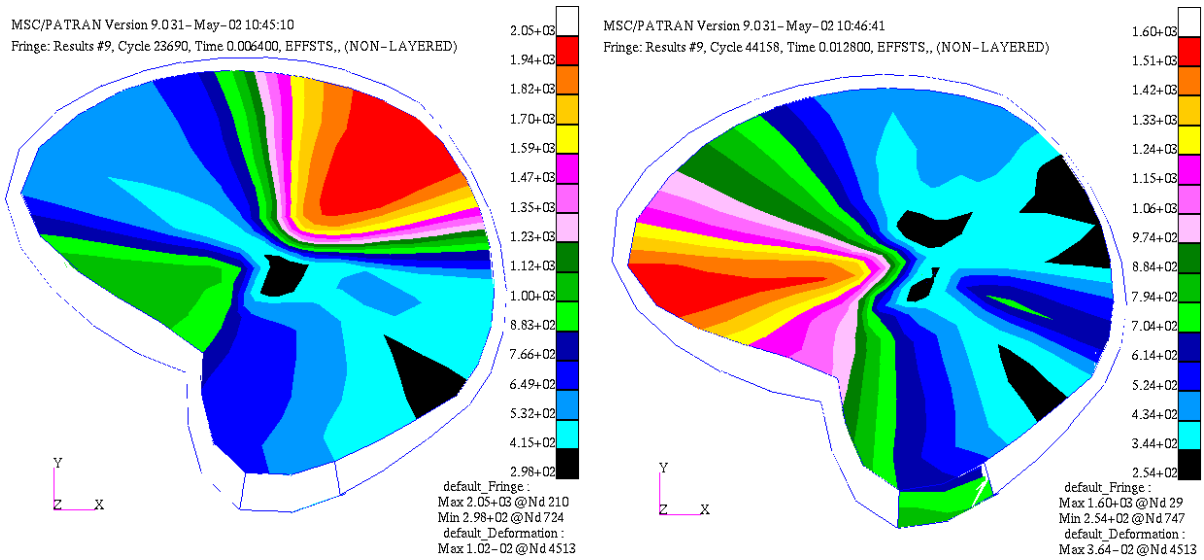

(a) Instants of maximum coup and contrecoup stresses for hard occipital impact.

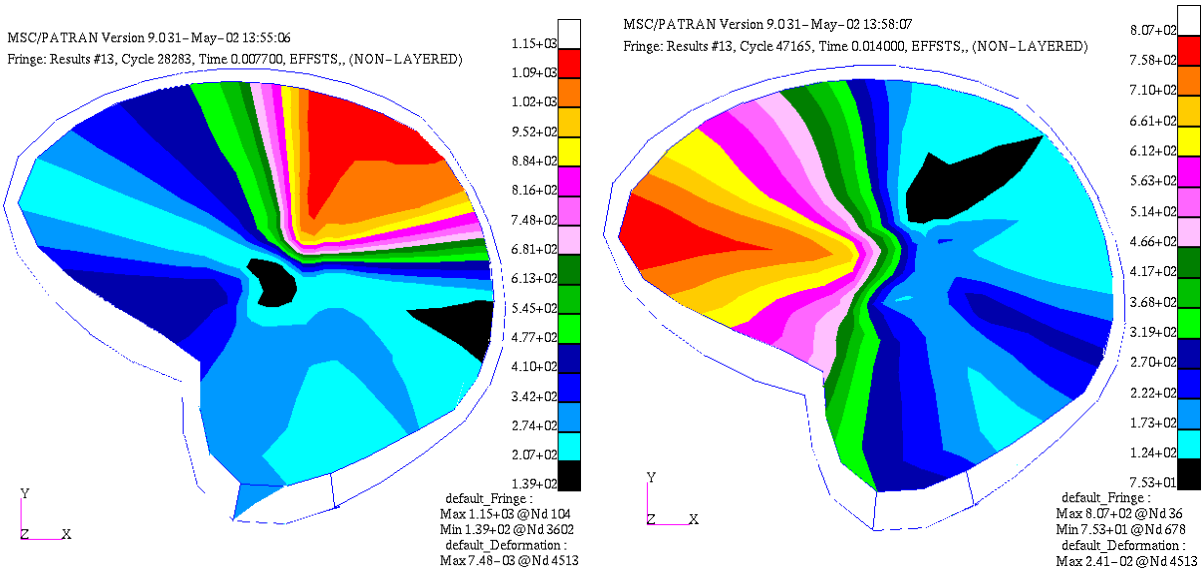

(b) Instants of maximum coup and contrecoup stresses for soft occipital impact.

Figure 5.21: Von Mises stress distributions during impacts against hard and padded surfaces.

5.6 Discussion and Conclusions

The finite element model developed in this chapter is the first published model of a baby's head specifically designed to model shaken baby syndrome and which incorporates a realistically modelled fluid and fluid/solid interactions. Normally finite element models need to be verified against experiments of a similar nature to the situations being analysed before any validity can be given to the results of the model, but in this case that is impossible since no experimental data exists that is comparable to this model. Previous reports involving head injury modelling claim to have verified the models against the experiments of Nahum *et al.* (1977) in which the intracranial CSF pressure is reported during impacts, and yet these models (which do not include any fluid elements) were then employed to model very different scenarios and concentrated on different, unverified results. Furthermore, Section 4.4 demonstrated that these fluid-as-soft-solid models cannot even yield correct results for relative brain displacement under simple horizontal acceleration conditions, and Section 5.4 showed that the wide range of different material parameters used for the brain tissue in these previous models produce significantly different results. Therefore the practice of verifying models against one set of limited experiments and then trusting the results of the model when modelling different scenarios needs to be questioned.

While it is impossible to verify this new model against experimental data, care was taken to ensure that the modelling software used was physically capable of accurately modelling fluid/solid interactions (as reported in Chapter 4), and then subsequent improvements to the model geometry, boundary conditions and material parameters were individually verified to be as accurate as possible. As Chapter 3 concluded, the inherent variability of biological tissue samples and the difficulties involved in testing the failure properties of bridging veins means that even if it were possible to completely verify the current model against some experimental data, it would still be impossible to derive accurate tolerance criteria for shaken baby syndrome based purely on the modelling results. Nevertheless, this new model does give an important new insight into the probable magnitude of relative brain motion and bridging vein strain during shaken baby syndrome

and has produced various other conclusions in the process.

The investigation into the effect of various brain material properties used in previous finite element models has highlighted the fact that the wide range of properties causes a very significant difference to the results of this model. Therefore more care needs to be taken in the choice of material properties in future finite element models, and the results of previous research which used unrealistic properties perhaps need to be regarded with caution. The sources of the properties used (where available) are listed in this chapter and show a range of sometimes questionable sources and conversions. The properties used by Zhou *et al.* (1996) were shown to be the only set which have a reliable source and an acknowledged interconversion technique (which was verified in this chapter), and therefore these were the properties used in the current model.

This chapter has demonstrated that the average added mass coefficient of the human infant brain/skull geometry is approximately 14.5, and hence the combined effect of the buoyancy and acceleration reaction forces on the brain is to reduce its relative translational acceleration to only 0.22% of the translational acceleration applied to the skull. This is a very important effect, and it explains why impacts and inertial accelerations which produce mainly translational head accelerations are unlikely to cause severe brain injury. For example, the literature is peppered with clinical observations (and animal experiments, including Ommaya and Gennarelli, 1974) of straight-line head impacts with fast-moving rigid bodies causing severe skull fractures in which the patients do not even experience concussion.

This explains the next conclusion which is that the rotational component of the shaking motion is responsible for approximately 93% of the bridging vein strain. The tentorium cerebelli which probably provides the brain with most of its protection against sagittal rotation — and was shown by this model to reduce the bridging vein strain by 61% — is still not as effective as the CSF is at providing protection against translation, and therefore rotational accelerations are extremely dangerous to humans and animals. The relative danger of rotation compared to translation has been well acknowledged since Holbourn

(1943) and has been demonstrated in primate experiments by Ommaya and Gennarelli (1974) and observations of woodpeckers by May *et al.* (1979), all of which are reviewed in Section 2.2.4. However, all these previous researchers have attributed this difference to brain tissue's very high ratio of bulk modulus to shear modulus as highlighted by Holbourn (1943), but this research has gives support the hypothesis of Hodgson, Shippen and Sunderland (2001) which is that the CSF almost perfectly protects the brain against translational accelerations but effectively acts as a lubricant to brain rotation.

The relative insignificance of the brain translation means that although MSC.Dytran has problems modelling buoyancy with irregular geometries and relative densities close to unity, the effect of this problem on the current model is negligible. Therefore, this research has shown that MSC.Dytran is a reliable and useful tool for modelling shaken baby syndrome and the fluid/solid interactions involved, although care should be taken if it is to be used to model situations where head translation dominates.

The stretch ratio histories presented in this chapter show that maximum bridging vein strain is experienced as the skull is at the rear extremity of its motion and accelerating forwards. At this point in the motion the higher density brain rotates backwards relative to the skull (which is starting to rotate forwards), stretching the bridging veins which drain forwards from the brain surface to the midsagittal sinus. This is in agreement with the general understanding that the brain is more susceptible to injury from occipital impacts than frontal impacts, and hence when characterising head motion for comparison with or development of head injury tolerance criteria care should be taken since lower magnitude forwards rotational acceleration may cause more damage than higher magnitude backwards rotational accelerations.

Comparison of the stretch ratio of the bridging veins in different locations showed that the veins closest to the vertex experience the most strain, which is logical since the vertex is the area furthest from the centre of rotation and therefore undergoes the highest tangential velocities and relative tangential motion between the brain and skull.

Most importantly this chapter has shown that the maximum bridging vein stretch ra-

tio is very sensitive to shaking frequency, especially at frequencies between 2–5 Hz. This means that a relatively small increase in shaking frequency will cause a disproportionate increase in bridging vein strain and hence dramatically increase the likelihood of bridging vein rupture and subdural haematoma. Chapter 3 concluded that while the average ultimate stretch ratio of bridging veins was found to be approximately 1.5, some veins may fail at ratios of as little as 1.15. This chapter has shown that shaking at a frequency of 4 Hz and amplitude of $\pm 60^\circ$ can produce a stretch ratio of approximately 1.26, therefore this chapter can conclude that subdural haematoma may well be a possible result of manually shaking a baby. The chances of subdural haematoma are increased with increasing shaking frequency and amplitude, but less vigorous shaking could also be dangerous in infants which for whatever reason have weaker bridging veins, or if veins are weakened by repeated, milder shaking. Furthermore, the amplitude of $\pm 60^\circ$ was measured without applying any excessive force to the heads of healthy babies, therefore it is likely that forced shaking may cause oscillations of a higher amplitude and hence proportionally higher bridging vein strain.

The results of modelling impacts show that shaking a baby can cause as much if not more bridging vein strain than impacts against hard surfaces, and can easily cause more strain than impacts against soft surfaces. Although the accelerations produced during impacts are considerably higher, the longer duration of the shaking episodes gives more time for whole brain movement and thus are more likely to cause subdural haematoma. Conversely, internal brain stresses which are responsible for concussion and diffuse axonal injury can develop extremely quickly and are therefore more significant in high acceleration, sort duration impacts.

The results from the modelling suggest that, at least for purely sinusoidal oscillations, the relationship between bridging vein strain and peak angular acceleration is approximately linear. Therefore, from Equation 5.18, at a given amplitude of oscillation the stretch ratio is proportional to the square of angular velocity, and for a given angular velocity the stretch ratio is proportional to the amplitude.

CONCLUSIONS

6.1 Conclusions

Each chapter of this thesis has brought relevant information to the shaken baby syndrome debate, including opinions of previous research and the collated statistics of relevant clinical observations to date, through to the deficiencies of previous head injury finite element models and the technical problems involved in overcoming these deficiencies. Finally, the successful development of a sophisticated finite element model of shaken baby syndrome, which for the first time includes the fluid/solid interactions involved was presented, and the model employed to develop approximate injury criteria for causing subdural haematoma by shaking a baby, as well as various other observations.

The motivation for this research was the current lack of understanding of the forces involved in shaken baby syndrome, the impossibility of conducting direct experiments on infants and awareness of the controversy regarding causative mechanisms including whether shaking alone or shaking/impact are needed to cause it. Since the early 1970's clinical observations have been mounting which suggest high incidence of subdural haematoma without any evidence of impact, and Caffey's 'whiplash shaken infant syndrome' (1974) gained acceptance. However, head injury specialists — aware of the very high energies involved in road traffic accident related head injuries — continued to believe that some form of impact must be necessary. Then in 1987 an experimental study seemed to confirm this belief, when Duhaime *et al.* appeared to prove that impact must be necessary to cause subdural haematoma, and since then the term 'shaken/impact' syndrome gained

wider acceptance. This thesis has presented two major facts which cast doubt on the findings of Duhaime *et al.* (1987), including:

- It appears that the primate experiments upon which the study was based involved shaking the animals head's at frequencies of approximately 100 Hz, whereas the study itself produced frequencies up to only 4 Hz when human adults manually shook life-like baby dolls. Therefore, the transferability of the results is questionable.

- The method employed to scale the tolerance levels from the adult monkey experiments to human babies was originally based on internal brain stresses as the cause of injury and only takes into account the different brain masses. Therefore it ignores the greater CSF layers present in babies and also the different nature of concussion and DAI (which are caused by internal brain stresses) compared to SDH (which is caused by movement of the brain as a whole)

This leads to the first major conclusion of this thesis, which is that (as summarised in Table 2.1) on average the published clinical investigations into subdural haematoma in which evidence of even minor head impact or lack thereof is reported, almost one-third of all cases have *no evidence of impact*. Therefore, there is strong clinical evidence in favour of shaken baby syndrome, and little or no evidence capable of categorically disproving shaken baby syndrome.

The review of previous data on material properties of the head contents highlighted that the mechanical testing of human biological samples was very limited, and all tests vary in quality, method and results. This, combined with the fact that biological samples are by their very nature extremely variable in their dimensions and properties, means that the choice of material constituent properties for analytical or finite element models is a great source of error.

This problem is evident from Figure 5.4 in which the previously used brain material properties resulted in bridging vein stretch ratios between 1.015 and 1.300. However, investigating the source of all these properties led to the conclusion that the properties

developed by Zhou *et al.* (1996) are the only set which have a reliable source and verifiable interconversion technique.

The shortcomings of the previous research into bridging vein failure criteria led to additional experiments on human infant bridging veins, and in fact were the first such experiments to use bridging veins from infants. Unfortunately various external circumstances (mainly the enquiry into the Liverpool Alder Hey Hospital organ retention) arose which made it impossible to obtain an adequate number of samples. The limited number of experiments did produce results within the range previously reported (see Table 3.5), although improved precision or data on the effect of strain rate were unobtainable. It was possible to conclude that bridging veins are very small and extremely delicate, and their properties can vary significantly between individuals. This makes it very difficult to rely on tolerance criteria quoted in previous research which are themselves just the averages of a wide range of values. The results of this and previous research indicates that for some veins stretches of as little as 1.15 (ie. strains of only 15%) may be enough to cause failure, therefore shaken baby syndrome tolerance criteria based on the commonly quoted average ultimate stretch of 1.5 may be significantly over-estimated. It must also be remembered that shaken baby syndrome is usually caused when bridging veins fail, but is most likely to occur when the *weakest* veins fail.

The review of previous finite element models then showed that there is a distinct lack of models specifically designed to answer questions about shaken baby syndrome, and that all models either omitted the cerebrospinal fluid layer or modelled it as a very soft solid. Section 4.4 of this thesis demonstrates how such models are incapable of modelling even very simple systems for which the theoretical results is known, and demonstrated how modern modelling software can accurately model these fluid/solid interaction problems. This means that the results of the previous modelling attempts should be regarded with caution, especially where brain displacement and bridging vein strain is concerned.

An important stage of this research was complete when it was shown that the finite element modelling package MSC.Dytran was indeed capable of modelling the complex

interactions between fluids and solids, paving the way for the development of the first finite element model specifically designed to answer questions about shaken baby syndrome, and to our knowledge the first model of head injury to include the cerebrospinal fluid layer accurately. The final model was created using infant brain and skull geometry digitised from a series of MRI scans, and included a viscoelastic brain and brain stem material, rigid skull, linearly elastic tentorium cerebelli membrane, non-linearly elastic bridging veins and of course the cerebrospinal fluid modelled using fluid elements. Immediately various conclusions were demonstrated by the model, including:

- The significant effect of the brain material properties, as already mentioned.
- The combined effect of buoyancy and acceleration reaction forces reduces the translation of the brain relative to the skull to only 0.22% of the translational acceleration applied to the skull.
- The tentorium cerebelli provides significant protection against rotationally induced subdural haematoma by reducing the bridging vein strain by approximately 61%.
- Bridging vein elasticity itself has only the small but not insignificant effect of reducing bridging vein strain by 5%.
- The rotational component of the shaking motion is responsible for approximately 93% of the bridging vein strain.
- Internal brain stresses are significantly lower during shaking than during short-duration impacts. Furthermore the inclusion of the cerebrospinal fluid produces an energy and displacement absorption mechanism which causes lower brain stresses compared to previous models without cerebrospinal fluid.
- At low frequencies or amplitudes of shaking, the bridging vein strain is caused by the movement of the brain as a whole and thus is very sensitive to the input conditions, being roughly proportional to the amplitude and to the square of the frequency. In

other words, the bridging vein strain is proportional to the peak angular acceleration of the head.

- At higher input accelerations, once the bridging veins are stretched by about 50%, further vein strain is caused by brain deformation against the skull and is therefore less sensitive to input conditions.

The importance of rotation to brain injury has been well acknowledged since the early 1940's (see Section 2.2.4), but previously this has been thought to be the result of the brain being much more delicate in shear than it is in compression, since the brain is sheared in rotational motion but compressed in straight-line motion. However, the findings of this research agree with the hypothesis of Hodgson, Shippen and Sunderland (2001) which is that the CSF greatly reduces the translation of the brain within the skull but does very little to stop the brain rotating.

The model has also confirmed that forwards head rotation is considerably more dangerous than backwards head rotation, because bridging veins drain forward from the brain to the skull and hence forwards head rotation (as caused by occipital impacts) stretches the bridging veins whilst backwards head rotation relaxes the bridging veins.

Finally, in order to meet the original objective of this research tolerance levels for causing subdural haematoma by shaking a baby can be estimated from Figure 5.16, however these tolerance levels are only an approximate guide for many reasons, including:

- The variability of human bridging vein failure criteria means that veins could fail at strains usually between 30%–70%, but perhaps as little as 15% for some weaker veins.

- Geometric and material property approximations involved in the creation of the model.

- The infinite differences in size, shape, strength, etc. between individual infants and suspected shakers.

- The shaking motion modelled in this research is a purely sinusoidal rotation of the head about a pivot in the neck, and hence is only an approximation of real head motions during shaking. It is likely that real head motion would contain superimposed components of higher and lower frequencies, and hence may cause more damage.

In essence, this thesis can conclude that shaking of an infant could produce bridging vein stretch ratios of approximately 1.25, ie. strains of 25%. Depending on the interpretation of the bridging vein failure criteria this may or may not be enough to cause subdural haematoma, however it should probably be accepted that it could well be enough, especially in extraordinary circumstances such as weaker, underdeveloped children, repeated shaking, etc. Furthermore, proportionally higher bridging vein strain would be caused if forced shaking were shown to produce head oscillations of a higher amplitude than than the passive amplitude of $\pm 60^\circ$ used as a maximum in this research.

6.2 Further Work

Some deficiencies of the current model have already been mentioned, and given time and adequate data there are various other factors in the model which could be improved. These include:

- Motion studies of a range of life-like baby dolls being shaken at various degrees of violence by different adults would produce more accurate inputs for the current model.

- Different models could be developed for multiple infants of different ages/weights to determine the effect this might have on susceptibility to subdural haematoma by shaking.

- Brain geometry could be improved, by separating the cerebellum from the cerebrum, and dividing the cerebrum into distinct hemispheres. However, this would

produce significant problems of geometry and mesh generation which would have to be overcome.

- Other head anatomy could be included, such as the various layers of dura surrounding the cerebrum, the falx cerebri which separates the left and right hemispheres of the cerebrum, more accurate placement of the bridging veins, fontanelle, foramen magnum allowing flow of CSF, brain ventricles, separate grey/white matter, etc.

- The brain stem which provides an important mechanical link between the brain and neck motion could be modelled more accurately.

- The skull could be modelled as a non-rigid body allowing impacts to be modelled more realistically.

- Inclusion of the ocular cavity and discrete eye components would also allow retinal haemorrhages to be investigated.

While adding components to the model may make it look more realistic (and hence more believable in many peoples eyes), unless it is done with great care at every stage it may easily just add to the model's dependence upon unknown variables and hence detract from the model's overall predictive power. Every additional complexity must be justified and the individual effect of changes in the new variables must be investigated.

LIST OF REFERENCES

ABEL, J.M., GENNARELLI, T.A. and SEGAWA, H. (1978). "Incidence and severity of cerebral concussion in the rhesus monkey following sagittal plane angular acceleration". *Proc. 22nd Stapp Car Crash Conf.* Warrendale, Pa: Society of Automotive Engineers, 35–53.

ACKERMAN, N.L. and ARBHABHIRAMA, A. (1964). "Viscous and boundary effects on virtual mass". *Journal of Engineering Mechanics, Proc. of the Am. Soc. of Civil Engineers*, **EM4**, 123–130.

AL-BSHARAT, A.S., HARDY, W.N., YANG, K.H. and KHALIL, T.B. (1999). "Brain/skull relative displacement magnitude due to blunt head impact: new experimental data and model". *Proc. 43rd Stapp Car Crash Conf.* SAE Paper 99SC22, 321–332.

ALEXANDER, R., SATO, Y., SMITH, W. and BENNETT, T. (1990). "Incidence of impact trauma with cranial injuries ascribed to shaking". *American Journal of Diseases of Children*, **144**, 724–726.

BARLOW, K.M. and MINNS, R.A. (1999). "The relation between intracranial pressure and outcome in non-accidental head injury". *Developmental Medicine and Child Neurology*, **41**, 220–225.

BARLOW, K.M., GIBSON, R.J., McPHILLIPS, M. and MINNS, R.A. (1999). "Magnetic resonance imaging in acute non-accidental head injury.". *Acta Pæditricia*, **88**, 734–740.

BECKER, J.C., LIERSCH, R., TAUTZ, C., SCHLUETER, B. and ANDLER, W. (1998). "Shaken baby syndrome: report on four pairs of twins". *Child Abuse & Neglect*, **22(9)**, 931–937.

BILSTON, L.E., LIU, Z. and PHAN-THEIN, N. (1997). "Linear viscoelastic properties of bovine brain tissue in shear". *Biorheology*, **34(6)**, 377–385.

BROWN, J.K. and MINNS, R.A. (1993). "Non-accidental head injury, with particular reference to whiplash shaking injury and medico-legal aspects". *Developmental Medicine and Child Neurology*, **35**, 849–869.

CAFFEY, J. (1946). "Multiple fractures in the long bones of infants suffering from chronic subdural hematoma". *American Journal of Roentgenology and Radium Therapy*, **56**, 163–173.

CAFFEY, J. (1972). "On the theory and practice of shaking infants". *American Journal of Diseases of Children*, **124(2)**, 161–169.

CAFFEY, J. (1974). "The Whiplash Shaken Infant Syndrome: manual shaking by the extremities with whiplash-induced intracranial and intraocular bleedings, lined with

residual permanent brain damage and mental retardation". *Pediatrics*, **54(4)**, 396–403.

CHRISTENSEN, R.M. (1982). "Theory of viscoelasticity, 2nd ed". *Academic Press*. ISBN 0121742520.

CHU, C-C., LIN, M-S., HUANG H-M. and LEE, M-C. (1994). "Finite element analysis of cerebral contusion". *Journal of Biomechanics*, **27(2)**, 184–194.

CLARK, C. and BLECHSCHMIDT, C. (1965). "Human transportation fatalities and protection against rear and side crash loads by the airstop restraint". *Proc. 9th Stapp Car Crash Conf.* Minneapolis: University of Minnesota.

DIMASI, F., MARCUS, J. and EPPINGER, H.C. (1991). "3-D anatomic brain model for relating cortical strains to automobile crash loading". *Proc. 13th Int. Techn. Conf. on Experimental Safety Vehicles*. Paper no. 91-S8-O-11.

DISCALA, C., SEGE, R., LI, G. and REECE, R.M. (2000). "Child abuse and unintentional injuries: A 10 year retrospective". *Archives of Pediatric and Adolescent Medicine*, **154**, 16–22.

DONNELLY, B.R. and MEDIGE, J. (1997). "Shear properties of human brain tissue". *Journal of Biomechanical Engineering*, **119**, 423–432.

DUHAIME, A.C., GENNARELLI, T.A., THIBAULT, L.E. *et al.* (1987). "The Shaken Baby Syndrome: A clinical, pathological, and biomechanical study". *Journal of Neurosurgery*, **66**, 409–415.

ELNER, S.G., ELNER, V.M., ARNALL, M. and ALBERT, D.M. (1990). "Ocular and associated systemic findings in suspected child abuse: a necropsy study". *Archives of Ophthalmology*, **108**, 1094–1101.

FALLENSTEIN, G.T., HULCE, V.D. and MELVIN, J.W. (1969). "Dynamic mechanical properties of human brain tissue". *Journal of Biomechanics*, **2**, 217–226.

GALBRAITH, C.G. and TONG, P. (1988). "Boundary conditions in head injury finite element modeling". *16th Annual In. Workshop on Human Subjects for Biomechanical Research*. 179–193.

GALFORD, J.E. and McELHANEY, J.H. (1970). "A viscoelastic study of scalp brain and dura". *Journal of Biomechanics*, **3**, 211–221.

GEDDES, J.F., VOWLES, G.H. and HACKSHAW, A.K. (2001*a*). "Neuropathology of inflicted head injury in children. 1: Patterns of brain damage". *Brain*, **124**, 1290–1298.

GEDDES, J.F., VOWLES, G.H. and HACKSHAW, A.K. (2001*b*). "Neuropathology of inflicted head injury in children. 1: Microscopic brain injury in infants". *Brain*, **124**, 1299–1306.

GENNARELLI, T.A. and THIBAULT, L.E. (1982). "Biomechanics of acute subdural hematoma". *The Journal of Trauma*, **22(8)**, 680–686.

GENNARELLI, T.A., THIBAULT, L.E., ADAMS, M.B. *et al.* (1982). "Diffuse axonal injury and traumatic coma in the primate". *Annals of Neurology*, **12**, 564–574.

GILLILAND, G.F. and FOLBERG, R. (1996). "Shaken babies—some have no impact injuries". *Journal of Forensic Sciences*, **14(1)**, 114-116.

GLECKMAN, A.M., BELL, M.D., EVANS, E.J. and SMITH T.W. (1999). "Diffuse axonal injury in infants with nonaccidental craniocerebral trauma". *Archives of Pathology and Laboratory Medicine*, **123**, 146–151.

GUTHKELCH, A.N. (1971). "Infantile subdural hematoma and its relationship to whiplash injury". *British Medical Journal*, **2**, 430–431.

HADLEY, M.N., SONNTAG, K.H., REKATE, H.L. and MURPHY, A. (1989). "The infant whiplash-shake injury syndrome: A clinical and pathological study". *Neurosurgery*, **24(4)**, 536–540.

HAUT, R.C. (1983). "Age-dependent influence of strain rate on the tensile failure of rat-tail tendon". *Journal of Biomechanical Engineering*, **105(3)**, 296–299.

HODGSON, D.C., SHIPPEN, J.M. and SUNDERLAND, R. (2001). "Protective role of cerebrospinal fluid in brain injuries [letter].". *Archives of Disease in Childhood*, **84(2)**, 187.

HOLBOURN, A.H.S. (1943). "Mechanics of Head Injuries". *The Lancet*, **2**, 438–441.

HOWARD, M.A., BELL, B.A. and UTTLEY, D. (1993). "The pathophysiology of infant subdural hematomas". *British Journal of Neurosurgery*, **7**, 355–365.

HUANG, H.-M., LEE, M.-C., HIU, W.-T. *et al.* (1999). "Three-dimensional finite element analysis of subdural hematoma". *Journal of Trauma*, **47(3)**, 538–544.

JAYAWANT, S., RAWLINSON, A., GIBBON, F. *et al.* (1998). "Subdural Haemorrhages in infants: population based study". *British Medical Journal*, **317**, 1558–1561.

KANG, H-S., WILLINGER, R., DIAW, B.M. and CHINN, B. (1997). "Validation of a 3D anatomic human head model and replication of head impact in motorcycle accident by finite element modeling". *Proc. 41st Stapp Car Crash Conf.* SAE Paper 973339, 329–338.

KEMPE, C.H., SILVERMAN, F.D, STEELE, B.F., *et al.* (1962). "The battered-child syndrome". *Journal of the American Medical Association*, **181(1)**, 17–24.

KHALIL, T.B. and VIANO, D.C. (1982). "Critical issues in finite element modeling of head impact". *Proc. 26th Stapp Car Crash Conf.* SAE Paper 821150, 87–102.

KOENEMAN, J.B. (1966). "Viscoelastic properties of brain tissue". *unpublished MSc thesis*. Case Institute of Technology.

KUIJPERS, A.H.W.M., CLAESSENS, M.H.A. and SAUREN, A.A.H.J. (1995). "The influence of different boundary conditions on the response of the head to impact: A two-dimensional finite element study". *Journal of Neurotrauma*, **12(4)**, 715–724.

LAZORITZ, S., BALDWIN, S. and KINI, N. (1997). "The whiplash shaken infant syndrome: Has Caffey's syndrome changed or have we changed his syndrome?". *Child Abuse & Neglect*, **21(10)**, 1009–1014.

LEE, M-C. and HAUT, R.C. (1989). "Insensitivity of tensile failure properties of human bridging veins to strain rate: implications in biomechanics of subdural hematoma". *Journal of Biomechanics*, **22(6/7)**, 537–542.

LEE, M-C., MELVIN, J.W. and UENO, K. (1987). "Finite element analysis of traumatic subdural hematoma". *Proc. 31st Stapp Car Crash Conf.* SAE Paper 872201, 67–77.

LÖWENHIELM, P. (1974*a*). "Dynamic properties of the parasagittal bridging veins". *Z Rechtsmedizin*, **74**, 55–62.

LÖWENHIELM, P. (1974*b*). "Strain tolerance of the vv. cerbri sup. (bridging veins) calculated from head-on collision tests with cadavers". *Z Rechtsmedizin*, **75**, 131–144.

MARGULIES, S.S., THIBAULT, L.E. and GENNARELLI, T.A. (1985). "A study of scaling and head injury criteria using physical model experiments". *International IRCOBI Conference on the Biomechanics of Impacts*. 223–234.

MARGULIES, S.S. and THIBAULT, L.E. (1989). "An analytical model of traumatic diffuse brain injury". *Journal of Biomechanical Engineering*, **111**, 241–249.

McCLELLAND, C.Q., REKATE, H., KAUFMAN, B. and PERSSE, L. (1980). "Cerebral injury in child abuse: A changing profile". *Child's Brain*, **7**, 225–235.

MAXEINER, H. (2001). "Demonstration and interpretation of bridging vein ruptures in cases of infantile subdural bleedings". *Journal of Forensic Science*, **46(1)**, 85–93.

MAY, P.R., FUSTER, J.M., HABER, J. and HIRSCHMAN, A. (1979). "Woodpecker drilling behaviour: an endorsement of the rotational theory of impact brain injury". *Archives of Neurology*, **36**, 370–373.

McCONNELL, K.G. and YOUNG, D.F. (1965). "Added mass of a sphere in a bounded viscous fluid". *Journal of Engineering Mechanics, Proc. of the Am. Soc. of Civil Engineers*, **EM4**, 147–164.

McELHANEY, J.H., MELVIN, J.W., ROBERTS, V.L. and PORTNOY, H.D. (1973). "Dynamic characteristics of the tissues of the head". In Kenedi, R.M., *Perspectives in Biomedical Engineering*. London: Macmillan Ltd..

MEANEY, D.F. (1991). "Biomechanics of acute subdural hematoma in the subhuman primate and man". *PhD Thesis, University of Pennsylvania, USA*.

MEANEY, D.F., THIBAULT, L.E. (1990). "Physical model studies of cortical brain deformation in response to high strain rate inertial loading". *International IRCOBI Conf. on the Biomechanics of Impacts*. 215–223.

MILLER, K. and CHINZEI, K. (1997). "Constitutive modelling of brain tissue: experiment and theory". *Journal of Biomechanics*, **30(11/12)**, 1115–1121.

MILNE-THOMPSON, L.M. (1968). "Theoretical hydrodynamics, 5th ed.". *London: MacMillan & Co Ltd*. ISBN: 0-486-68970-0.

MORRIS, M.W., SMITH, S., CRESSMAN, J. and ANCHETA, J. (2000). "Evaluation of infants with subdural hematoma who lack external evidence of abuse". *Pediatrics*, **105(3)**, 549–553.

NAHUM, A.M., SMITH, R. and WARD, C.C. (1977). "Intracranial pressure dynamics during head impact". *Proc. 21st Stapp Car Crash Conf.* 339–366.

OKA, K., RHOTON, A.L., BARRY, M. and RODRIGUES, R. (1985). "Microsurgical anatomy of the superficial veins of the cerebrum". *Neurosurgery*, **17(5)**, 711–748.

OMMAYA, A.K. (1968). "Mechanical properties of tissues of the nervous system". *Journal of Biomechanics*, **1**, 127–138.

OMMAYA, A.K. and GENNARELLI, T.A. (1974). "Cerebral concussion and traumatic unconsciousness". *Brain*, **97**, 633–654.

OMMAYA, A.K. and HIRSCH, A.E. (1971). "Tolerances for cerebral concussion from head impact and whiplash in primates". *Journal of Biomechanics*, **4**, 13–21.

OMMAYA, A.K., YARNELL, P., HIRSCH, A.E. and HARRIS, E.H. (1967). "Scaling of experimental data on cerebral concussion in sub-human primates to concussion threshold for man". *Proc. 11th Stapp Car Crash Conf.* New York: Society of Automotive Engineers.

OMMAYA, A.K. and YARNELL, P. (1969). "Subdural hæmatoma after whiplash injury". *The Lancet*, **2**, 237–239.

POLANYI, M. (1911). "Beitrag zur chemie der hydrocephlausflüssigkeit". *Biochem Zeitsch*, **34**, 205–210.

ROE, P.L. (1981). "Approximate Riemann solvers, parameter vectors, and difference schemes". *Journal of Computational Physics*, **43**, 357–372.

RUAN, J.S., KHALIL, T.B. and KING, A.I. (1993). "Finite element modeling of direct head impact". *Proc. 37th Stapp Car Crash Conf.* SAE Paper No. 933114, 69–81.

RUAN, J.S. and PRASAD, P. (1996). "Study of the biodynamic characteristics of the human head". *International IRCOBI Conference on the Biomechanics of Impacts.* 63–74.

SALADIN, K.S. (1998). "Anatomy and Physiology". *New York: McGraw-Hill.* 468.

SAUREN, A.A.H.J. and CLAESSENS, M.H.A. (1993). "Finite element modelling of head impact: The second decade". *International IRCOBI Conference of Biomechanics of Impacts.* 241–253.

SHUCK, L.Z., ADVANI, S.H. (1972). "Rheological response of human brain tissue in shear". *ASME Journal of Basic Engineering*, **Dec**, 905–911.

SHUCK, L.Z., HAYNES, R.R. and FOGLE, J.L. (1970). "Determination of viscoelastic properties of human brain tissue". *ASME paper 70-BHF-12.* The American Society of Mechanical Engineers.

SMITH, S.S. and HANSON, R. (1974). "134 battered children: a medical and psychological study". *British Medical Journal*, **3**, 666–670.

THIBAULT, L.E. and GENNARELLI, T.A. (1985). "Biomechanics of diffuse brain injuries". *Proc. of the Fourth Experimental Safety Vehicle Conference.* New York: American Association of Automotive Engineers.

THIBAULT, K.L. and MARGULIES, S.S. (1998). "Age-dependent material properties of the porcine cerebrum: effect on pediatric inertial head injury criteria". *Journal of Biomechanics*, **31**, 1119–1126.

TZIOUMI, D. and OATES, R.K. (1998). "Subdural hematomas in children under 2 years. Accidental or inflicted? A 10-year experience". *Child Abuse & Neglect*, **22(11)**, 1105–1112.

YAMASHIMA, T. and FRIEDE, R.L. (1984). "Why do bridging veins rupture into the virtual subdual space?". *Journal of Neurology, Neurosurgery and Psychiatry*, **47**, 121-127.

ZHOU, C., KHALIL, T.B. and KING, A.I. (1996). "Viscoelastic response of the human brain to sagittal and lateral rotational acceleration by finite element analysis". *International IRCOBI Conference on the Biomechanics of Impacts.* 35–48.

ZIMMERMAN, R.A., BILANIUK, L.T. and BRUCE, D. (1979). "Computed tomography of craniocerebral injury in the abused child". *Radiology*, **130**, 687–690.

